Integration of a Solar Energy System at the Future Building Laboratory of Concordia University: Simulation, Analysis, and Testing of Different Operational Modes

Jay Prajapati

A Thesis

in

The Department

of

Electrical and Computer Engineering

Presented in Partial Fulfillment of the Requirements

for the Degree of

Master of Applied Science (Electrical and Computer Engineering) at

Concordia University

Montréal, Québec, Canada

April 2025

CONCORDIA UNIVERSITY
SCHOOL OF GRADUATE STUDIES

This is to certify that the thesis prepared

By: Jay Prajapati

Entitled: Integration of a Solar Energy System at the Future Building Laboratory of Concordia University: Simulation, Analysis, and Testing of Different Operational Modes

and submitted in partial fulfillment of the requirements for the degree of

Master of Applied Science (Electrical and Computer Engineering)

complies with the regulations of this University and meets the accepted standards with respect to originality and quality.

Signed by the final examining committee:

______________________________ Chair
Dr. Luiz Lopes

______________________________ Examiner
Dr. Hua Ge

______________________________ Supervisor
Dr. Pragasen Pillay

Approved by: ______________________________
Dr. Abdelwahab Hamou-Lhadj, Chair
Department of Electrical and Computer Engineering

____
Dr. Mourad Debbabi, Dean,
Faculty of Engineering and Computer Science

ABSTRACT

Integration of a Solar Energy System at the Future Building Laboratory of Concordia University: Simulation, Analysis, and Testing of Different Operational Modes

Jay Prajapati

This research explores the development and integration of a solar photovoltaic (PV) system and a vehicle-to-home (V2H) backup power system at the Future Building Laboratory (FBL) of Concordia University, Montreal, Quebec. The study addresses the challenges of rural electrification, proposing renewable energy systems as sustainable and eco-friendly solutions for off-grid applications. A modified electrical power system is designed for the FBL, incorporating critical loads, a subpanel, manual transfer switches, grid-forming and grid-following converters, battery storage, and an electric vehicle with a vehicle-to-home inverter.

The system's performance is analyzed through simulation and experimental testing. Sunny Island (grid-forming/battery charger) and Sunny Boy (grid-following) were simulated in both standalone and grid-connected scenarios, with control strategies ensuring seamless operation in grid-forming and grid-following modes. Experimental results validate the simulations, demonstrating consistent performance of the converters under different operating conditions, including parallel operation.

The research also explores vehicle-to-load (V2L) and vehicle-to-home (V2H) systems, highlighting the capability of EVs to serve as reliable emergency backup power sources. The experimental results demonstrate that integrating V2H technology with renewable energy systems enhances the overall resiliency and flexibility of decentralized power systems. Moreover, this EV-to-home integration reduces reliance on traditional backup energy sources, thereby enhancing sustainability.

Thus, this study provides a comprehensive framework for integrating solar PV power and EV technologies into decentralized power systems, demonstrating their potential to create scalable, reliable, and environmentally sustainable solutions for rural and remote electrification needs.

Acknowledgment

"तस्मै श्रीगुरवे नमः।"

Salutations to that glorious teacher (God) who guides us.

I would like to express my heartfelt gratitude to my supervisor, Professor Pragasen Pillay, for granting me the opportunity to delve deeper into science under his invaluable guidance and support.

I am deeply appreciative of the mentorship and guidance provided by Dr. Akrem Aljehaimi and Dr. Mathews Boby throughout this research journey. Their insights and advice were instrumental in shaping this work.

I extend my warm thanks to my colleagues in the PEER group laboratory for creating a supportive, home-like environment. Special thanks to Mohammad, Rao, Ashutosh, Soliha, Nazanin, Amir, Neetusha, Bassam, Dr. Hyacinthe, Abraham, Hani and Kenneth for their camaraderie and encouragement.

Lastly, I wish to express my profound appreciation to my parents, Dipak and Jyoti, and my brother, Parth, for their unwavering love, support, and inspiration throughout this journey.

Table of Contest

List of Figure

List of Table

Nomenclature

A	Ampere
AC	Alternative Current
Ah	Ampere-Hour
C	Capacitor
DC	Direct Current
EV	Electric Vehicle
F	Farad
f	Frequency
FBL	Future Building Laboratory
FFT	Fast Fourier Transform
GFL	Grid-Following
GFM	Grid-Forming
H	Henry
hp	Horsepower
Hz	Hertz
I	Current
kW	Kilowatt
kWh	Kilowatt-Hour
MPPT	Maximum Power Point Tracking
PCC	Point of Common Coupling
PI	Proportional-Integral
PLL	Phase-Lock-Loop
PV	Photovoltaic
PWM	Pulse Width Modulation
RMS	Root Mean Square
s	Second
SOC	State of Charge
THD	Total Harmonic Distortion
V	Voltage
V2G	Vehicle-to-Grid
V2H	Vehicle-to-House
V2L	Vehicle-to-Load
W	Watt

1 Introduction

This chapter explains the issues regarding rural electrification and clean energy for remote residential areas using renewable resources. It discusses how traditional power infrastructure, which relies on large-scale grids, often struggles to reach these rural locations due to certain barriers. Additionally, typical centralized power grids have been reliant on fossil fuels such as coal, oil, and natural gas, which contribute to greenhouse gas emissions.

Micro-grids powered by renewable energy such as solar, wind, biomass, and hydro have the potential to significantly reduce carbon emissions. This chapter demonstrates some projects on renewable micro-grids as a promising solution to address the energy access challenge in rural areas.

1.1 Rural Electrification

Access to electricity is not just a convenience but a catalyst for change. It is crucial for alleviating poverty, driving economic growth, creating employment opportunities, and ensuring the delivery of essential social services such as education and healthcare. As of 2022, nearly 760 million people globally did not have access to electricity [1]. The majority of these people live in rural and remote areas [2]. Figure 1.1 shows the share of the world population having access to electricity in 2021 [3].

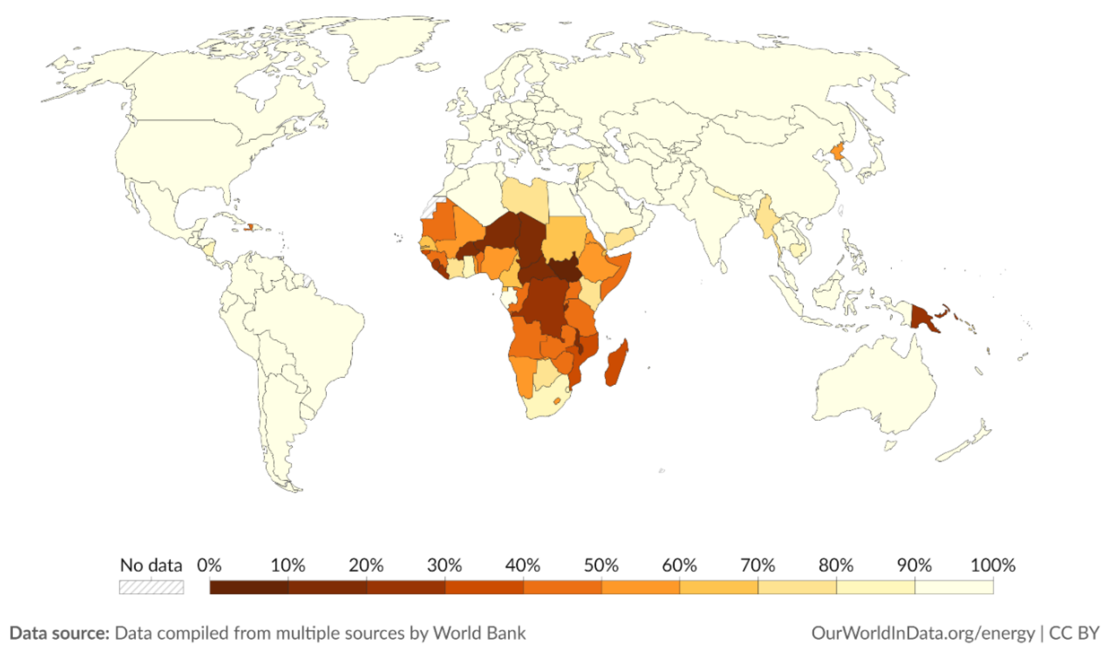

Figure 1.1 Share of Population with Access to Electricity, 2021 [3]

Approximately 178 Indigenous communities in Canada are not connected to the North American electricity grid and natural gas pipelines [4]. These off-grid communities primarily depend on costly diesel-fired generation for their electricity needs [4]. At the same time, some utilize smaller local or regional grids powered by hydroelectricity or trucked-in liquefied natural gas (LNG) [4].

1.2 Challenges for Rural Electrification

In recent years, rural electrification efforts have made substantial strides [5]. Through the combined efforts of government, non-profit organizations, and private companies, electricity access has been significantly expanded in remote regions [5]. However, electrification in remote areas continues to encounter challenges, such as:

- Geographical: Remote locations often face challenging terrains that make infrastructure development difficult and expensive. Excessive lengthening of the low-voltage network leads to significant network losses and increased costs [6]. Constructing long power lines for low-power consumers often increases transmission losses and costs, making it less usable economically [6].
- Maintenance and Sustainability: Ensuring the long-term sustainability and maintenance of electrification systems in remote areas presents several difficulties, including the availability of technical expertise, spare equipment, maintaining infrastructure, and a reliable energy source [7].
- Environmental Concerns: Diesel generators offer a convenient power solution for rural and remote areas but significantly contribute to greenhouse gas (GHG) emissions, contamination of water due to gasoline spillage. Many remote communities worldwide depend on diesel fuel for electricity. This dependency makes them vulnerable to fluctuating fuel prices and increases their GHG emissions as electricity demand rises. Adding more diesel generators to meet growing power needs only worsens the environmental impacts [8].

1.3 Renewable Energy System for Remote or Rural Areas

Renewable energy systems offer sustainable solutions for electricity generation in remote areas. These systems, including solar, wind, hydro, and biomass, provide reliable power while minimizing the environmental impact. Adopting renewable energy reduces reliance on diesel generators, lowering greenhouse gas emissions and protecting communities from volatile fuel prices. Additionally, these systems often have lower operational costs over time and can be scaled to meet growing energy demands.

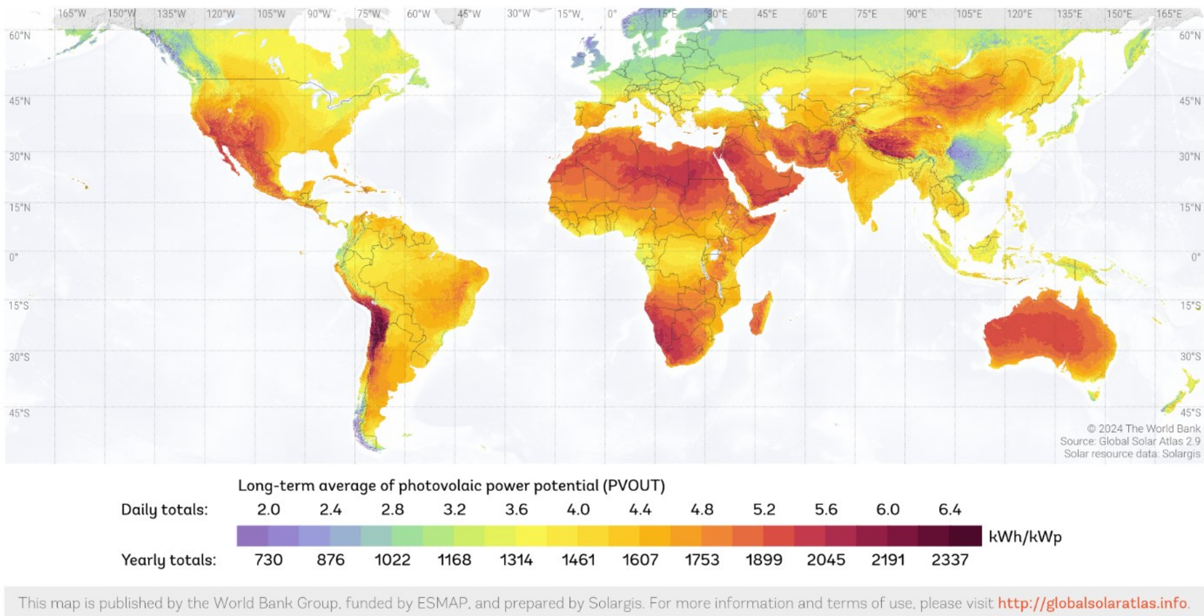

Figure 1.2 Photovoltaic Electricity Potential [9]

Solar energy systems are an excellent solution for providing electricity in remote areas. Key components of a solar energy system include solar panels, inverters, and batteries for energy storage. Implementing solar energy systems in remote regions involves initial assessments of energy needs, local solar potential, and the design of appropriate systems. Figure 1.2 shows the world map with the potential of solar photovoltaic electricity. If one compares the map with Figure 1.1, the population with less access to electricity has a good amount of photovoltaic potential. With proper planning and support, solar energy can significantly enhance the quality of life in remote communities by providing reliable, sustainable, and cost-effective electricity.

1.4 Off-grid Rural Electrification Projects

In March 2022, the government of Canada introduced its inaugural 2030 Emissions Reduction Plan (ERP) as part of the Canadian Net-Zero Emissions Accountability Act [10]. The aim is to achieve net-zero electricity by 2035 by expanding non-emitting energy sources nationwide, connecting regions to clean power, and providing a more reliable and affordable electricity supply

[10]. Some communities have developed off-grid, reliable solar-generated, and battery-storage systems for their electricity needs. Below are examples of such communities in Canada.

1.4.1 Three Nations Energy (3NE), Fort Chipewyan, Alberta

Fort Chipewyan, located in northern Alberta at the western end of Lake Athabasca, has the 3NE Solar Farm, the largest solar farm in a remote Canadian community with a capacity of 2.2 MW. Although the manufacturing process of solar panels emits CO2, the amount is negligible. This project successfully reduces the community's diesel usage for electricity generation by 25% [4]. Savings of 800,000 liters of diesel reduce greenhouse emissions by 2,145 tons of CO2 annually [11]. Figure 1.3 shows the 3NE Solar Project, battery bank, and backup diesel generator.

Figure 1.3 3NE Solar Farm Project [12]

1.4.2 Sree Vyaa (Old Crow Solar Project), Yukon

The fly-in community of Old Crow relies on diesel for heating and electricity [4]. Due to a lack of barge or winter road access, diesel is delivered by plane four times a year and stored in above-ground tanks [4]. ATCO Electric Yukon has initiated a project that includes 940 kW of solar panels and 616 kWh of battery storage [4]. This project cuts diesel usage by about 190,000 liters annually and reduces CO_2 emissions by 750 tons yearly [13]. Figure 1.4 shows the Old Crow Solar Project.

Figure 1.4 The Old Crow Solar Farm [14]

1.4.3 Giizis Energy Micro-grid, Gull Bay, Ontario

The community of Gull Bay is located on the western shores of Lake Nipigon, with a population of 392 people. The project was co-developed by Gull Bay First Nation and OPG (Ontario Power Generation). The solar-diesel hybrid microgrid features a 360 kW solar array and a 500 kWh battery. It is projected to decrease annual diesel usage by 25%, equivalent to 110,000 liters [4], [15]. Figure 1.5 shows the aerial view of the Giizis Energy Micro-grid project.

Figure 1.5 Giizis Energy Micro-grid in Gull Bay First Nation [16]

1.5 FBL (Future Building Laboratory)

A research facility is located in Loyola Campus, Concordia University, Montreal. The research facility is called the Future Building Laboratory. The building is equipped with a battery bank and different types of solar window panels such as STPV (Semi-Transparent Photovoltaics), BIPV/T (Building Integrated Photovoltaics/Thermal), power converters, V2L inverter, and EV charger. Figure 1.6 shows the FBL. The building has six test cells, each integrated with different types of solar panels, a mechanical room equipped with a water source heat pump, and an electrical room that has the electrical main panel, sub-panel, DC bus bar, battery bank, and ethernet communication rack for communicating with different devices of the building. The building also features some locations for the future connection of solar roof panels, wind turbines (WTs), and hydrogen loops.

Figure 1.6 FBL (Future Building Laboratory), Loyola Campus, Concordia University, Montreal

As part of this thesis, experiments were conducted on the different modes of operation of the available power sources and power converters. The current integrated system with energy sources and power converters is shown in Figure 1.7.

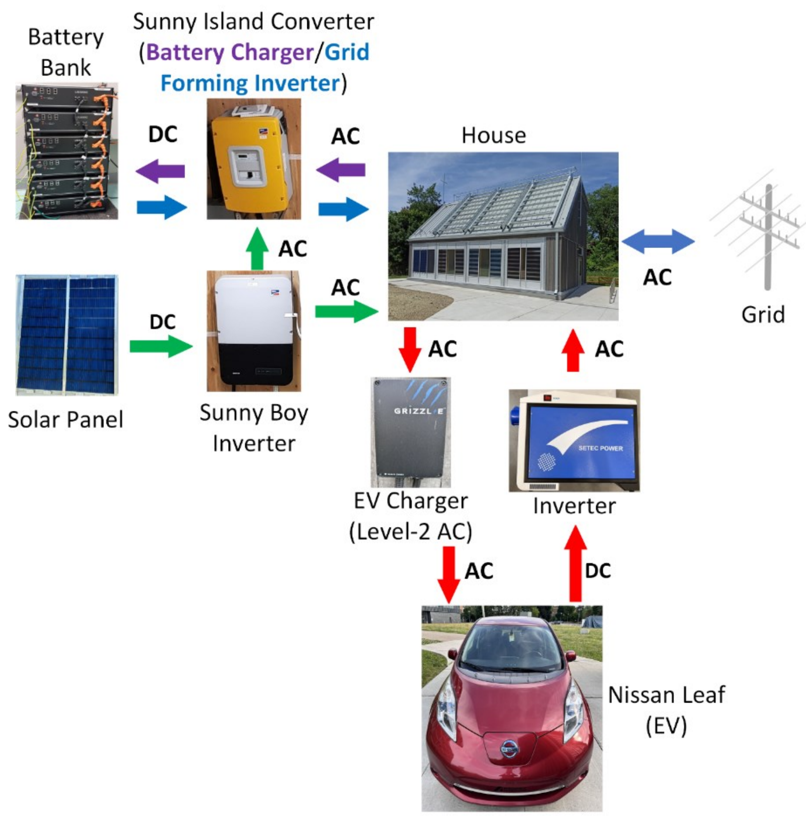

Figure 1.7 General Schematic: Energy sources and Power Electronic converters

1.6 Contribution

This thesis contributes to the understanding of grid-forming (GFM) converter design by thoroughly analyzing the internal components of the SMA Sunny Island converter. It further explores the design and control of the grid-following (GFL) inverter. Additionally, an electrical solar power system is designed and commissioned for the Future Building Laboratory (FBL) to integrate various energy sources, such as solar power, electric vehicles (EVs), and a battery bank, in conjunction with SMA solar converters and a vehicle-to-home (Setec) inverter. The system is tested in various modes of operation, both in off-grid and grid-connected conditions. From the behavior of the SMA converter setup, a frequency shift power control strategy is formed for the GFM and GFL converter to work together in off-grid conditions. The designed strategy is simulated, and the results are compared with the actual system's results. Out of this thesis, the following conference paper will be submitted to IEEE Symposium on Industrial Electronics conference.

J. Prajapati, A. M. Aljehaimi and P. Pillay, "Dynamics and Design Analysis of Grid-Forming and Grid-Following Converters of SMA Solar Technology." Will be submitted to *34th IEEE International Symposium on Industrial Electronics (ISIE 2025)*, Toronto, 20-23 June, 2025.

1.7 Thesis Organization

The thesis is structured as follows:

Chapter 2: This chapter discusses the FBL's electrical solar power system and its devices and reviews the different modes of operation of the electrical system.

Chapter 3: This chapter discusses the design of the SMA converters. The designed converters are simulated individually, followed by the integrated system.

Chapter 4: This chapter presents the experimental setup of the SMA solar system converters and some experimental results for different operating modes.

Chapter 5: This chapter discusses the experimental setups and results for vehicle-to-load (V2L) and vehicle-to-home (V2H) systems.

Chapter 6: Conclusion and future work are presented

2 FBL Electrical System and Modes of Operation

2.1 Introduction

This chapter presents the electrical power system of the FBL (Future Building Laboratory) and discusses Sunny Island's and Sunny Boy's different modes of operation.

2.2 Electrical Power System of the FBL

The electrical system of the building without any PV cells and batteries consists of a power supply of 600 V 3-phase 60 Hz from the grid, a 3-phase 150 kVA delta/star connected transformer which steps down the 600 V to 208 V (line) or 120 V (phase), and a 3-phase distribution panel which distributes the power to different loads. The total load of the building is almost 70 kVA. The electrical system is shown in Figure 2.1. Table 2.1 shows the characteristics of the 3-phase transformer used in the house.

For experimental purposes, some of the loads of the house are transferred from the main panel to the sub-panel, as shown in Figure 2.2. Two transfer switches are used to supply the sub-panel loads from the grid, the solar battery system, or the EV. So, even if the solar battery system malfunctions, the grid can supply the household loads. The transferred loads in the sub-panel are shown in Table 2.2. For emergency backup power needs, the AC socket for the EV is connected to the single-phase inverter that takes power from the EV traction battery. The transfer switch is put on the EV mode, and then the AC socket for the EV is connected to the C-phase loads of the sub-panel.

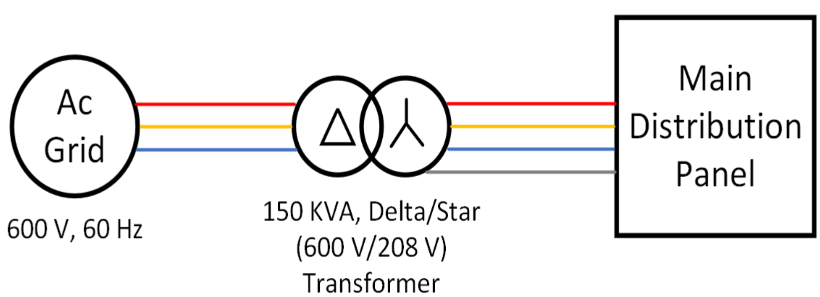

Figure 2.1 Electrical Power System of FBL

For integrating the electrical power from the PV modules in the house, the inverters Sunny Island and Sunny Boy are used along with the battery storage system. The electrical wiring diagram presented in [17] is updated to add other converters and energy sources to the house. The input in disconnector 1 (DSC 1) comes from the main distribution panel; then, each phase goes to Sunny Island's input terminal AC2 (Gen/Grid). The Sunny Islands' output AC1 (Loads/Sunny Boys) is connected to the three PCC lines. Two lines of the PCC are connected to the outputs L1 and L2 of the Sunny Boys in 208 V wye connection fashion, as shown in Figure 2.2. These PCC lines are connected to the house's loads. Figure 2.3 shows the transfer switches and sub-panel installed in the house.

The Sunny Islands' DC terminals are connected to the Battery Bank system through the DC busbar of the respective polarity. Each PV array is connected to one of the Sunny Boy's MPPs. C+ and C- terminals are used for PV array connections.

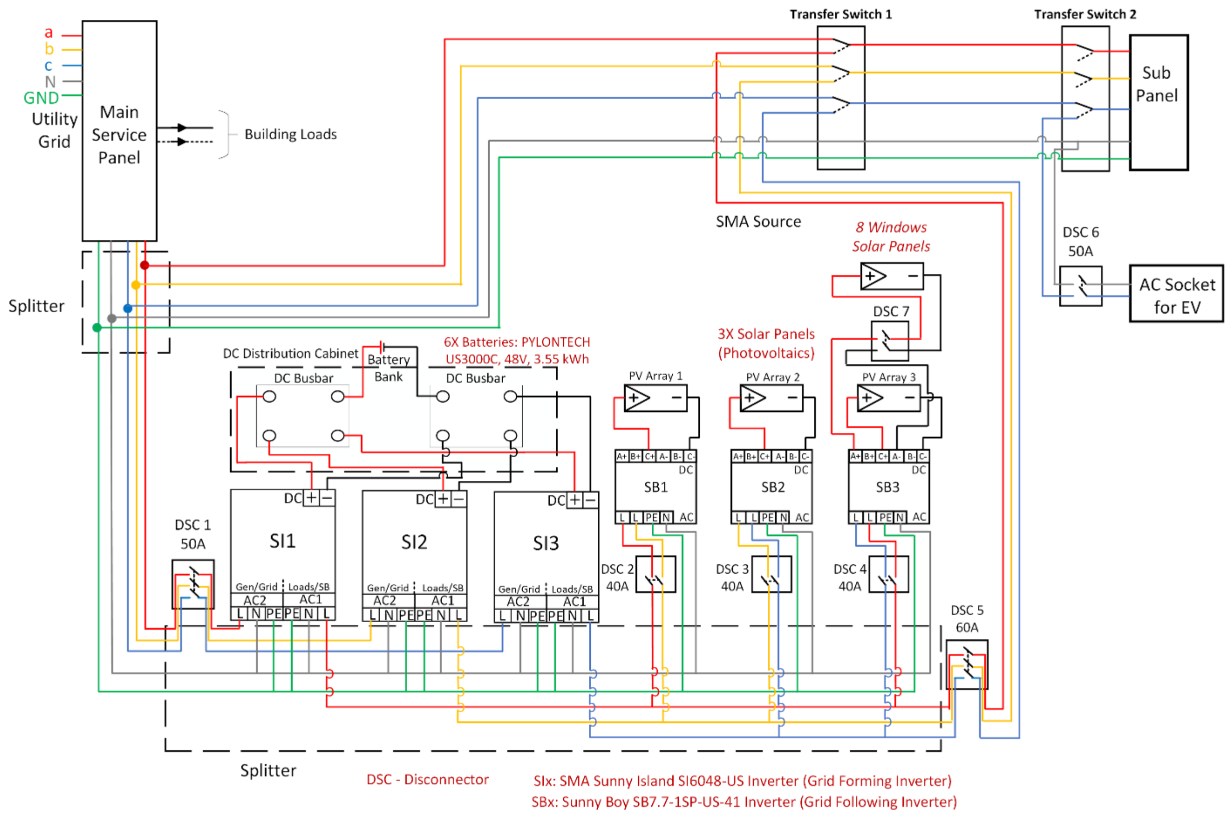

Figure 2.2 Electrical Wiring Diagram of the FBL with different Energy Sources

Table 2.1 150 KVA Transformer Characteristics [21]

Make and Model	Characteristics	
REX POWER MAGNETICS BC150J-M/S1/T80/X/Z3	kVA Rating	150 kVA
	Frequency	60 Hz
	% IMP	4.0 %
	BIL	10 kV
	Primary Voltage	600 V Delta
	Secondary Voltage	208Y/120 V

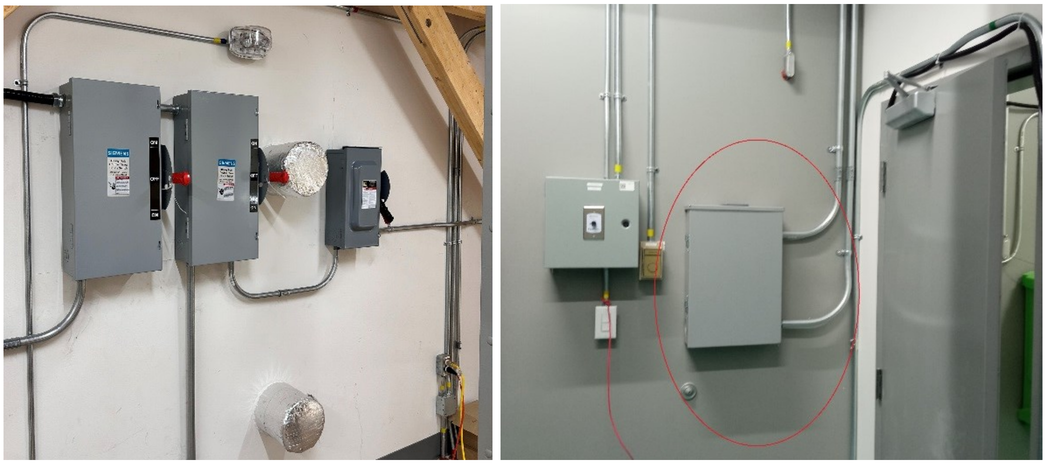

Figure 2.3 Transfer Switches and Sub-panel

Table 2.2 Transferred Loads in Sub-panel

No	Load	Phase A (VA)	Phase B (VA)	Phase C (VA)
1	EXTERIOR LIGHTING (CIR. 1)	105		
2	MEZZANINE LIGHTING AND LIGHT PIT (CIR. 2)	826		
3	GROUND FLOOR LIGHTING (CIR. 3)			891
4	GROUND FLOOR LIGHTING (CIR. 4)			1424
5	Heater (CIR. 13)	750		
6	Heater (CIR. 15)		750	
7	HU1-001-110.00-SH (Humidifier) (CIR. 17)		2025	
8	HU1-001-110.00-SH (Humidifier) (CIR. 19)	2025		
9	DSC INTRUSION ALARM BOX (CIR. 18)			500
10	VE1-002-110.01-SH (Greenheck Fan) (CIR. 29)			75
11	EC1-002-110.01-SH (Air Exchanger) (CIR. 35)			500
12	COMMUNICATION PANEL WITH... (CIR. 51)			500
13	FIRE ALARM CONTROL PANEL (CIR. 53)			500
14	ISTAR PANEL (Door Controller) (CIR. 54)			100
Total		3706	2775	4490

2.3 Major Components of the Power System

In the system shown in Figure 2.2, the Sunny Island and Sunny Boy are the Grid-Forming and Grid-Following Inverters, respectively. Six batteries are connected in parallel to the DC bus bar of their respective polarities.

2.3.1 Sunny Island (Grid Forming Inverter)

The grid-forming inverters create a grid-like voltage when the grid is shut down. Its primary significance is that it can start without any external supply source [19]. It uses the 48 V house battery bank as a power supply. The grid-forming inverter controls the voltage and frequency according to the power requirement of the load [20]. The Sunny Island works as a rectifier and battery charger to charge the battery from the grid under normal conditions. When the grid is shut down, it works as a grid-forming inverter. It creates a grid-like voltage by converting the battery's DC power to AC power to supply the loads. Table 2.3 gives the specification details of the Sunny Island inverter.

Table 2.3 SMA Sunny Island SI6048-US Inverter Specifications [22]

Make and Model	Characteristics	
SMA Solar Technology America LLC SMA Sunny Island SI6048-US Inverter	**Output Data**	
	Nominal AC Voltage (Adjustable)	120 V (105 V to 132 V)
	Nominal AC Current	48.0 A
	Nominal AC Power	5750 W
	Nominal Frequency	60 Hz (55 to 65 Hz)
	Input Data	
	Input Voltage (Adjustable)	120 V (80 V to 150V)
	Input Frequency (Adjustable)	60 Hz (54 Hz to 66 Hz)
	Maximum AC input Current (Adjustable)	56 A (0 A to 56 A)
	Maximum Input Power	6.7 kW
	Battery Data	
	Battery Voltage (range)	48 V (41 V to 63 V)
	Maximum battery charging Current	140 A
	Continuous charging Current	110 A
	Battery Type	Lead-acid battery: VRLA/FLA/NiCd battery Lithium-ion battery

2.3.2 Sunny Boy (Grid Following Inverter)

The grid-following inverters create an output voltage in phase with the grid's voltage. In doing this, the grid supply is required. The grid-following inverters control the output power by measuring the angle of the grid's voltage using a phase-lock-loop (PLL) [20]. In this configuration, the Sunny Boy follows the phase of the voltage created by Sunny Island when the grid is off. The Sunny Boy works in one direction only, i.e., it converts the DC power of the PV cell into AC power to supply power to the load, to charge the battery, or to supply power to the grid. The specification of the Sunny Boy inverter is shown in Table 2.4.

Table 2.4 SMA Sunny Boy SB7.7-1SP-US-41 Specifications [23]

Make and Model	Characteristics	
SMA Solar Technology America LLC SMA Sunny Boy SB7.7-1SP-US-41	**Dc Input**	
	Maximum PV Array Power	12320 Wp
	Maximum Input Voltage	600 V
	Minimum Input Voltage	100 V
	Maximum Input Current per input	10 A
	Number of independent MPP inputs	3
	AC Output	
	Rated Grid Voltage	208 V / 240 V
	Rated Power at 208 V / 240 V	6650 W / 7680 W
	Nominal AC Current at 208 V / 240V	32 A / 32 A
	Operating range at AC power Frequency 60 Hz	59.3 Hz to 60.5 Hz
	AC Voltage range at 208 V	183 V to 229 V
	AC Voltage range at 240 V	211 V to 264 V

2.3.3 Pylontech Battery Bank

Six batteries are connected in parallel to form a battery bank. The battery bank is connected to the bus bar of the respective polarity. The battery has an inbuilt BMS (Battery Management System) for charge management and protection functions such as over-discharge, over-charge, over-current, and high/low temperature. The six batteries are connected via Ethernet cables.

Table 2.5 PYLONTECH-US3000C Li-ion Battery Specifications [24]

Make and Model	Characteristics	
Pylon Technologies Co., Ltd. PYLONTECH-US3000C Li-ion Battery	Nominal Voltage	48 V
	Nominal Capacity	3552 Wh
	Usable Capacity	3374.4 Wh
	Depth of discharge	95 %
	Discharge Voltage	44.5 V to 53.5 V
	Charge Voltage	52.5 V to 53.5 V
	Recommended Charge/Discharge Current	37 A
	Communication	RS485, CAN

2.3.4 Communication Network

The master SI inverter is embedded with the RS-485 Piggy-back for RS-485 communication with the EDDM (SMA Data Manager); it also communicates with the battery bank on CAN protocol and other SI inverters (slave1, slave2). The six batteries communicate through LINKPORT; the first battery behaves like the master battery. The Sunny Boy inverters' communication ports are connected in a daisy chain, with one end connected to the EDDM. The EDDM is connected to the internet for remote access to the system. Figure 2.4 shows the detail of the communication network. The detailed commissioning process and remote monitoring platform are discussed in the appendix.

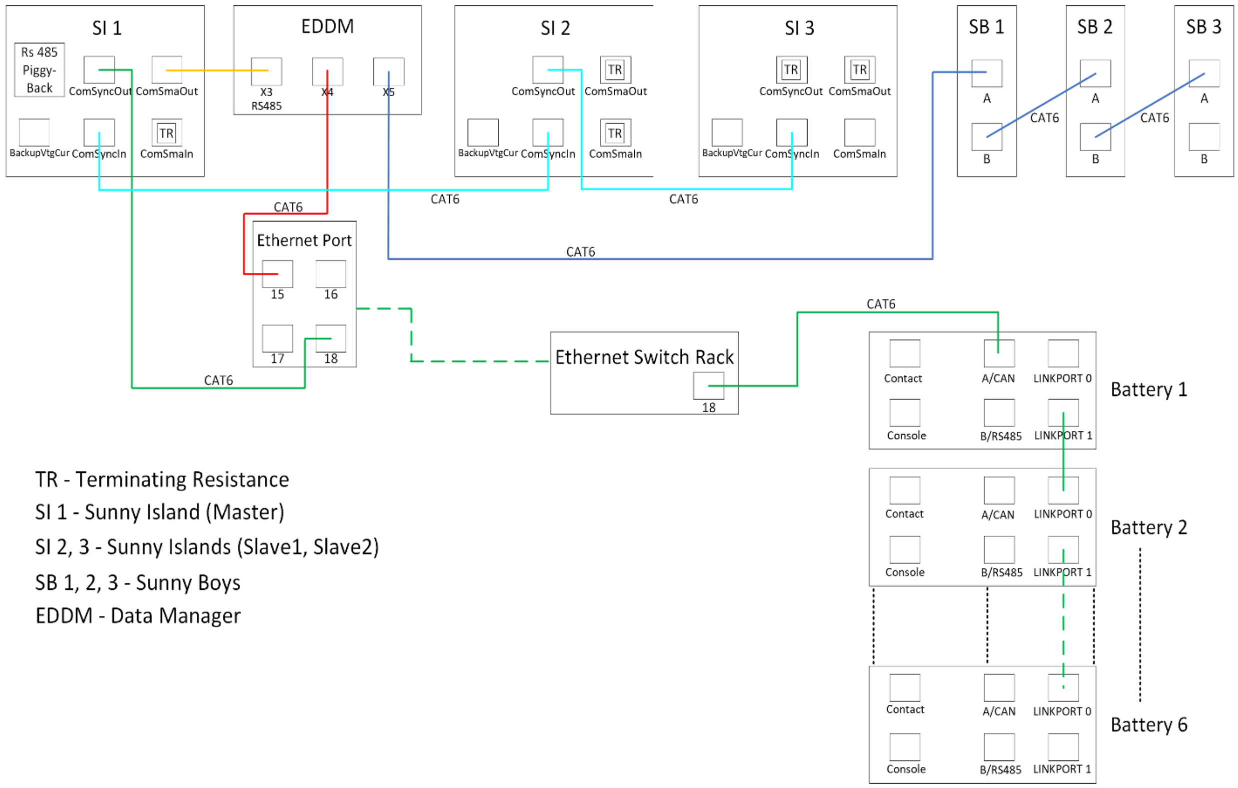

Figure 2.4 Communication Network of the SMA converters

2.4 Modes of Operation

The working mode of these inverters varies depending on the conditions. Conditions such as grid power, house battery state of charges, power generation from solar modules, and power consumed by the house loads at a particular time will decide the mode of the inverters and the power flow in the system. The different scenarios are discussed below.

2.4.1 When the Grid is ON, and the battery is not fully charged

In this case, two sub-conditions arise depending on the house's power consumption.

a) Solar modules are producing less power than the required house load power:

The power from the grid will be used to charge the battery through the Sunny Islands. In this case, the Sunny Islands work as a battery charger. The house loads will be fed from the grid and solar power. The Sunny Boys will work as grid-following inverters; they supply power to the house loads on the grid voltage and frequency of that moment, as shown in Figure 2.5.

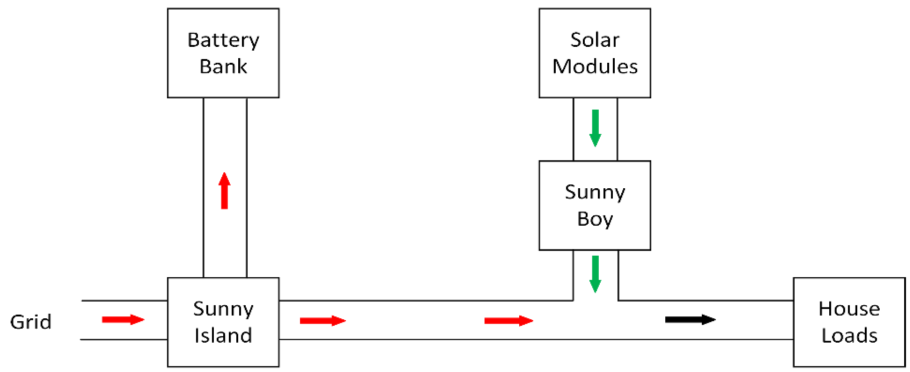

Figure 2.5 Power flow mode 1

b) Solar modules are producing more power than the required house load power:

Solar modules satisfy the power requirement of the house loads and generate excess power, which is used for charging the battery system. At that time, no power is taken from the grid, as shown in Figure 2.6.

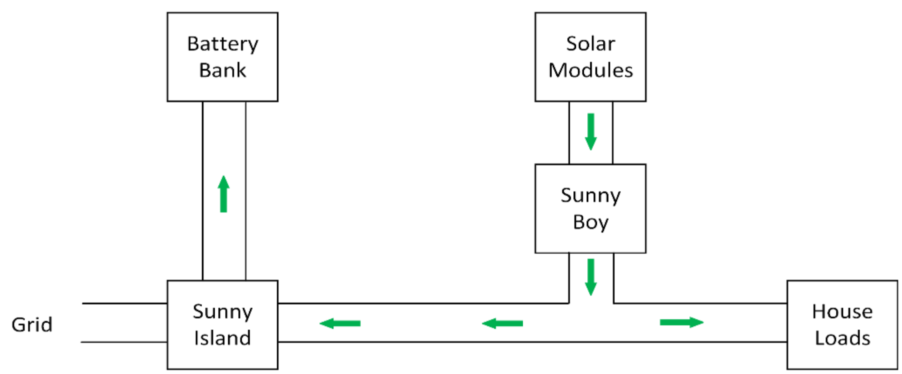

Figure 2.6 Power flow mode 2

2.4.2 When the Grid is ON and the battery is fully charged

Same as the above two conditions. There are two modes depending on the power consumption habit of the house loads.

a) Solar modules are producing less power than the required house loads:

As the battery is fully charged, the power from the grid bypasses the sunny island and gives power to the house loads. Also, the power generated from the solar modules will contribute to house loads. As shown in Figure 2.7.

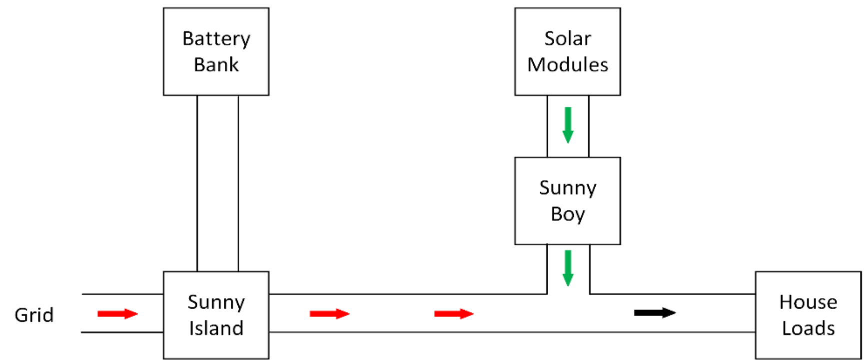

Figure 2.7 Power flow mode 3

b) Solar modules are producing more power than the required house load power:

In this case, the excess power generated by the solar modules will be injected into the grid when the battery is fully charged, as shown in Figure 2.8.

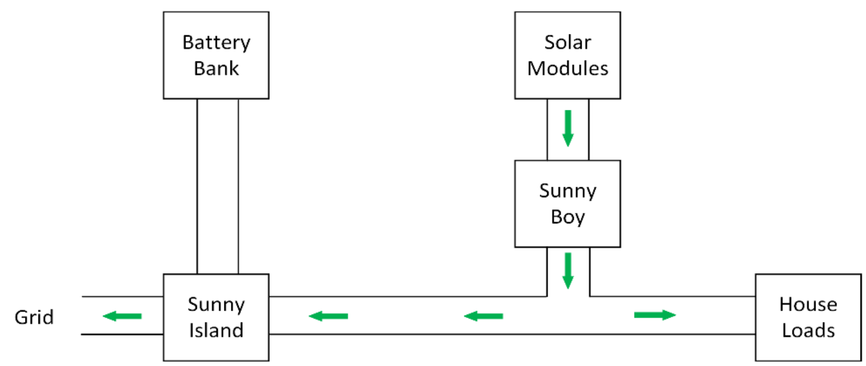

Figure 2.8 Power flow mode 4

2.4.3 When Grid is OFF

Here, two scenarios will also occur based on solar power generation.

a) Solar modules are producing less power than the required house load power:

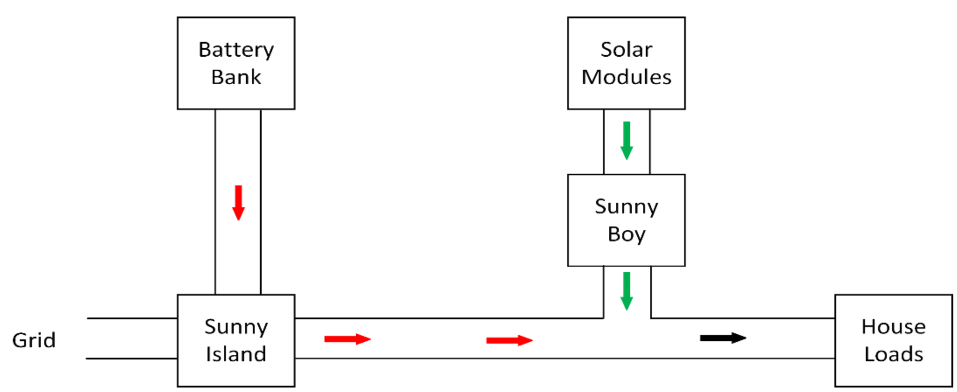

Figure 2.9 Power flow mode 5

In this case, the Sunny Island uses the battery power to create a grid-like voltage and frequency. The Sunny Boy follows the created voltage and frequency to inject solar power into the PCC to feed the house loads, as shown in Figure 2.9.

b) Solar modules are producing more power than the required house load power:

As shown in Figure 2.10, the Sunny Islands will use the excessive power generated by solar panels to charge the battery bank.

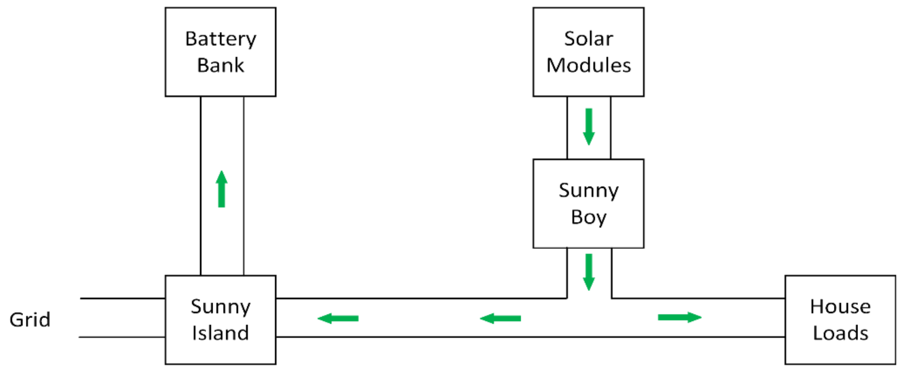

Figure 2.10 Power flow mode 6

3 Modelling and Simulation of Converters

3.1 Introduction

In this chapter, the Sunny Island (Grid Forming) and Sunny Boy (Grid Following) converters are simulated separately first, then together in an off-grid condition.

3.2 Grid Forming Converter (Sunny Island)

Currently, most inverters in engineering use a grid-following inverter control architecture, employing vector current control to manage the output current [25]. Traditionally, synchronous generators provide the voltage needed by inverters. However, with more new energy generation devices connecting to the grid via converters, the proportion of synchronous generators is decreasing, weakening the grid's strength [26]. Grid-forming inverters are seen as a key solution for power grids with a high proportion of power electronics penetration [27-28]. Grid-forming inverters can independently generate AC output voltage, allowing them to operate in isolation or on weak grids, offering a significant advantage in power systems [29].

3.2.1 Investigation of the internal hardware of Sunny Island

For a clear understanding of the topology of the grid-forming converter to form a model, internal hardware and component investigation is necessary. Figure 3.1 shows the inside of the Sunny Island converter.

Sunny Island uses 32 MOSFETs in the H-bridge; each eight MOSFETs are connected in parallel to form one switch. The switching frequency is found by measuring the output voltage from the H-bridge using an oscilloscope. The results are shown in Figure 3.2. From Figure 3.2, the converter uses a unipolar PWM scheme. The time period (ts) is found to be 100 µs, as illustrated in Figure 3.3. Hence, the switching frequency of the Mosfets in the H-bridge is 10 kHz. The DC side of the H-bridge has a total capacitor value of 48.6 mF.

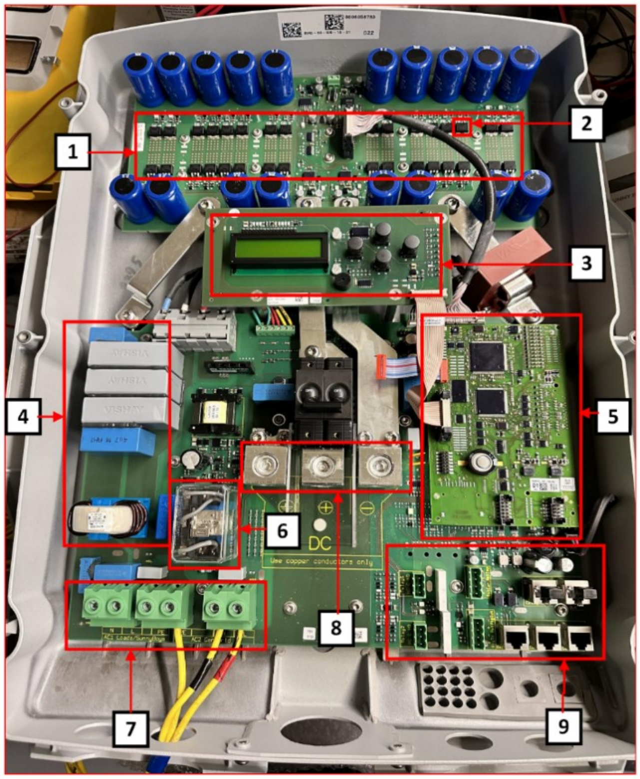

Figure 3.1 Sunny Island Converter: 1) H-bridge converter, 2) MOSFET (Infineon-IRF2907Z), 3) Display and parameter setting buttons, 4) Filter Components, 5) Controller and Processor Unit, 6) Relay, 7) AC Terminals: Load side and Grid side, 8) DC Terminals, 9) Communication Unit

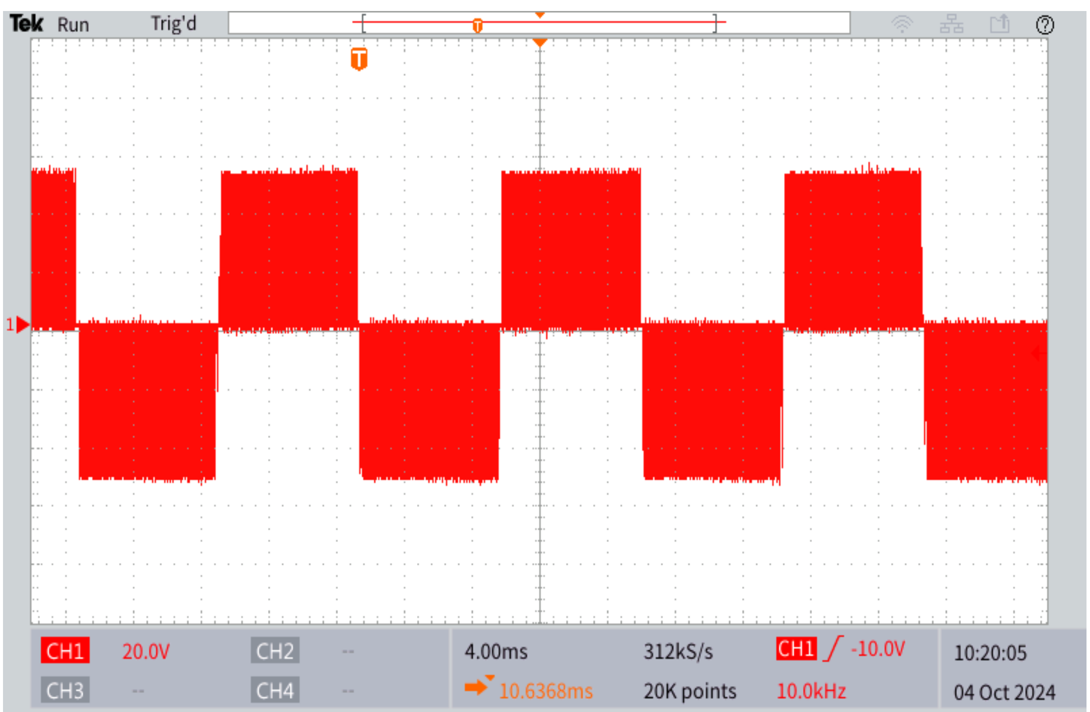

Figure 3.2 Sunny Island H-bridge output voltage waveform (4 ms/div)

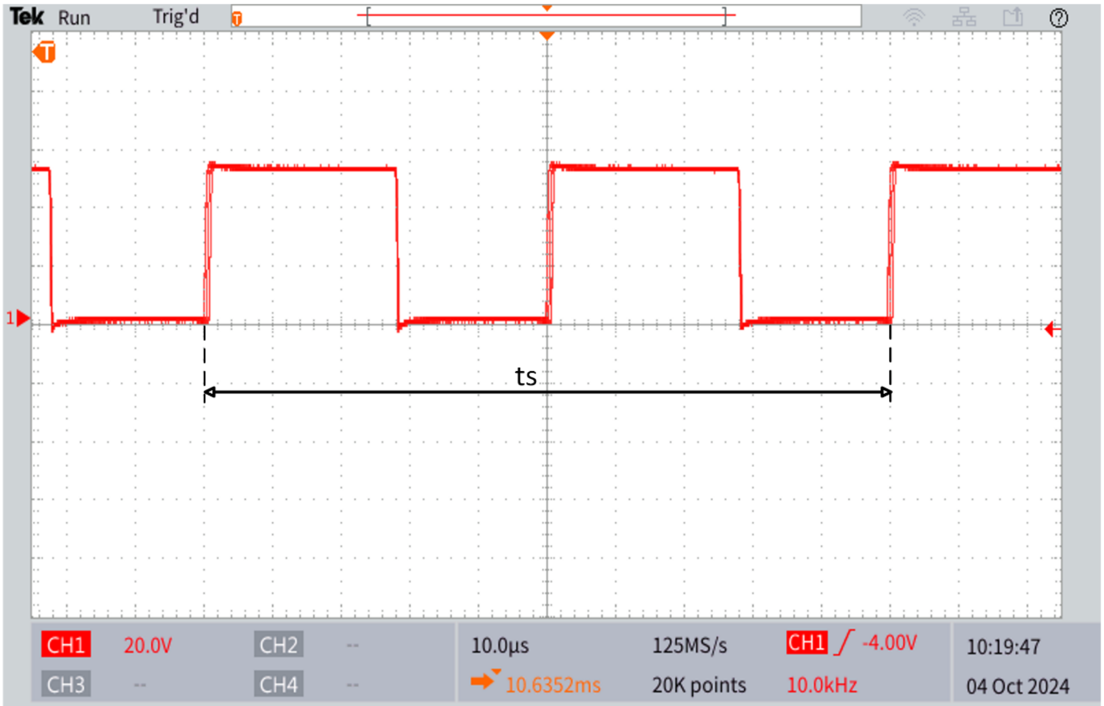

Figure 3.3 Sunny Island H-bridge output voltage waveform (10 µs/div)

A transformer is used after the H-bridge to boost the AC voltage. The transformer is installed on the back side of the Sunny Island. Figure 3.4 shows the transformer removed from the Sunny Island. A relay is connected between the AC1 (Sunny Boy/Load) and AC2 (Grid). This relay is connected as a safety device for islanding mode. Apart from the mentioned components, there are voltage sensors, current sensors, fans for cooling, and a flyback converter. The following tests are performed to obtain the parameters of the transformer.

a) Transformer Turns Ratio Test:

A transformer turns test is performed to obtain the transformer's turns ratio. Table 3.1 shows the data obtained from the transformer turns test. The approximate value of the ratio comes out to 1:4.5. If this ratio is used with a 48 V battery voltage, the maximum AC output voltage will be 145.1 V with a modulation index of 0.95. This obtained ratio is used in the simulation. Also, the label on the transformer mentions a voltage rating of 27V/120V and a power rating of 3300 VA.

Table 3.1 Transformer Turns Test

No.	LV	HV	Ratio
1	20.2	92.4	1:4.57
2	25.3	113.3	1:4.48
3	26.6	120.2	1:4.52

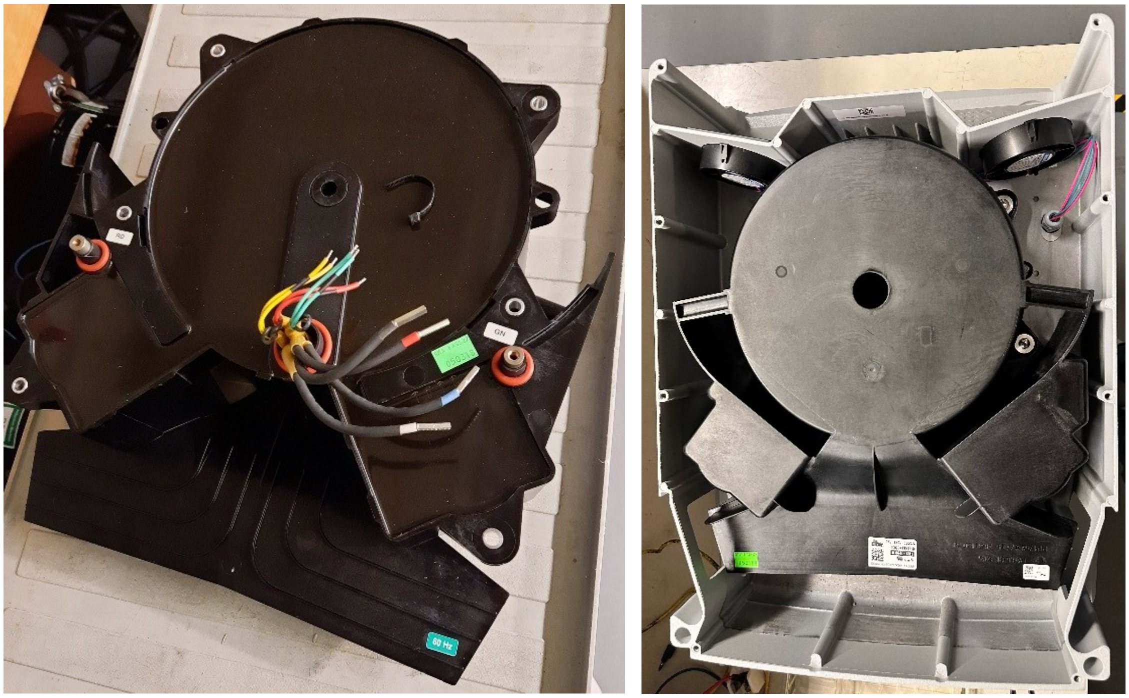

Figure 3.4 Sunny Island’s Transformer

b) Transformer Open Circuit (OC) Test:

An open circuit test is performed to obtain the transformer's no-load losses. This test gives the value of the shunt branch parameter of the transformer equivalent circuit. In the OC test, the LV (Low Voltage) side rated voltage is supplied using a variac, and the HV (High Voltage) side is kept open. Current and power are measured on the LV side winding. Figure 3.5 shows the transformer test setup. Table 3.2 represents the data obtained from the transformer OC test.

Table 3.2 Transformer Open Circuit Test

V_{oc} (Open Circuit Voltage)	I_{oc} (Open Circuit Current)	P_{oc} (no load losses)
27.3 V	0.596 A	13.75 W

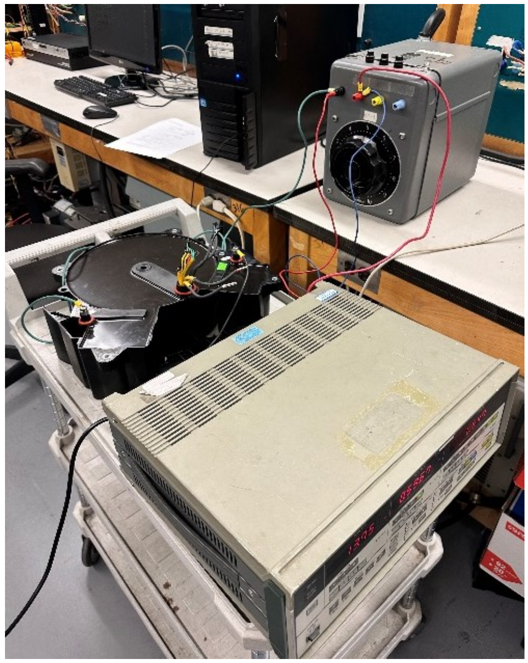

Figure 3.5 Transformer OC and SC test setup

The equivalent shunt branch parameters (R_c and L_m) on the primary side of the transformer are calculated as follows:

$$R_c = \frac{V_{oc}^2}{P_{oc}} \tag{3.1}$$

$$R_c = 54.2\ \Omega$$

$$\cos\varphi = \frac{P_{oc}}{V_{oc} \times I_{oc}} \tag{3.2}$$

$$\varphi = 32.32°$$

$$X_m = \frac{P_{oc}}{I_{oc} \times \sin\varphi} \tag{3.3}$$

$$X_m = 85.65\ \Omega$$

$$L_m = 227.25\ mH$$

c) Transformer Short Circuit (SC) Test:

A short circuit test is performed to obtain the series parameters of the transformer equivalent circuit. The LV side is short-circuited, and the rated current is applied on the HV side. The rated current is calculated from the transformer's rating of 3300 VA. The voltage on the HV side of the transformer is increased slowly to reach the full load current of 27.5 A. The measured power on the HV side is the copper loss of the transformer at full load. The readings are mentioned in Table 3.3.

Table 3.3 Transformer Short Circuit Test

V_{sc} (Short Circuit Voltage)	I_{sc} (Short Circuit Current)	P_{sc} (Full load losses)
16.56 V	27.9 A	159.6 W

$$R_{02} = \frac{P_{sc}}{I_{sc}^2} \tag{3.4}$$

$$R_{02} = 0.205\ \Omega$$

$$Z_{02} = \frac{V_{sc}}{I_{sc}} \tag{3.5}$$

$$Z_{02} = 0.5935\ \Omega$$

$$X_{02} = 0.557\ \Omega$$

$$L_{02} = 1.48\ mH$$

3.2.2 Circuit Design

For the inverter mode of operation, the power is fed from the battery. The DC voltage of 48 V from the battery is converted into 120 V AC. The H-bridge converter is used for the voltage conversion from DC to AC. The voltage obtained from the H-bridge is of a lower magnitude. So, to step up the voltage, a transformer is connected. The design of the topology is such that it can work in both directions. The power is controlled by the controller. Finally, a filter is used to attenuate the unwanted harmonics. L and R2 are the equivalent inductance and resistance of the transformer and filter. A simplified circuit diagram is shown in Figure 3.6.

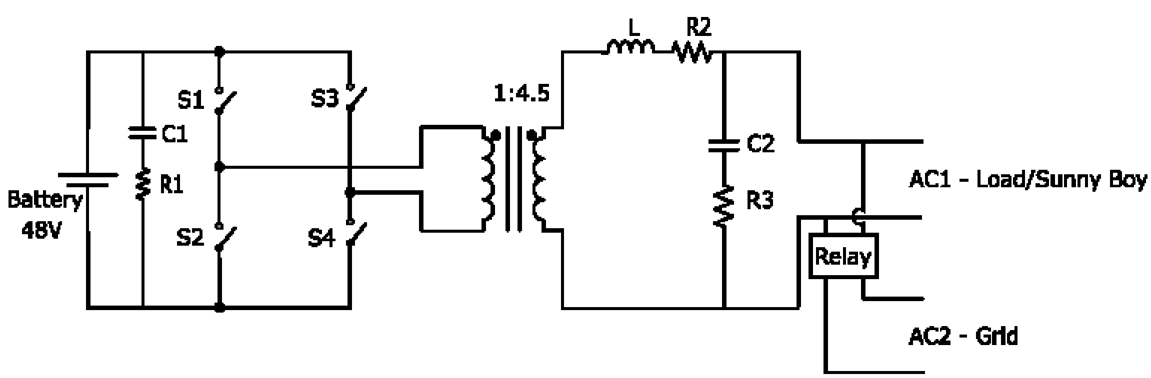

Figure 3.6 Simplified Circuit Diagram of Sunny Island

3.2.3 Controller Design

The AC output voltage from Sunny Island is 120 V. The H-bridge's output voltage is controlled to a desired value so that the transformer then steps up the voltage to 120 V. A closed-loop voltage control is used to control the inverter's output voltage at the desired value. The loop has a PI controller and a unipolar SPWM scheme circuit. The carrier frequency of the SPWM is 10 kHz. The reference triangular signal is 10 kHz. A dead time of 1 µs is assumed to avoid a short circuit in the leg of the H-bridge. The closed loop controller maintains the output AC voltage constant even if the battery voltage and loads change. The chosen values for the PI controller of the AC output voltage are presented in Table 3.4. Kp is the proportional gain, and Ki is an integral gain of the PI controller.

Table 3.4 PI Controller Parameter

K_p	3
K_i	40

3.2.4 Filter Design

Consider a 5% voltage drop in the design of the LC filter inductor. The Sunny Island converter is rated at 5.75 kW.

V=120 V RMS, 60 Hz

I = 48 A RMS

$$Vd = 2\pi f * L * I \tag{3.6}$$

$$L \cong 0.33\ mH$$

From the investigation of the Sunny Island converter, it is found that the transformer used in the converter has an equivalent inductance of 1.48 mH on the HV side. The measured equivalent resistor of the transformer on the HV side is 0.205 Ω. It is also considered in the simulation. The transformer's inductance is considered when calculating the filter capacitance.

L_f=0.33mH + 1.48mH = 1.81mH

$$f_c = \frac{1}{2\pi\sqrt{L_f C_f}} \tag{3.6}$$

$$f_c \leq \frac{f_s}{10}, \qquad f_s = 10\ kHz, \qquad f_c \leq 1\ kHz$$

The cut-off frequency found from the measured value of capacitor and inductor is 722.65 Hz.

$$C_f = 26.8\ \mu F$$

The measured value of Sunny Island's filter capacitance is 25.8 µF. The selected values of the filter for simulation are shown in Table 3.5.

Table 3.5 Sunny Island Filter Parameter

	Calculated	Measured	Simulation
L_f	1.81 mH	1.88 mH	1.88 mH
C_f	26.8 µF	25.8 µF	25 µF

3.2.5 Simulation

Figure 3.7 shows the simulation circuit with the controller. The turn's ratio and shunt parameter of the transformer are considered in the simulation. Table 3.6 shows the battery parameters selected for the simulation. In simulation, the load side of the converter is connected to a resistive load of 10 Ω. The converter is loaded for 1200 W which is 20.86 % loading of the inverter.

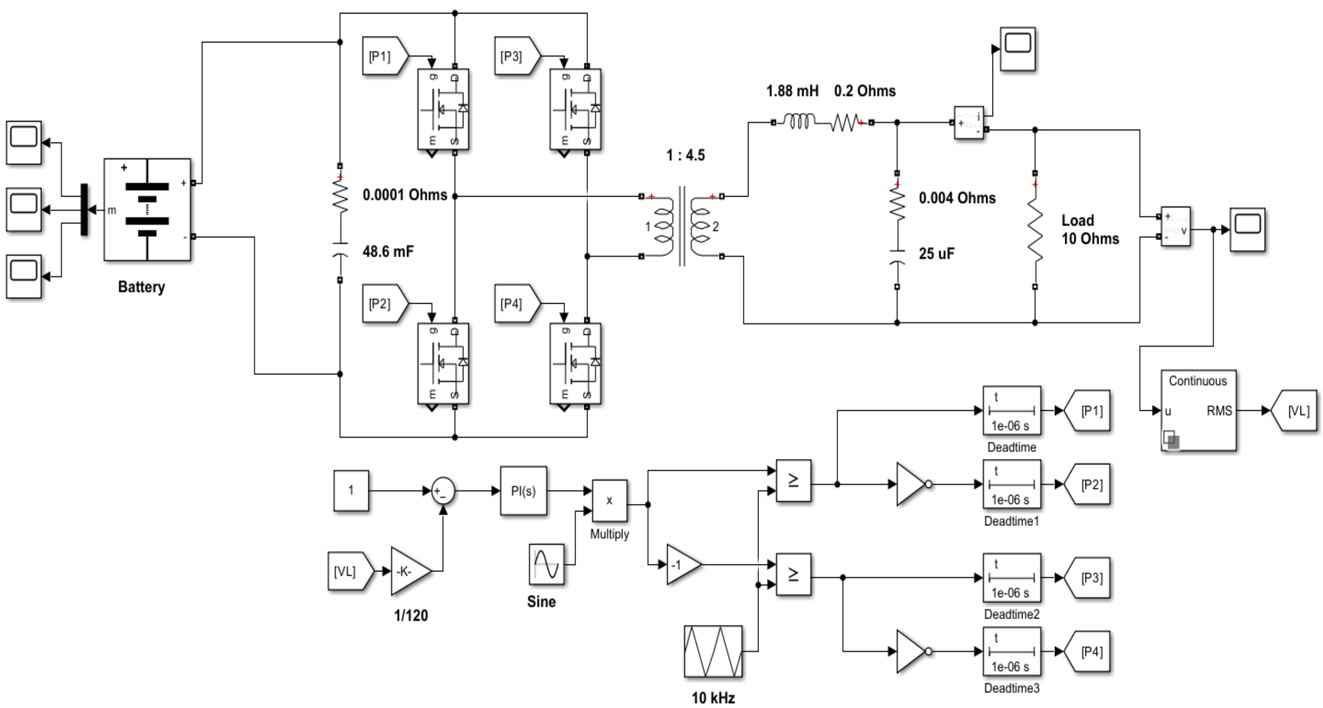

Figure 3.7 Grid Forming converter with PI controller for voltage control in Simulink

Table 3.6 Battery Parameters in Simulation

Nominal Voltage V	48 V
Ah	74 Ah
SOC	80%
Fully Charged Voltage V	55.87 V

3.2.6 Results

The simulation results in the time domain are shown in Figures 3.8 and 3.9.

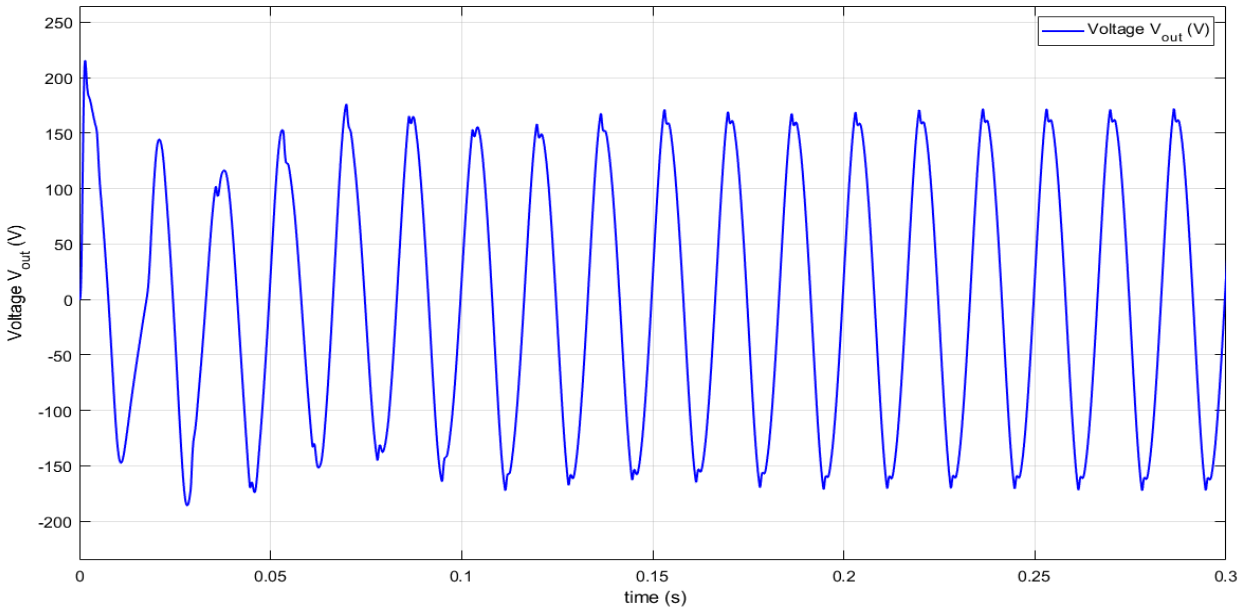

Figure 3.8 Simulation result of the grid-forming converter; output voltage (time segment: 0 - 0.3s)

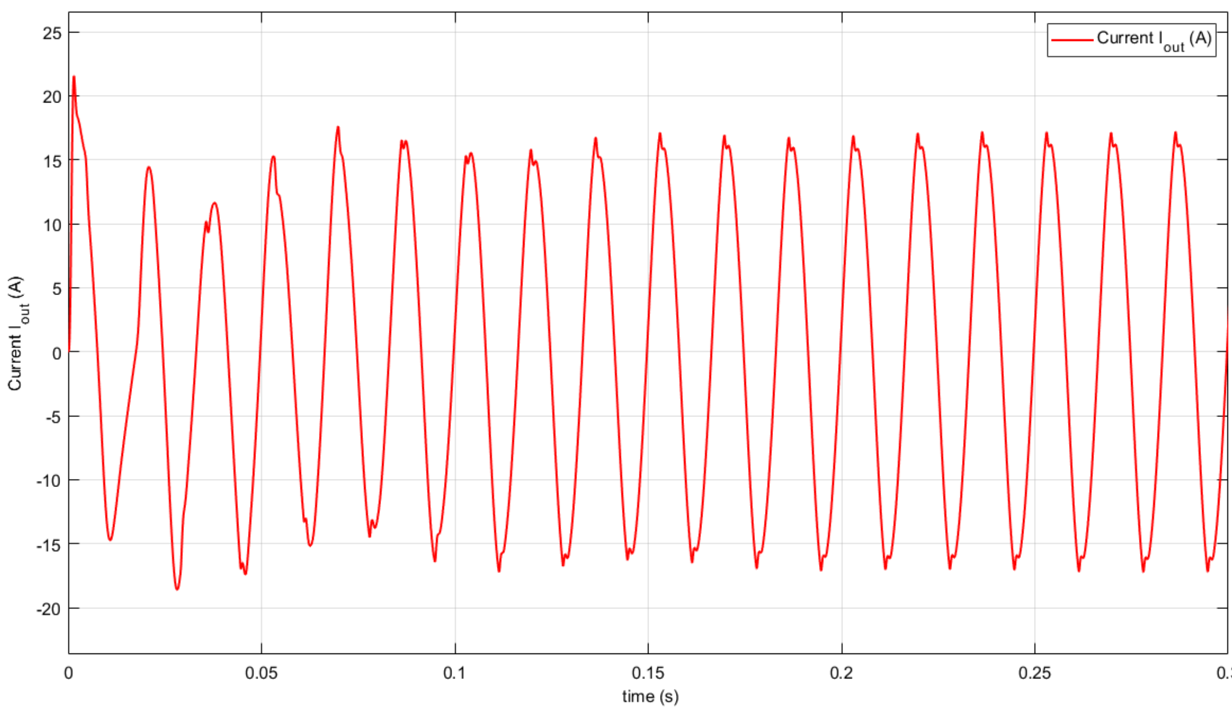

Figure 3.9 Simulation result of the grid-forming converter; output current (time segment: 0 - 0.3s)

Figures 3.8 and 3.9 show that the output voltage and current take 0.2 - 0.25s to reach a steady state.

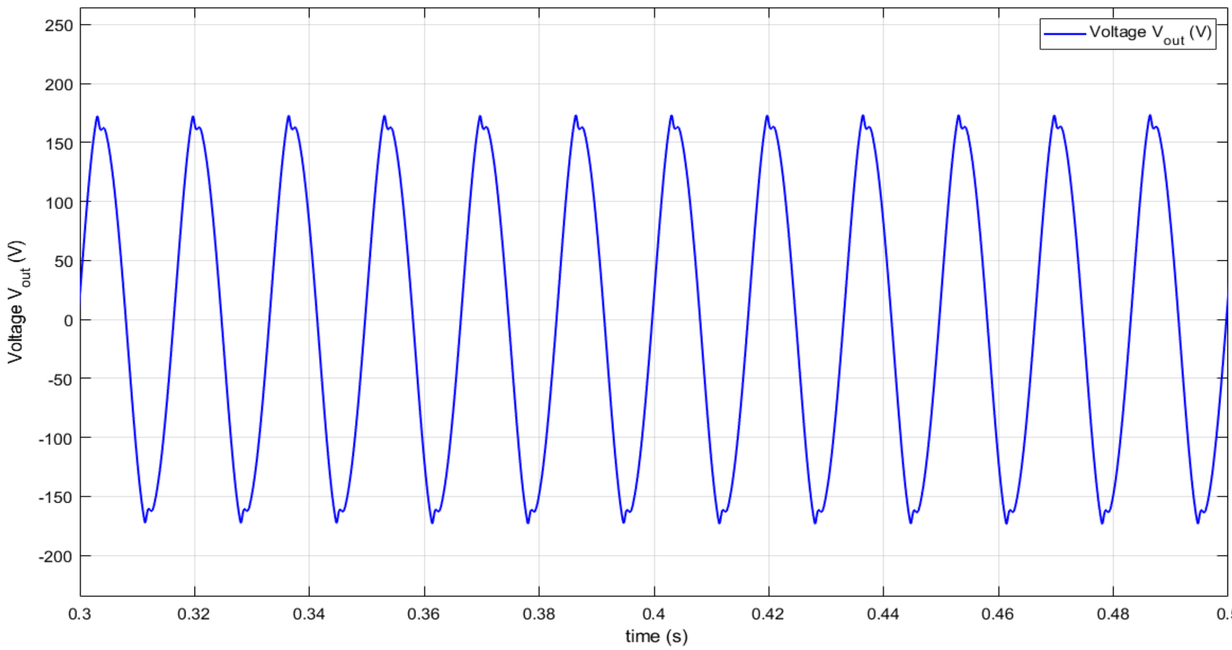

Figure 3.10 Simulation result of the grid-forming converter; the output voltage. (time segment: 0.3 - 0.5s)

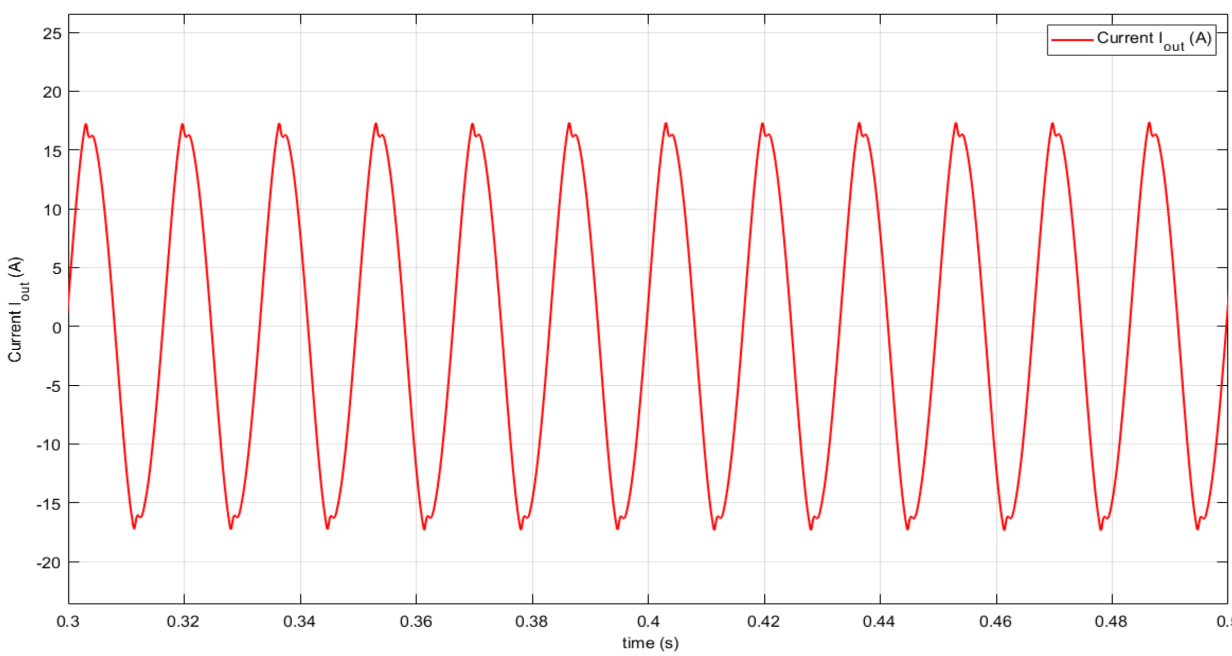

Figure 3.11 Simulation result of the grid-forming converter; the output current. (time segment: 0.3-0.5s)

Figure 3.10 shows a sinusoidal voltage waveform and the RMS value of voltage is 119.9 V. The current drown by the 10 Ω loads is 11.99 A RMS as depicted in Figure 3.11.

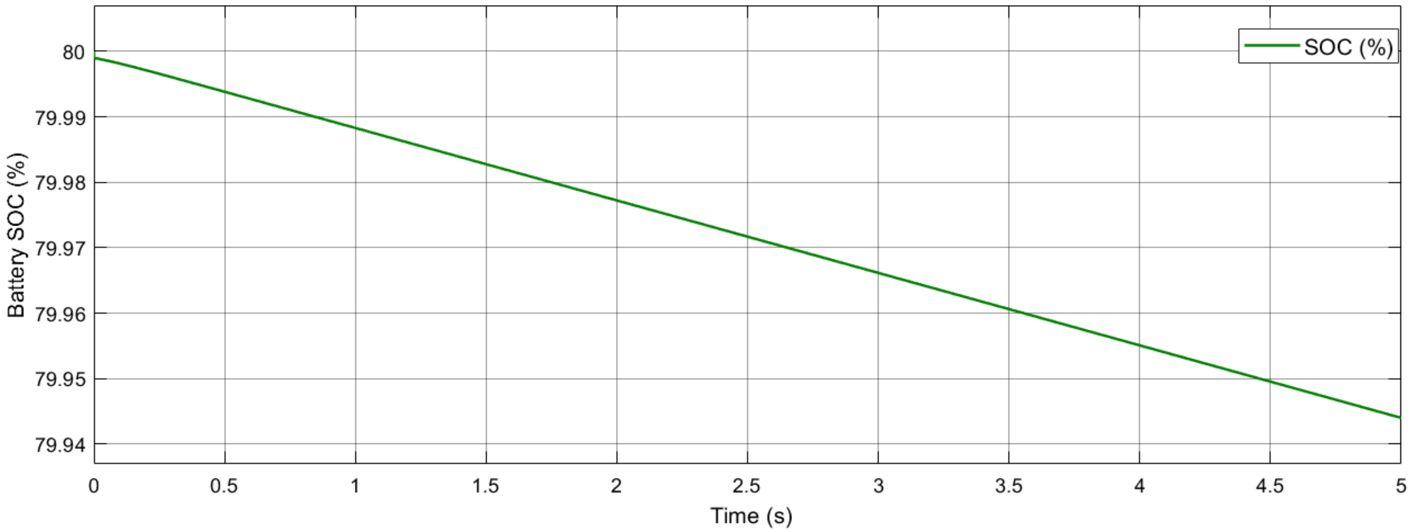

Figure 3.12 Simulation result of the grid-forming converter; the state of the charge (SOC) of the battery in the first 5 seconds of simulation. A decreasing SOC is observed

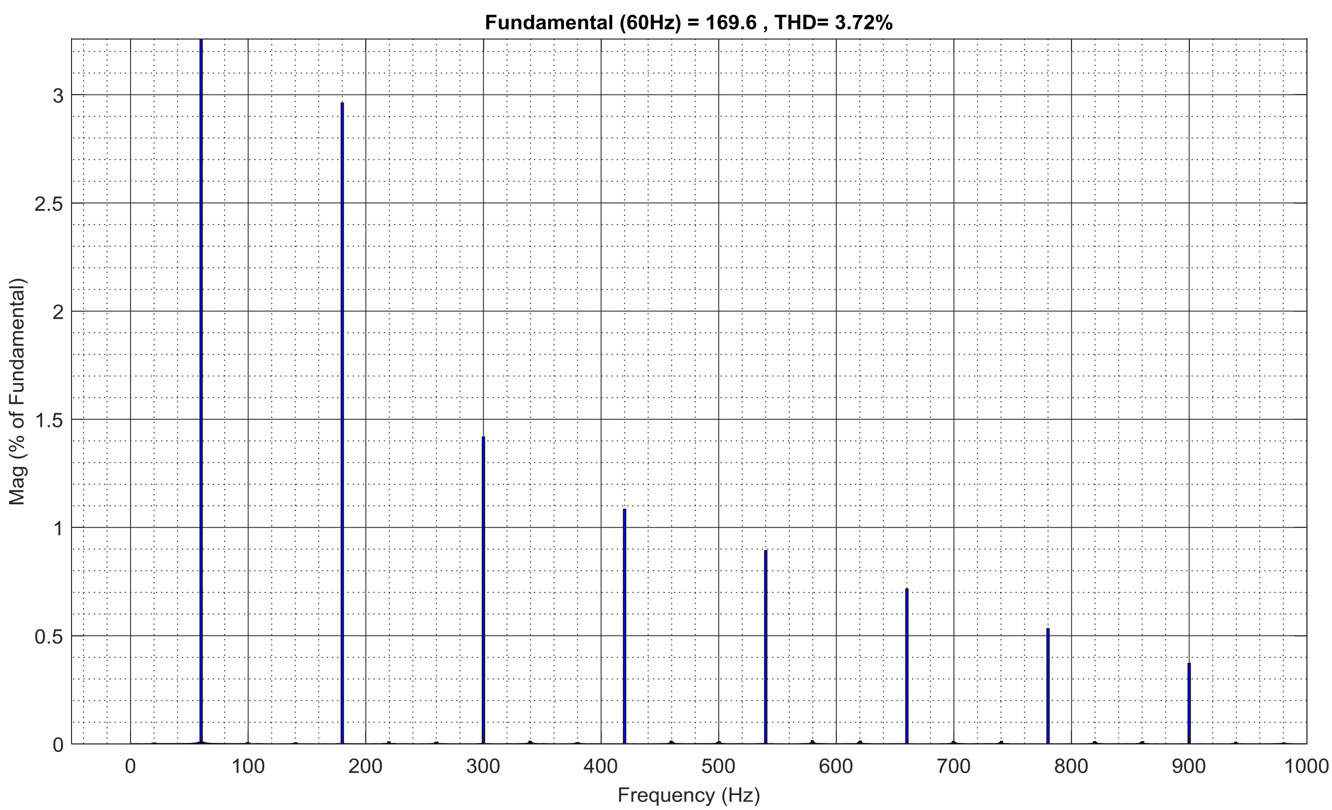

Figure 3.13 FFT analysis of the output voltage of the grid-forming converter.

A FFT analysis of the voltage and current are shown in Figures 3.13 and 3.14. The dominant odd harmonics 3rd, 5th, 7th, 9th , etc are present. The THD of voltage and current waveform is 3.72%.

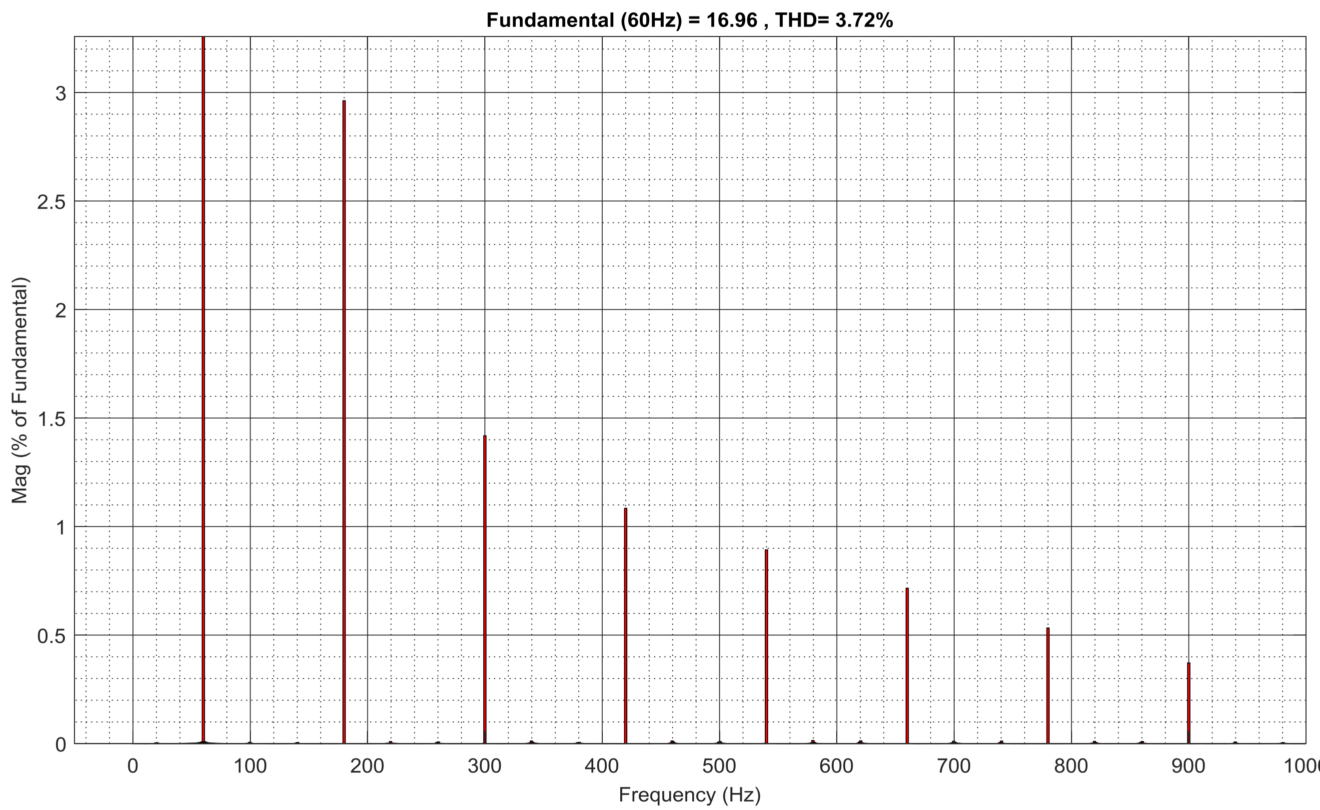

Figure 3.14 FFT analysis of the output current of the grid-forming converter.

3.3 Grid Following Inverter (Sunny Boy)

The grid-following inverter is a controlled current source synchronized with the grid [30-31]. A grid or a grid-like supply is required. The grid-following inverters control the output power by measuring the angle of the grid's voltage using a phase-lock-loop (PLL) [32].

3.3.1 Circuit Design

The grid-following inverter consists of an H-bridge to convert the DC to AC and an LCL filter to attenuate the harmonics caused by the H-bridge's semiconductor devices (MOSFETs). The circuit diagram of the grid-following inverter is shown in Figure 3.15.

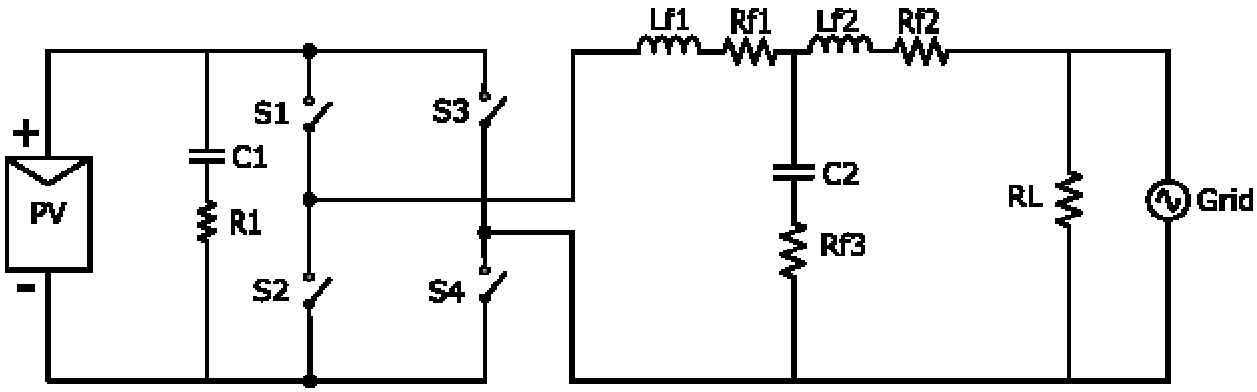

Figure 3.15 Circuit diagram of the grid-following (Sunny Boy) Inverter

3.3.2 Controller Design

The control circuit of the grid-following inverter is shown in Figure 3.16. An orthogonal signal generator (OSG) converts the inverter feedback current to alpha-beta axes. I_{d_ref} and I_{q_ref} are the reference currents for controlling the active power and reactive power, respectively [33]. A phase Lock Loop (PLL) block is used to obtain the phase of the grid voltage. This phase from the PLL is used for the axes transformation. V_{dff} and the V_{qff} are the feed-forward terms [34]. Generally, when the inverter is connected to the grid, the reference current I_{d_ref} comes from the maximum

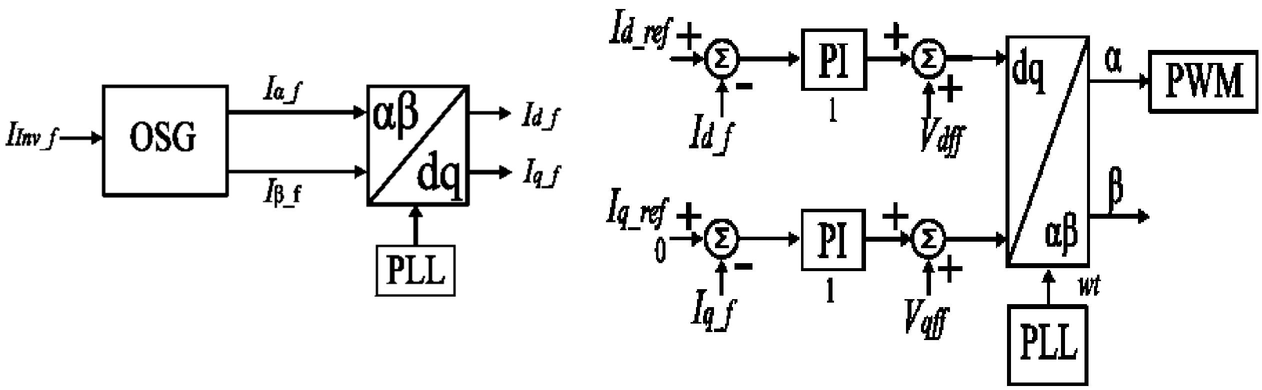

Figure 3.16 Grid Following Inverter Control Circuit

power point tracking (MPPT) block, as shown in Figure 3.17. However, during the off-grid conditions, the current is controlled based on the load requirement. The current control loop has a PI controller and a unipolar SPWM scheme circuit. The carrier frequency of the SPWM is 10 kHz. A dead time of 1 μs is assumed for the simulation.

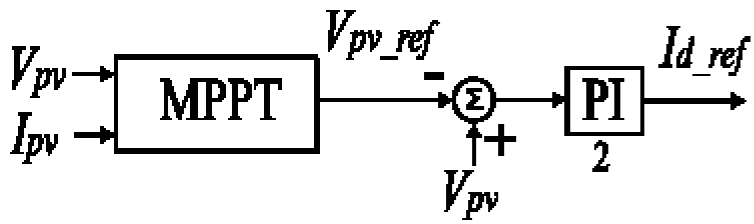

Figure 3.17 Id_ref generated from the MPPT block using a PI controller

3.3.3 MPPT

The perturbation and observation MPPT algorithm is commonly used in many PV systems [35-36]. In simulation, the MPPT block is written in a MATLAB function block and follows the algorithm shown in Figure 3.18.

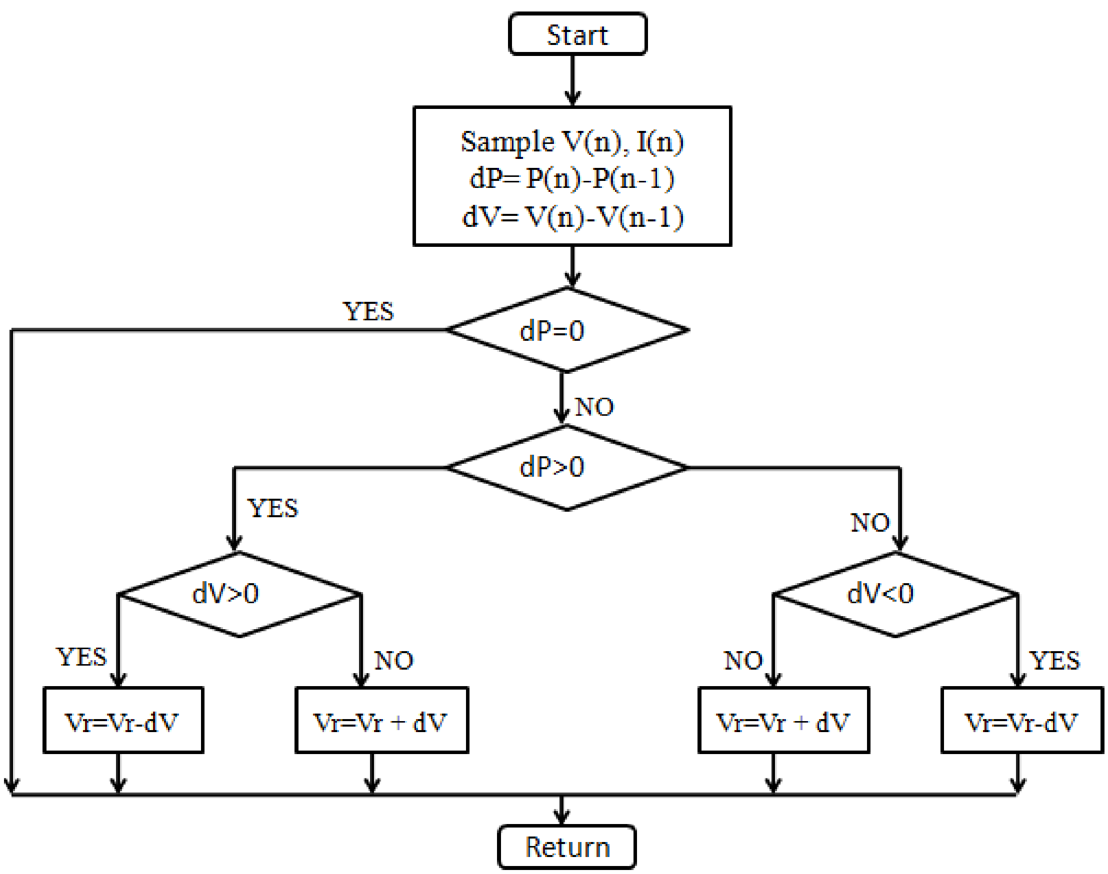

Figure 3.18 Flowchart of the P&O MPPT algorithm [37]

3.3.4 Filter Design

As shown in Figure 3.19, LCL filters are commonly used in grid tie inverter applications. When designing the filter capacitor, 5% of the total power is considered a reactive power requirement. The Sunny Boy inverter's total power rating is 7800 W.

$$Q_c = V^2 \omega_o C_{max} \tag{3.7}$$

$$C_{max} \cong 72\ \mu F$$

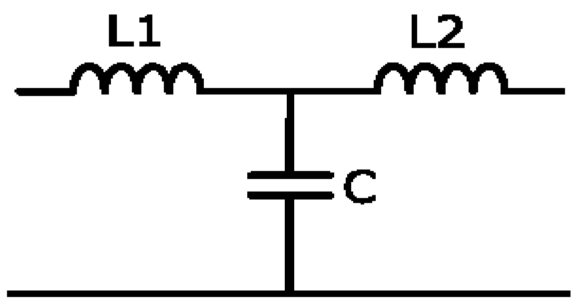

Figure 3.19 LCL Filter

For the inductor design, considering a voltage drop of 5%,

$$I = \frac{P}{V} = \frac{7800}{120} = 65\ A$$

$$V_L = X_L * \mathrm{I} \tag{3.8}$$

$$L \cong 0.25\ mH$$

The total value of the inductor is obtained; it is divided into two equal parts for the LCL filter. For the lowest current ripple, the values of L1 and L2 are the same.

$$L1 = L2 = 125\ \mu H$$

Table 3.7 Filter Parameter

	Calculated	Simulation
L1, L2	125 µH	125 µH
C	72 µF	25 µF

The calculated value of the capacitor (72 µF) is the maximum value. In simulation, the used capacitor value is 25 µF.

3.3.5 Simulation

Case I: Sunny Boy inverter supplying power to the grid

The simulated system is shown in Figure 3.20. In this simulation, the grid-following inverter is connected to a PV module on the DC side, and the AC side is connected to the grid. The specification of the PV module selected is given in Table 3.8. In a string, a total of 10 modules are connected in series. Sun irradiance and cell temperature are kept at 1000 W/m^2 and 25℃. The current and voltage controller values are mentioned in Table 3.9. The q-axis (reactive current component) reference current is kept at zero in the simulation, so the output power from the inverter is purely active. The GFL inverter is simulated at 43% power capacity.

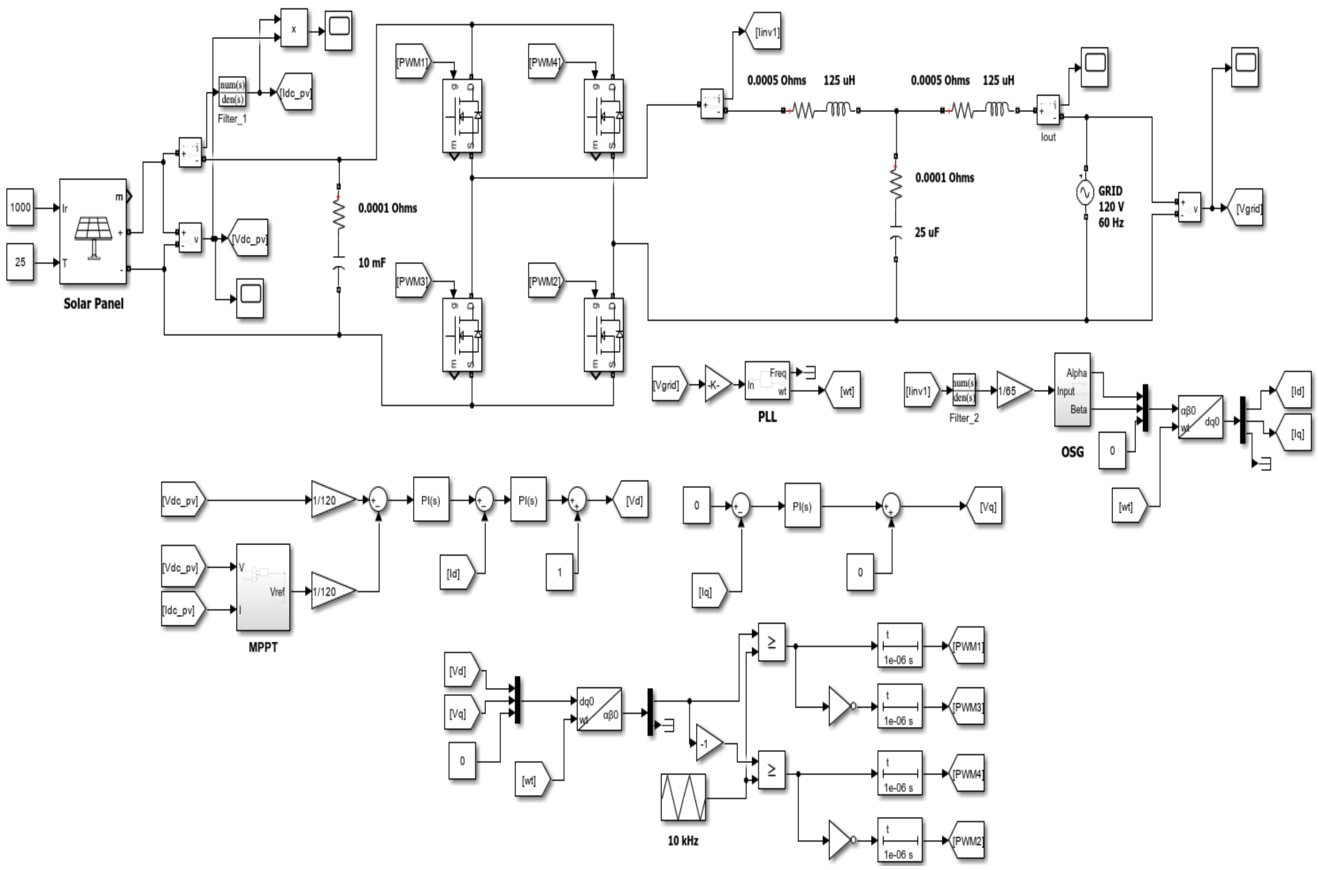

Figure 3.20 Grid-following inverter feeding grid system in Simulink

Table 3.8 Specifications of a PV module

Open-Circuit Voltage V_{oc}	51.5 V
Short-Circuit Current I_{sc}	9.4 A
Voltage at maximum power point V_{mp}	430 V
Current at maximum power point I_{mp}	8.13 A

Table 3.9 PI Controller Parameter

Current Controller PI (PI-1)	K_p	8
	K_i	200
Voltage Controller PI (PI-2)	K_p	-0.01
	K_i	10

Case II: Sunny Boy inverter supplying power to the grid and 1.5 kW load

In this simulation, all parameters of the above simulation are kept the same, and a 1.5 kW (9.6 Ω) load is added, as illustrated in Figure 3.21. The PV power feeds the load and the extra PV power is fed back to the grid.

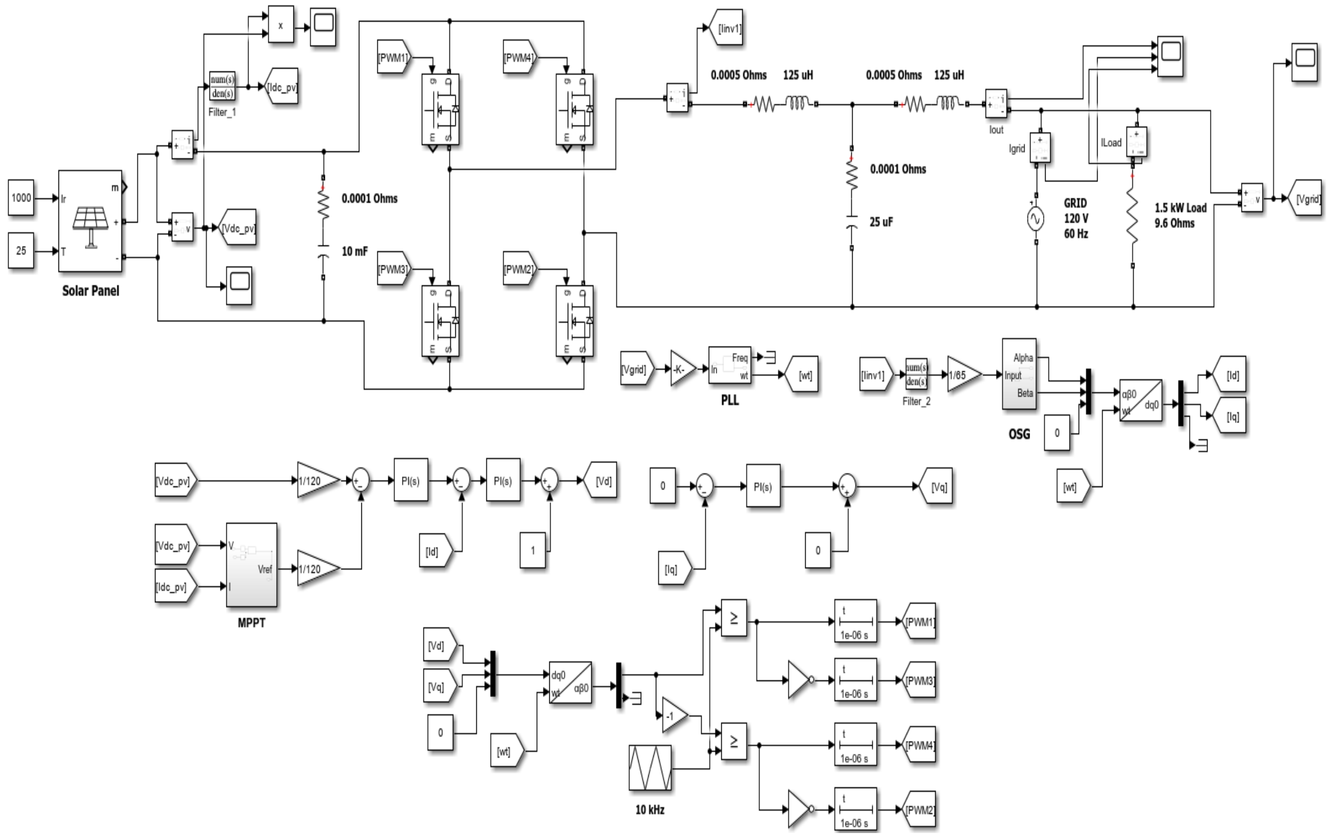

Figure 3.21 Grid-following inverter feeding grid and load system in Simulink

3.3.6 Results

Case I: Sunny Boy inverter supplying power to the grid

The results of the simulation are shown in Figures 3.22 to 3.25.

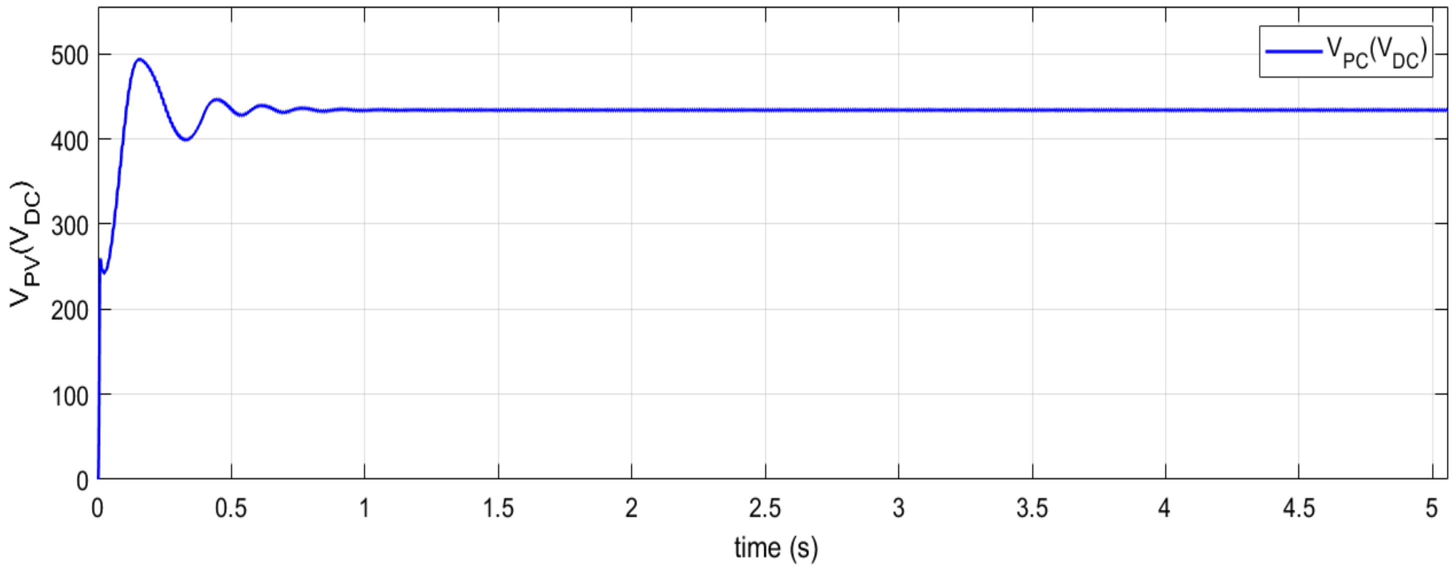

Figure 3.22 Simulation results for the grid-following inverter; the input DC voltage from the PV.

Figure 3.22 shows that the DC voltage achieves a maximum power point (MPP) voltage of 434.3 V at the steady state. Figure 3.23 also shows the inverter reaches the maximum power point (MPP) in less than one second.

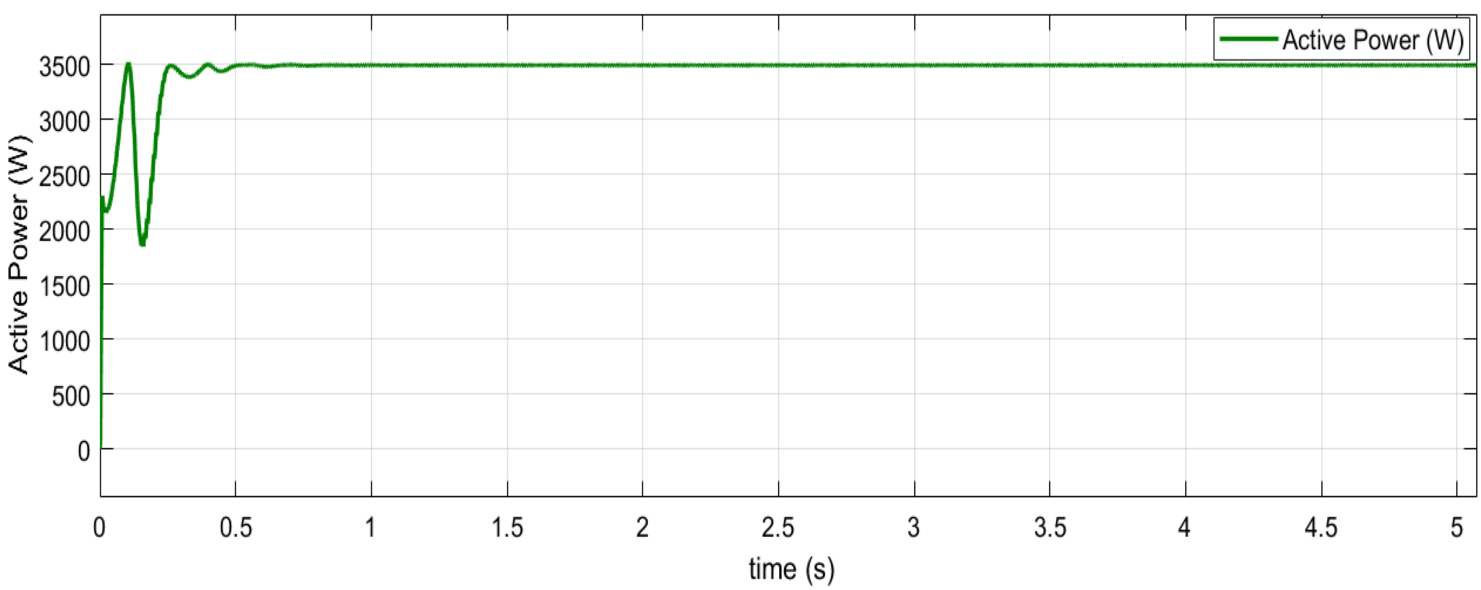

Figure 3.23 Simulation results for the grid-following inverter; the PV power.

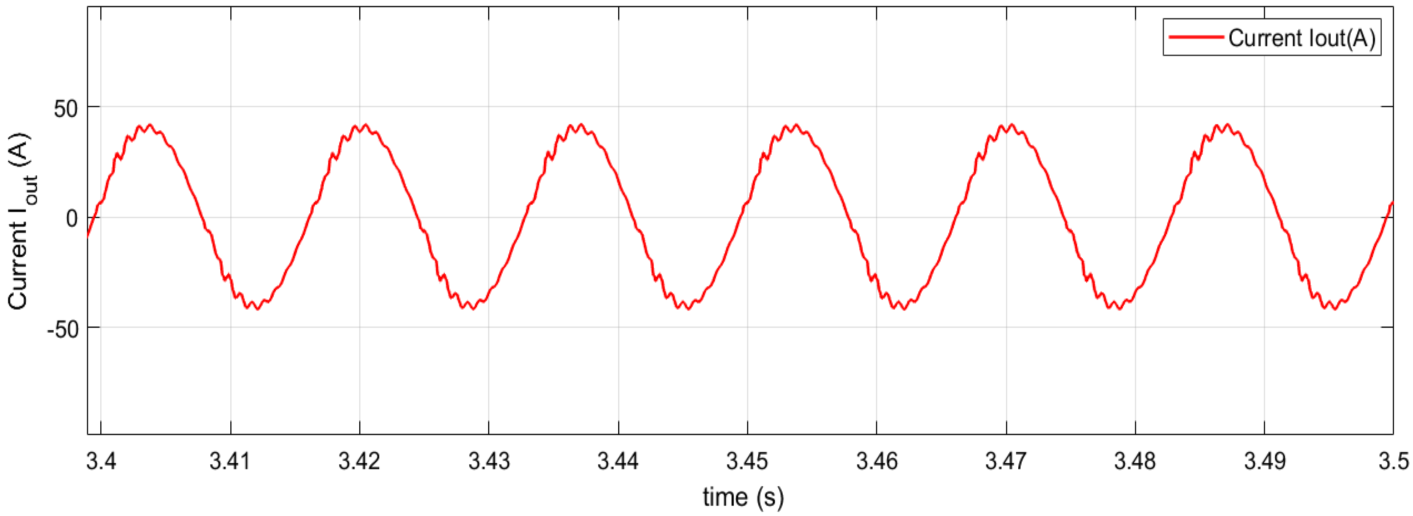

Figure 3.24 Simulation results for the grid-following inverter; the inverter output current.

The output current waveform is sinusoidal with some ripple at the peaks, as illustrated in Figure 3.24. The injected current into the grid is 28.6 A RMS.

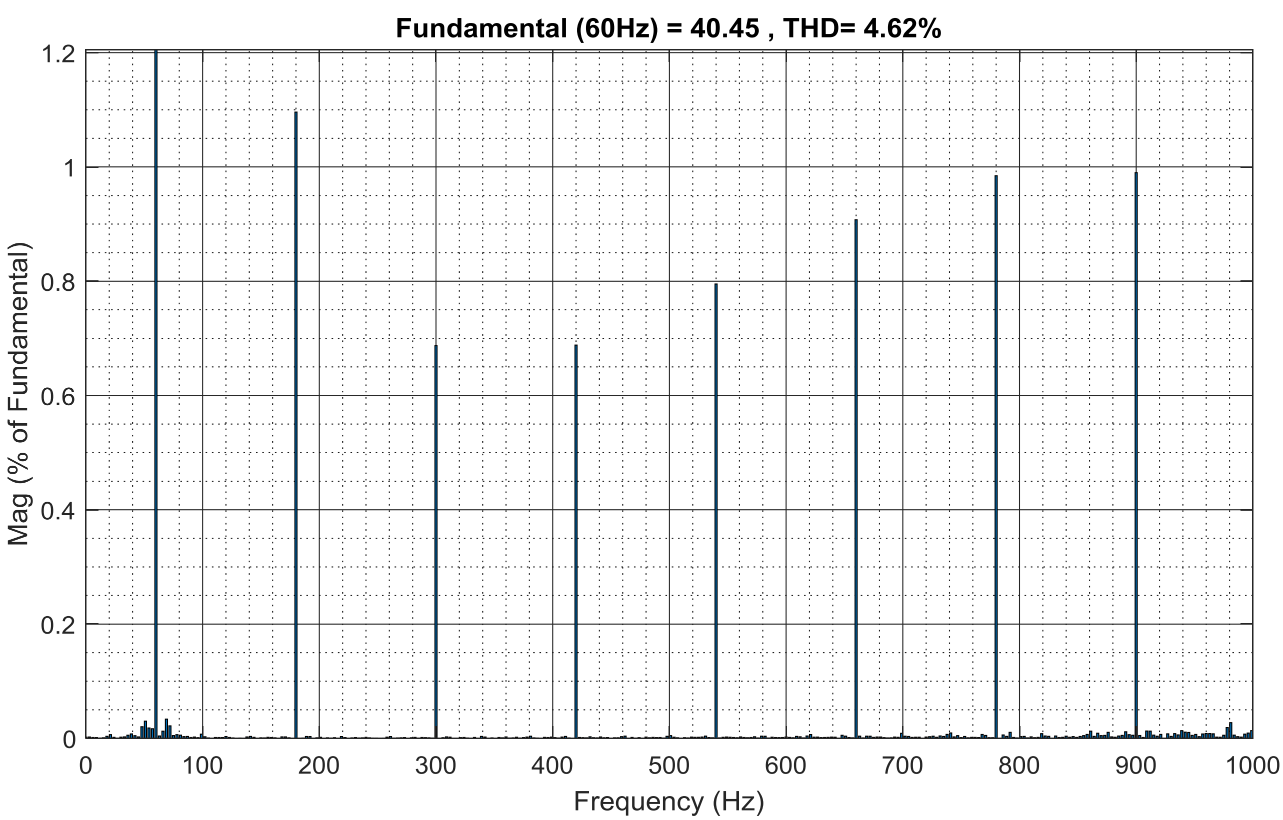

Figure 3.25 FFT analysis of grid following inverter output current

The FFT analysis of the current waveform is shown in the Figure 3.25. The dominant odd harmonics are present in the analysis. Total harmonic distortion (THD) of the output current of the grid following inverter is 4.62%.

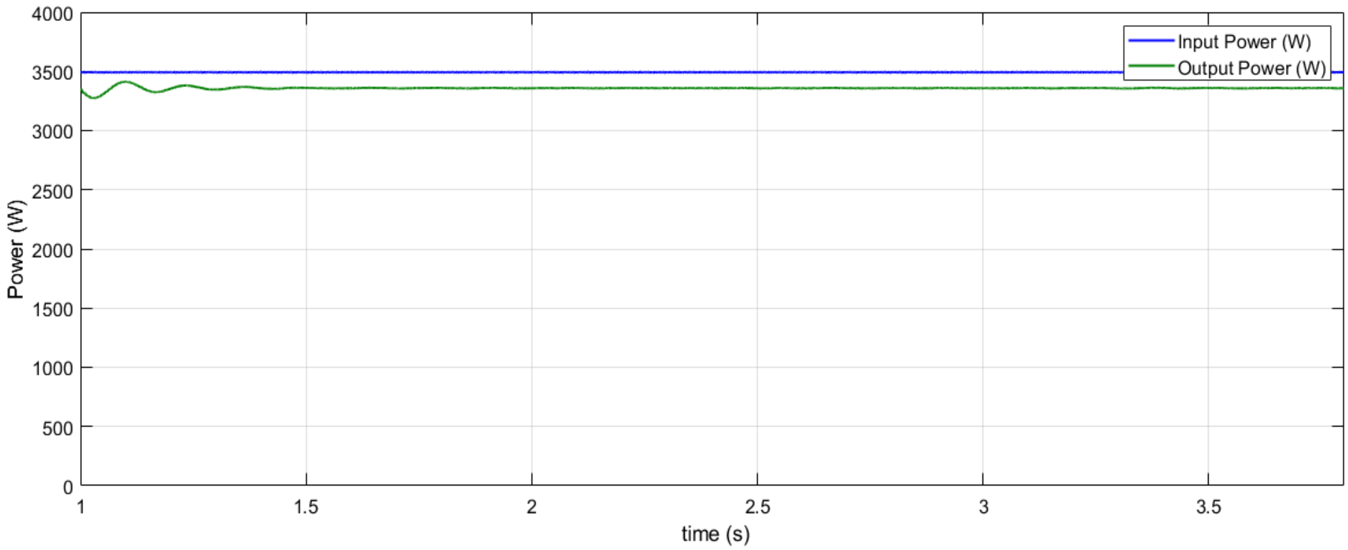

Figure 3.26 Simulation results for the grid-following inverter: the blue trace is the DC input power of the PV panels, and the green trace is the AC output power of the inverter.

From Figure 3.26, the inverter's output power is 3360 W, and its input power is 3493 W. Thus, the inverter's efficiency is 96.2 %.

Case II: Sunny Boy inverter supplying power to the grid and 1.5 kW load

The output current waveform of the Sunny Boy inverter, the load current, and the grid current are shown in Figure 3.27. The RMS values of these three currents are 28.59 A, 12.5 A, and 16.53 A, respectively.

Figure 3.28 shows the power generated by the Sunny Boy inverter, the power consumed by the load, and the power fed back to the grid. The values are 3360 W, 1500 W, and 1859 W, respectively. The solar power satisfies the load requirement, and the excess power is fed back to the grid.

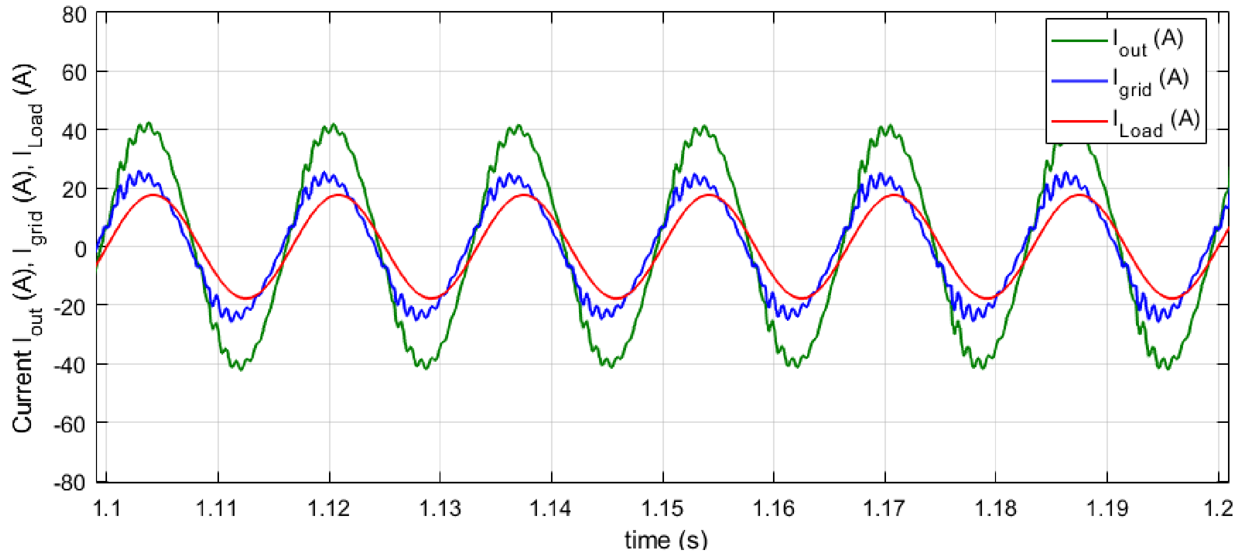

Figure 3.27 Steady-state simulation results for the grid-following inverter feeding the load and the grid: currents.

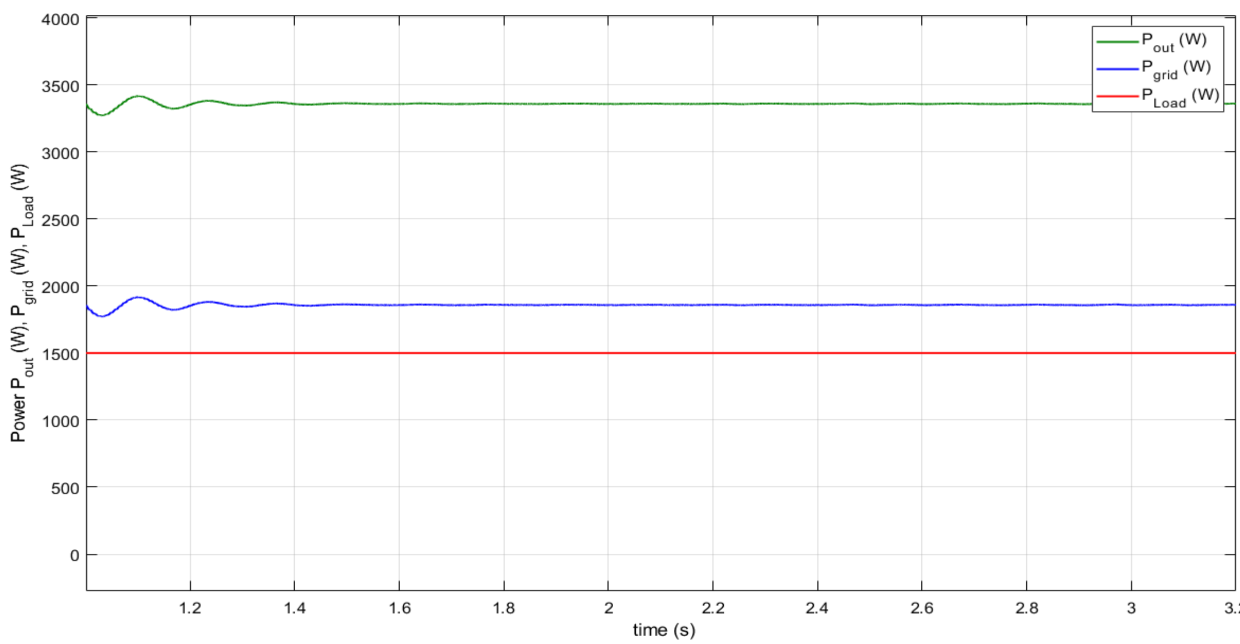

Figure 3.28 Steady-state simulation results for the grid-following inverter feeding the load and the grid: powers.

3.4 Integrated System

The integrated system consists of grid-forming (GFM) and grid-following (GFL) converters connected in parallel. The simulation mainly focuses on the off-grid condition when there is excessive solar power generation. In [38], [39], and [40], different control strategies of the GFM and GFL inverters are mentioned. Reference [39] uses a frequency droop to control the power of the GFM inverter. Reference [40] divides the controlled voltage between the GFL and the GFM inverters. Reference [41] discusses various control techniques for power synchronization, along with the issues of angle and current stability. Reference [42] shows the adjustment of active and reactive powers of the GFL inverter using the measured frequency and voltage magnitudes.

3.4.1 Controller Design

In the proposed strategy, the power demand is first detected using a frequency droop. After that, the current is controlled so that the maximum power is generated by the GFL inverter first, and then the power from the GFM converter is used if the load demand is greater than the solar-generated power. This way, the maximum solar power is utilized. The controllers of the GFM and GFL inverters are updated to work in off-grid conditions.

3.4.1.1. Updated GFM Converter Controller

The controller shown in Figure 3.29 focuses on the inverter mode during off-grid conditions. P_m is the active power of Sunny Island converter (GFM). The “f” block in the controller decides the operating frequency of the GFM converter in an off-grid condition based on the value of P_m. Figure 3.30 shows the flowchart of the “f” block. In the GFL inverter connected condition, the frequency is shifted so that the power of the GFL inverter is controlled using the shifted frequency.

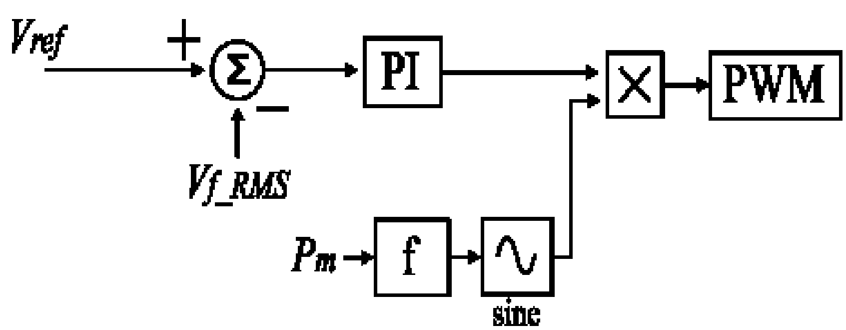

Figure 3.29 Updated controller of the GFM converter

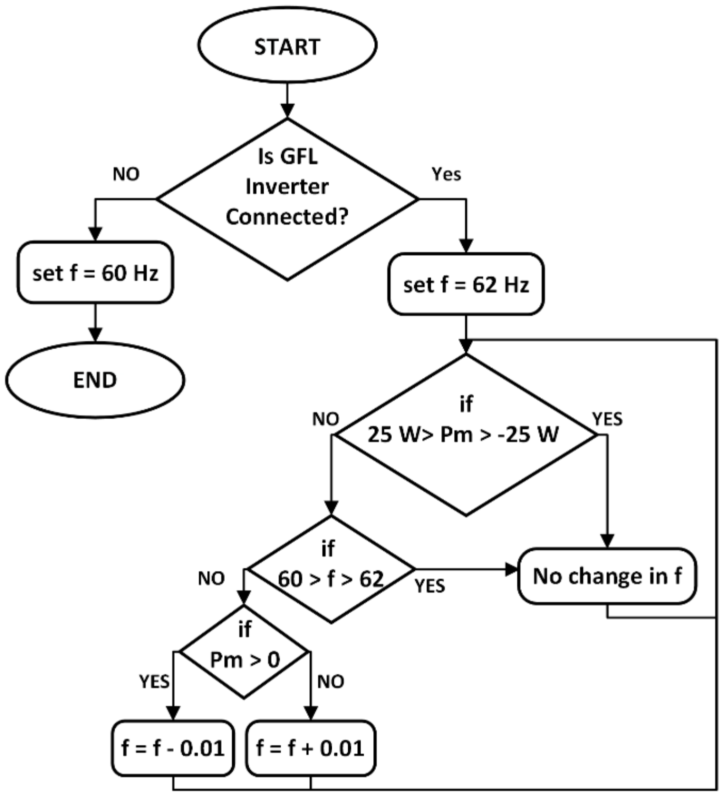

Figure 3.30 Flowchart of the "f" block of the GFM converter in off-grid conditions

3.4.1.2. Updated GFL Inverter Controller

The output power of the GFL inverter is controlled using the inverter current. When the GFL inverter is connected to the grid, it works in the MPPT condition. In off-grid conditions, when the GFL inverter is connected to the GFM converter, the output power is controlled using the frequency reference from the GFM converter. The output power control with respect to frequency is shown in Figure 3.31. The power output varies between 60 to 62 Hz. The power-varying frequency bandwidth is 2. At the startup, the GFL inverter works in MPPT mode and obtains the value of maximum power (P_{MPPT}). The slope is calculated as shown in equation 3.9.

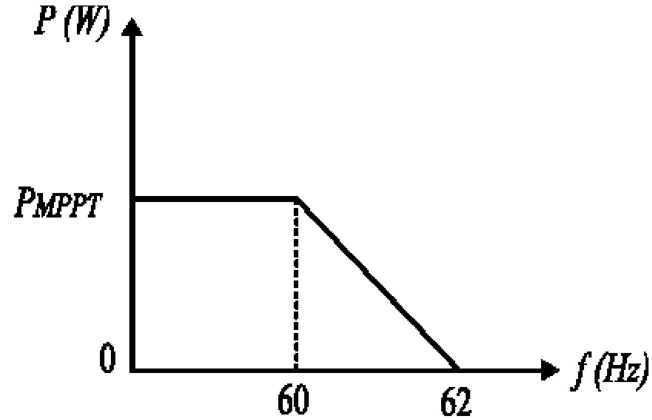

Figure 3.31 Frequency shift power curve

$$Slope\ (S) = \frac{P_{MPPT}}{2} \tag{3.9}$$

To obtain the required power from the frequency,

$$P = S * (62 - f) \tag{3.10}$$

When the frequency exceeds 62 Hz, the GFL inverter shuts down. Figure 3.32 shows the generation of the *d*-axis reference current. Initially, the switch (SW) is at S1, and the GFL inverter works in MPPT and obtains the value of maximum power (*PMPPT*). From the value of (*PMPPT*), the slope is determined using equation 3.9. The switch (SW) transfers to S2 if the GFL inverter is connected to the GFM converter. Otherwise, the switch remains on S1 if the GFL inverter is connected to the grid. The P(f) block calculates power from frequency using equation 3.10. By dividing the power by the voltage (V), the current (I) is obtained.

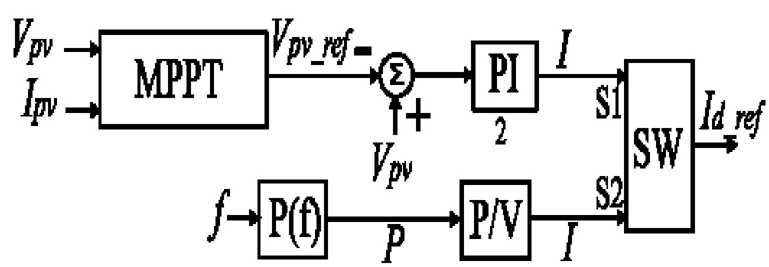

Figure 3.32 Generating d-axis reference current

3.4.2 Simulation

Case I: When load consumption is less than PV generation

GFM and GFL converters are simulated together to test the control strategy of frequency shift power control. The combined control strategy focuses mainly on the off-grid condition. In this integrated system, the GFM converter is connected to a 48 V battery, which is 100% charged, and the GFL inverter is connected to the solar panel module. The PV module's ratings are 3.49 kW, 515 V open circuit voltage, and 9.4 A short circuit current. The circuit diagram is shown in Figure 3.33. To test the frequency shift power control method, the loads are changed from 25 Ω to 40 Ω in steps of 5 Ω. To achieve this, equivalent parallel branch resistors are removed one by one (150Ω, 210 Ω, 280 Ω).

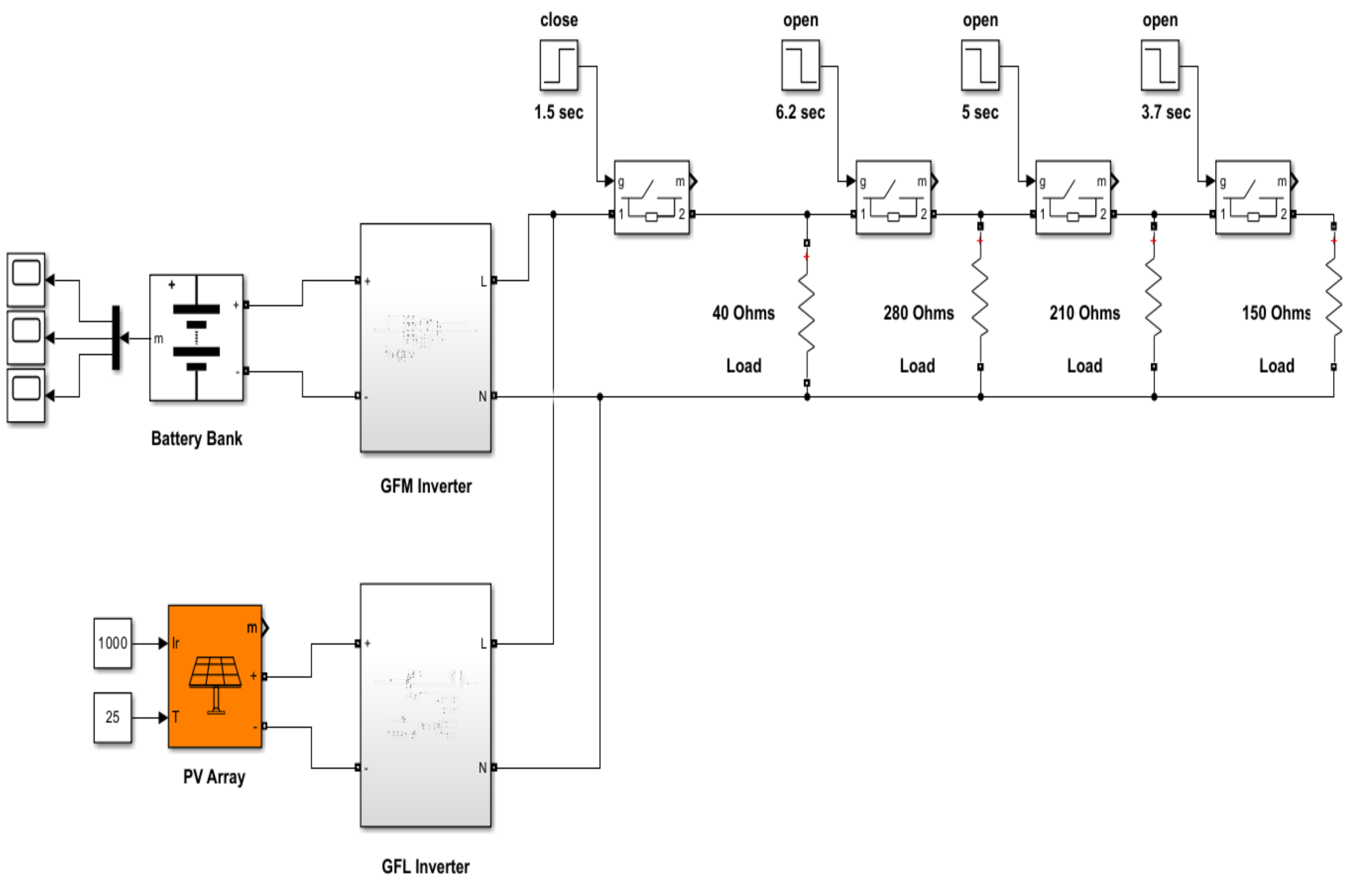

Figure 3.33 Integrated System in Simulink; load consumption is less than PV generation

Case II: When load consumption is more than PV generation

The GFM and GFL converters are simulated together to feed the 2.5 kW (5.76 Ω) resistive loads. The rated PV power is 3.49 kW, with an irradiance of 500 W/m^2 considered in the simulation. The generated PV power becomes nearly half the rated power, which is insufficient for the 2.5 kW load. In that case, the battery power contributes to feeding the load through the GFM converter. In simulation, the 2.5 kW load is connected to the system at 1.5 s. The combined system with the load is shown in Figure 3.34.

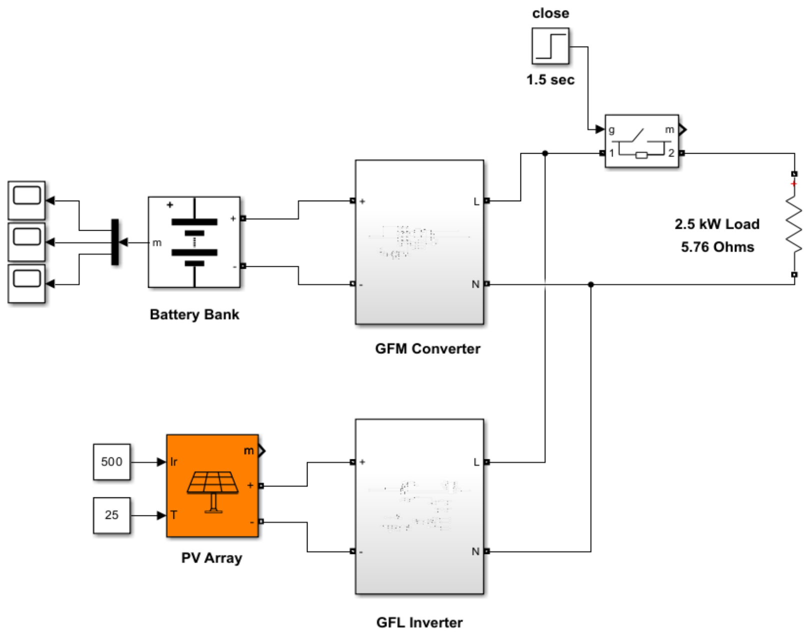

Figure 3.34 Integrated System in Simulink; load consumption is more than PV generation

3.4.3 Results

Case I: When load consumption is less than PV generation

Figures 3.35 and 3.36 show the simulated results of the integrated system. Figure 3.35 shows the power of the GFL inverters, the GFM inverter, and the load. Figure 3.36 shows that as the load decreases, the system's frequency increases, and the GFL inverter's output power decreases. The GFM converter consumes some power to charge the battery momentarily until the GFL inverter output power reaches a steady state.

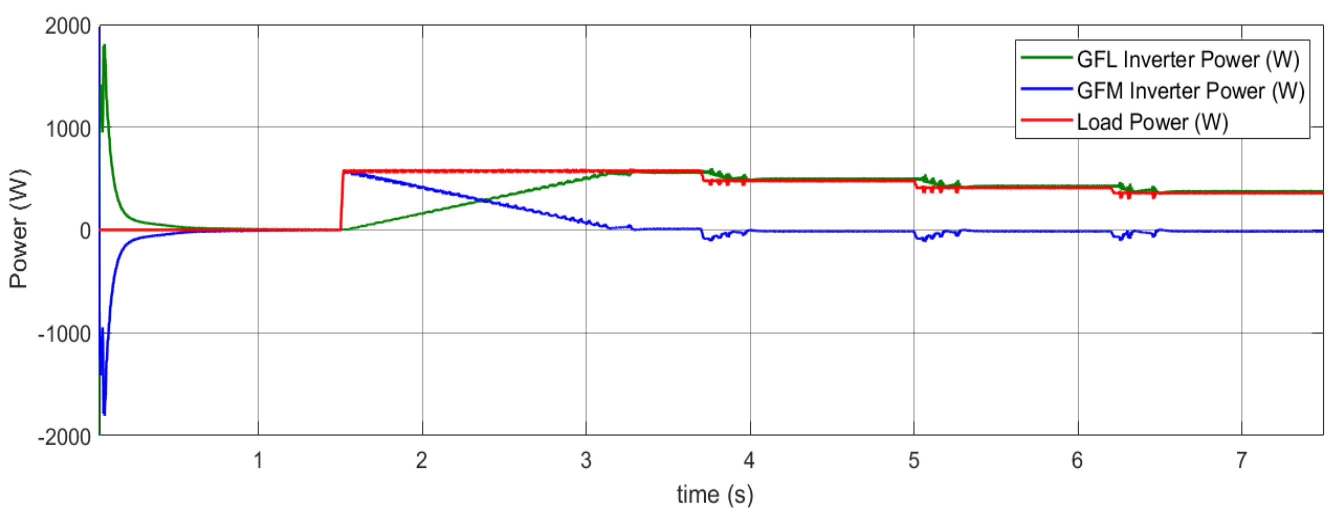

Figure 3.35 Simulation results of the integrated system; system reaches stability after 1 sec then load is applied at 1.5 sec

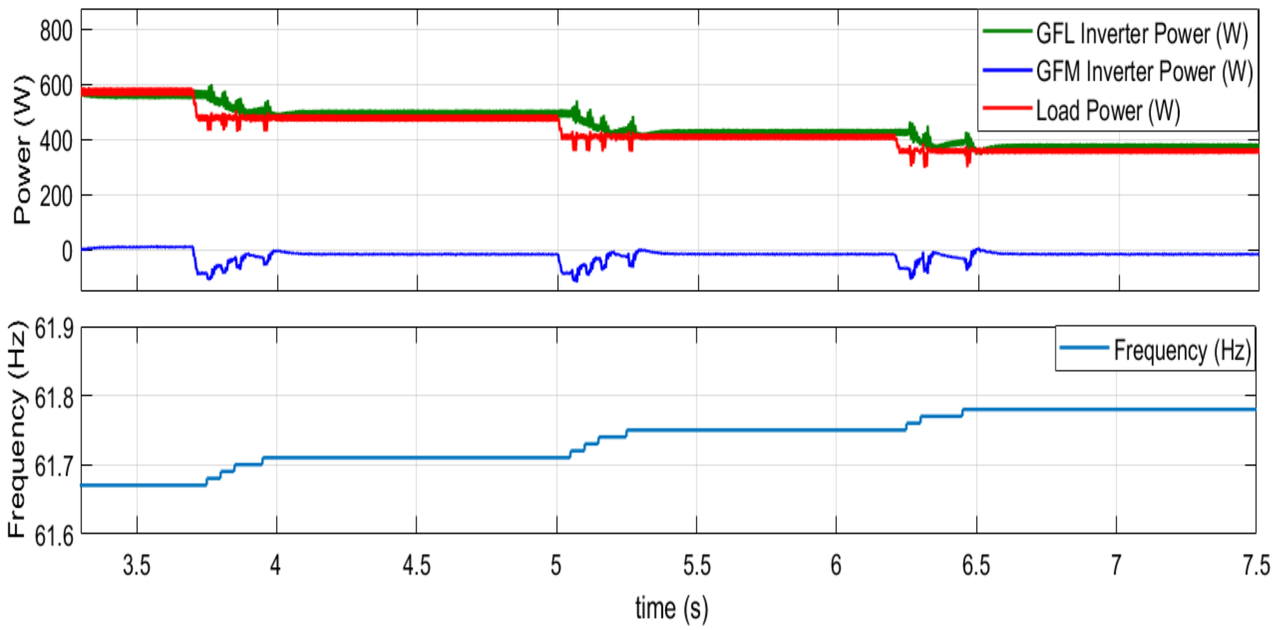

Figure 3.36 Simulation results of the integrated system; frequency shift power control when the load decreases. A zoomed-in version of Figure 3.35

Case II: When load consumption is more than PV generation

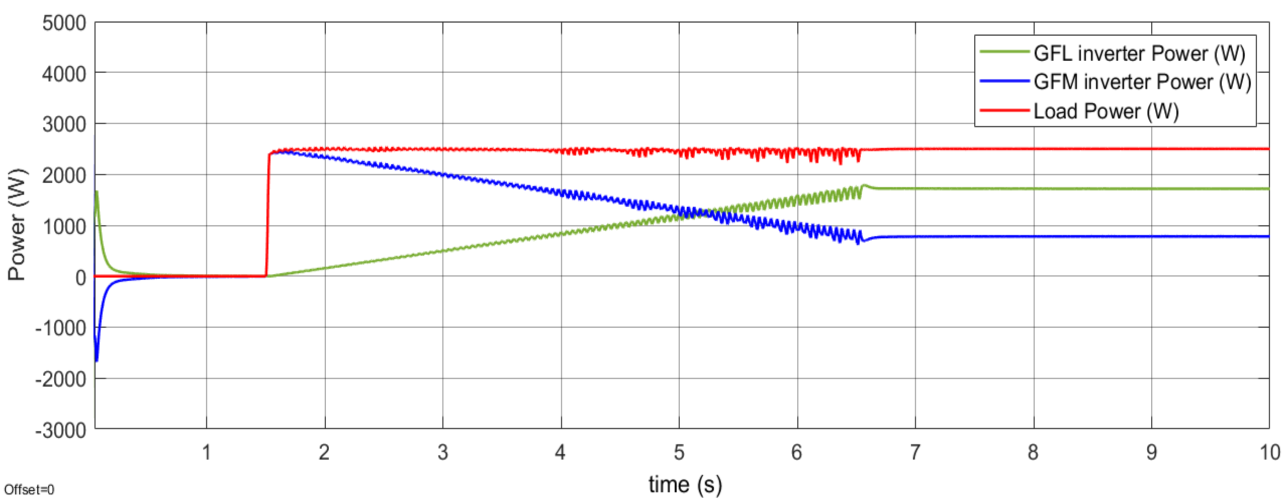

Figure 3.37 Simulation results of the integrated system; GFL and GFM inverters both contribute to load

The GFL inverter contributes the maximum possible PV power, and the remaining power is contributed by GFM inverter. From 1.5s to 6.5s, the frequency shift power control method increases the GFL inverter power to the maximum of 1718 W, and the remaining 782 W is generated by the GFM inverter, as shown in Figure 3.36.

4 Experimental Analysis of Converters

4.1 Introduction

This chapter presents the results of the Sunny Island (Grid Forming) and Sunny Boy (Grid Following) converters obtained from the performed experiments at the FBL.

4.2 Sunny Island Converter

The Sunny Island converter output voltage and current waveforms are obtained by connecting the decided load in off-grid conditions. In this condition, the converter works as an inverter and supplies AC power to the connected load.

4.2.1 Experimental Setup

The schematic diagram of the experiment setup is shown in Figure 4.1. The grid, which is generally connected to the AC2 side of the Sunny Island, is disconnected by a grid disconnect switch (DSC 1). The load side is connected to the Chroma variable load device, which is set to 10 Ω during the experiment. The Sunny Island is tested for 20.86% loading, which is the same as in the simulation.

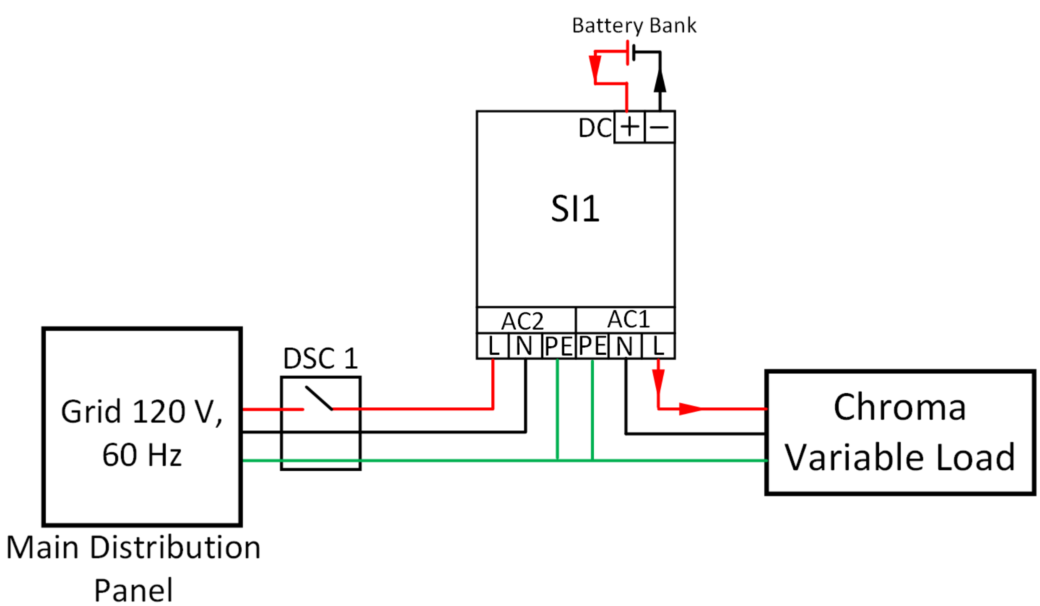

Figure 4.1 Schematic of Sunny Island and load experiment setup.

Voltage and current at the load side are measured using an oscilloscope. Figure 4.2 illustrates the experimental setup to obtain the waveforms.

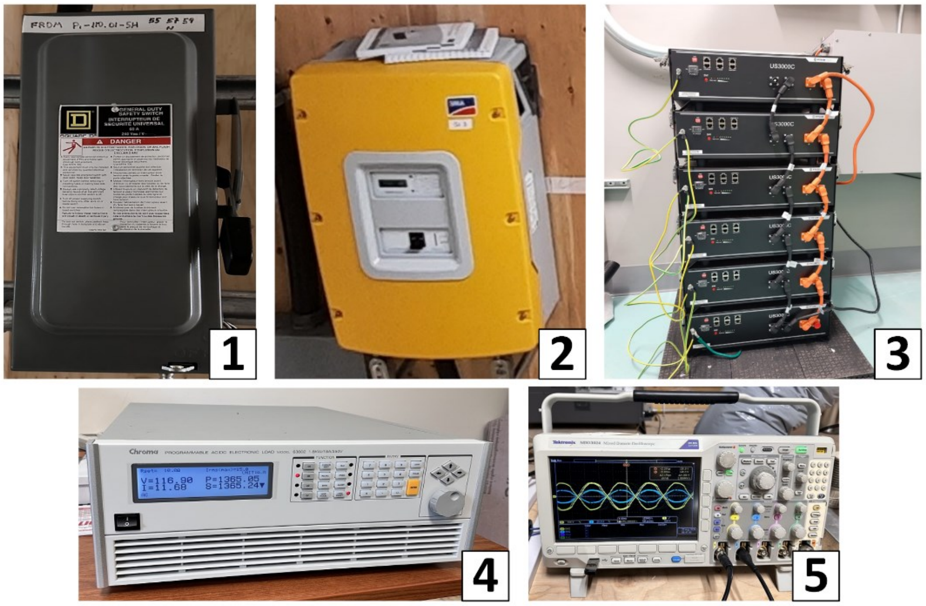

Figure 4.2 Sunny Island experimental setup: 1) Disconnect switch (DSC-1), 2) Sunny Island converter, 3) Battery bank, 4) Chroma variable load device, 5) Oscilloscope.

4.2.2 Observations

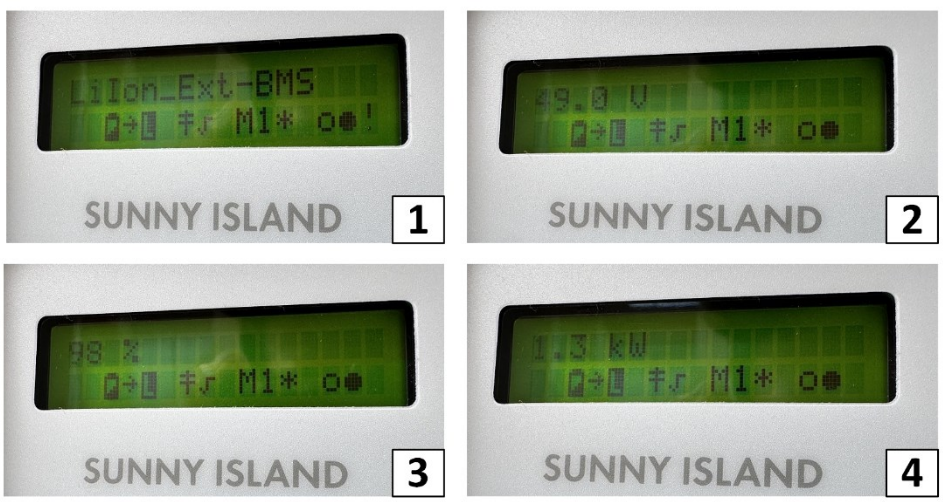

Figure 4.3 Sunny Island display: 1) Battery type, 2) Battery voltage, 3) Battery SOC, 4) Total inverter output power.

Figure 4.3 shows the display indication of Sunny Island during the experiment. The battery-to-load arrow indicates that the battery bank is feeding the load.

4.2.3 Experimental Results

The voltage and current waveform results of the Sunny Island experiment are shown in Figures 4.4 and 4.5.

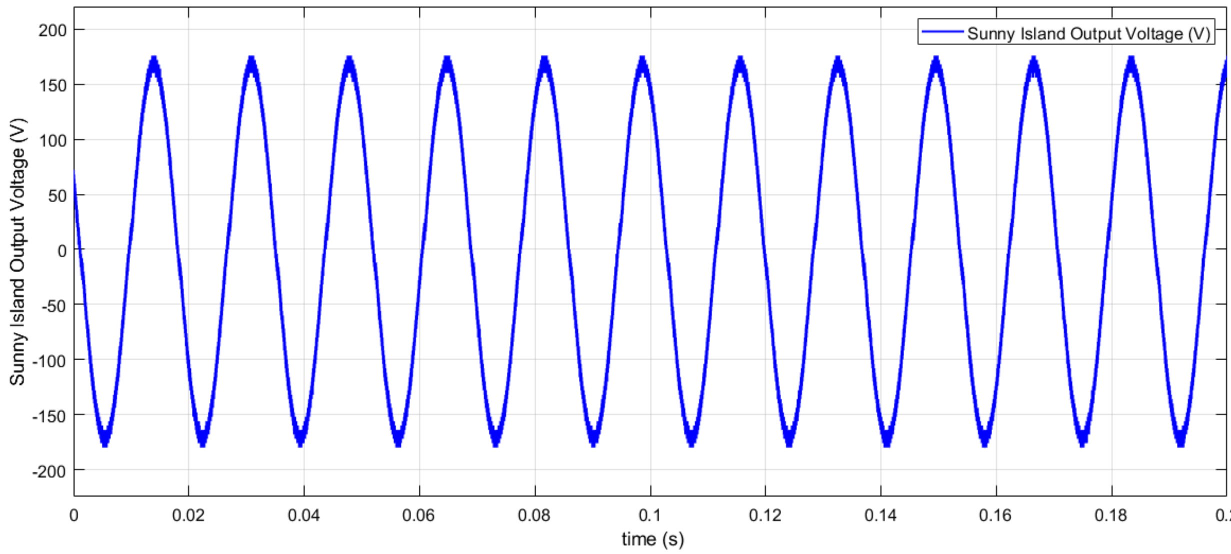

Figure 4.4 Experimental result of Sunny Island converter, output voltage (time segment: 0-0.2s).

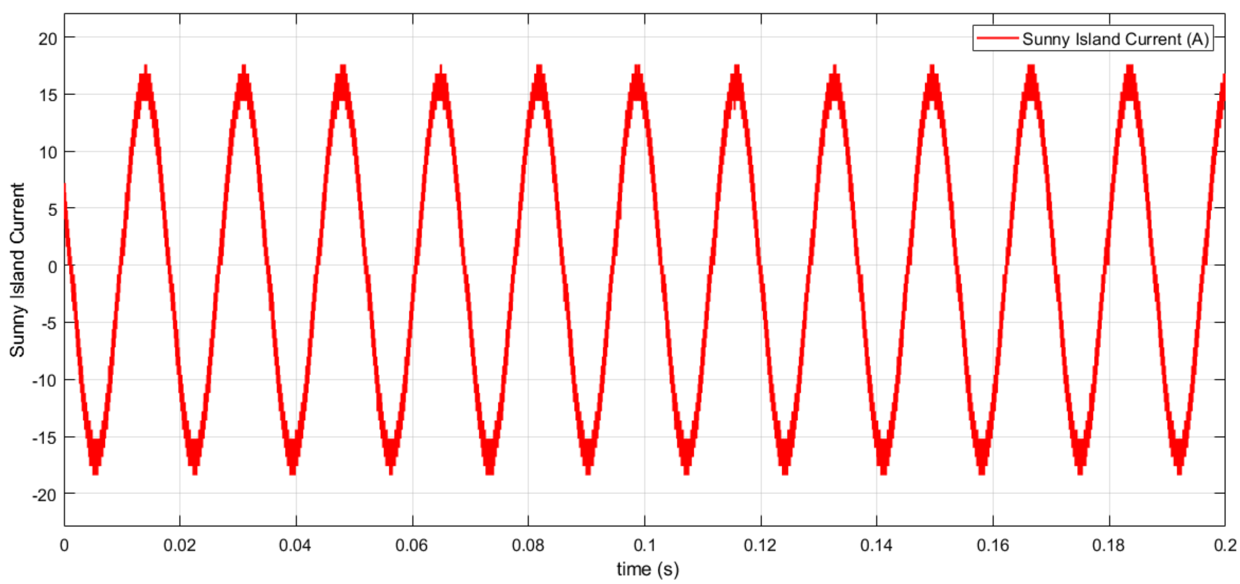

Figure 4.5 Experimental result of Sunny Island converter, output current (time segment: 0-0.2s).

As shown in Figures 4.4 and 4.5, the Sunny Island voltage and current waveforms are sinusoidal in nature, and their RMS values are 119.4 V and 11.2 A, respectively.

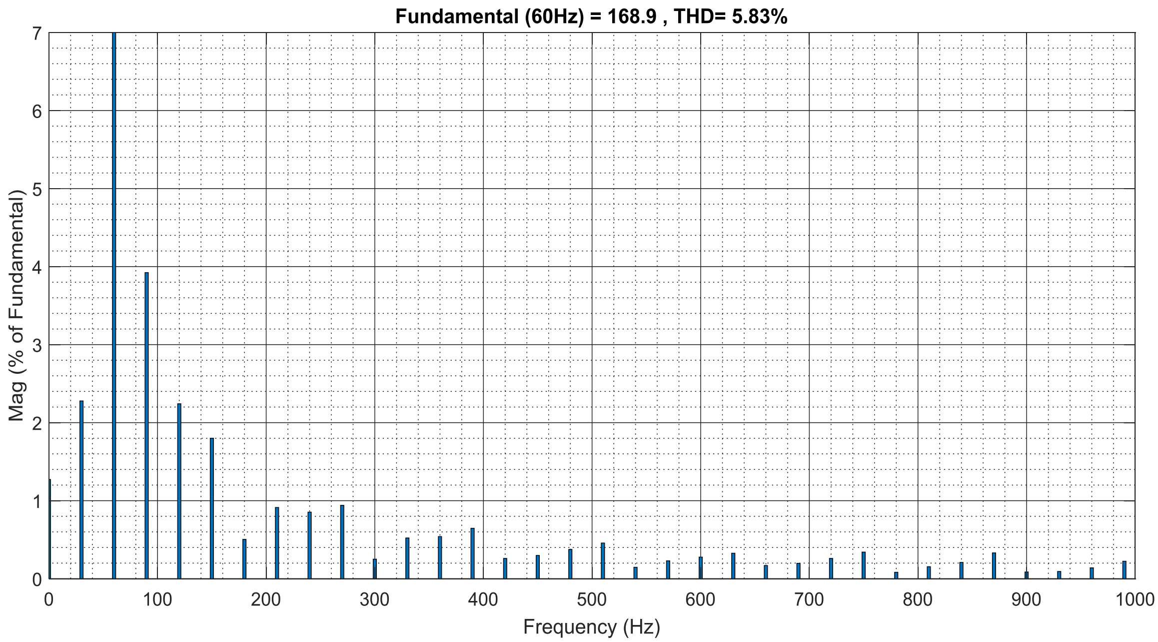

Figure 4.6 FFT analysis of the output voltage of Sunny Island

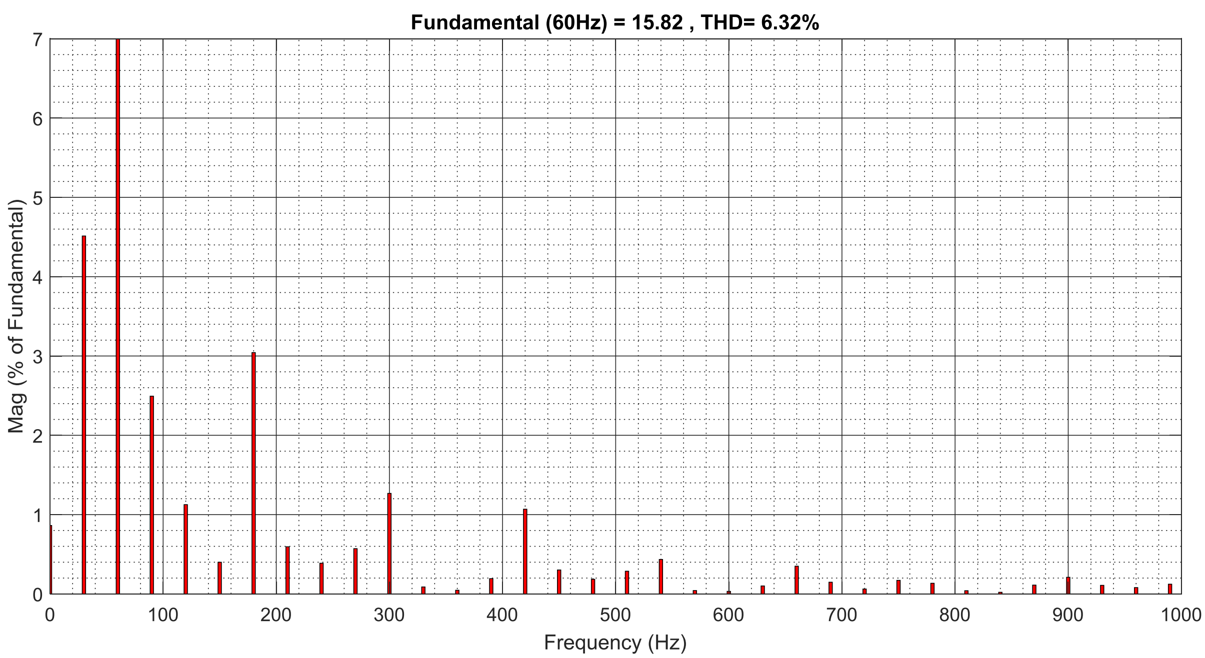

Figure 4.7 FFT analysis of the output current of Sunny Island converter.

According to IEEE 519, for a voltage level less than 1 kV, the voltage THD should be under 8%, and the individual harmonics distortion should be less than 5%. From Figure 4.6, the voltage

THD is 5.83%, which is within the limit of the IEEE standards. Also, the individual harmonics are less than 5%. From the FFT analysis of the waveforms, the presence of 30 Hz harmonic is noted. This sub-fundamental harmonic is due to the non-linearities of the inverter circuit, such as the switching actions of Mosfet. From the FFT analysis of the current in Figure 4.7, the THD is found to be 6.32%, and the dominant harmonics are 3rd, 5th, 7th, and 9th.

4.3 Sunny Boy Inverter

The Sunny Boy inverter is a grid-tie inverter. Excessive solar power generated by Sunny Boy either charges the battery bank connected to Sunny Island or is injected into the grid. Power generated by the Sunny Boy is calculated using the voltage and current waveforms and compared with the DC input power.

4.3.1 Experimental Setup

The FBL has window solar panels, but the voltage generated by the panels is insufficient to start the Sunny Boy inverter. The DC voltage cut-off level of the Sunny Boy inverter mentioned in the datasheet is 100 V. A variable DC source (Chroma PV simulator) is used to test the Sunny Boy. The DC source is capable of creating a PV-like DC source. The Chroma PV simulator can give a maximum of 150 V and 10 A. The open circuit voltage and short circuit current are decided according to these ratings. The configured parameters of the PV simulator are shown in Table 4.1. A real-time simulator (Opal-RT 4510) is used to log the Sunny Boy inverter's output voltage, current, and power. Figure 4.8 shows all the required connections for the experiment. The detailed experimental setup with the devices is shown in Figure 4.9.

Table 4.1 Configured parameters of the DC source

Open-Circuit Voltage V_{oc}	150 V
Short-Circuit Current I_{sc}	10 A
Voltage at maximum power point V_{mp}	130 V
Current at maximum power point I_{mp}	8.5 A

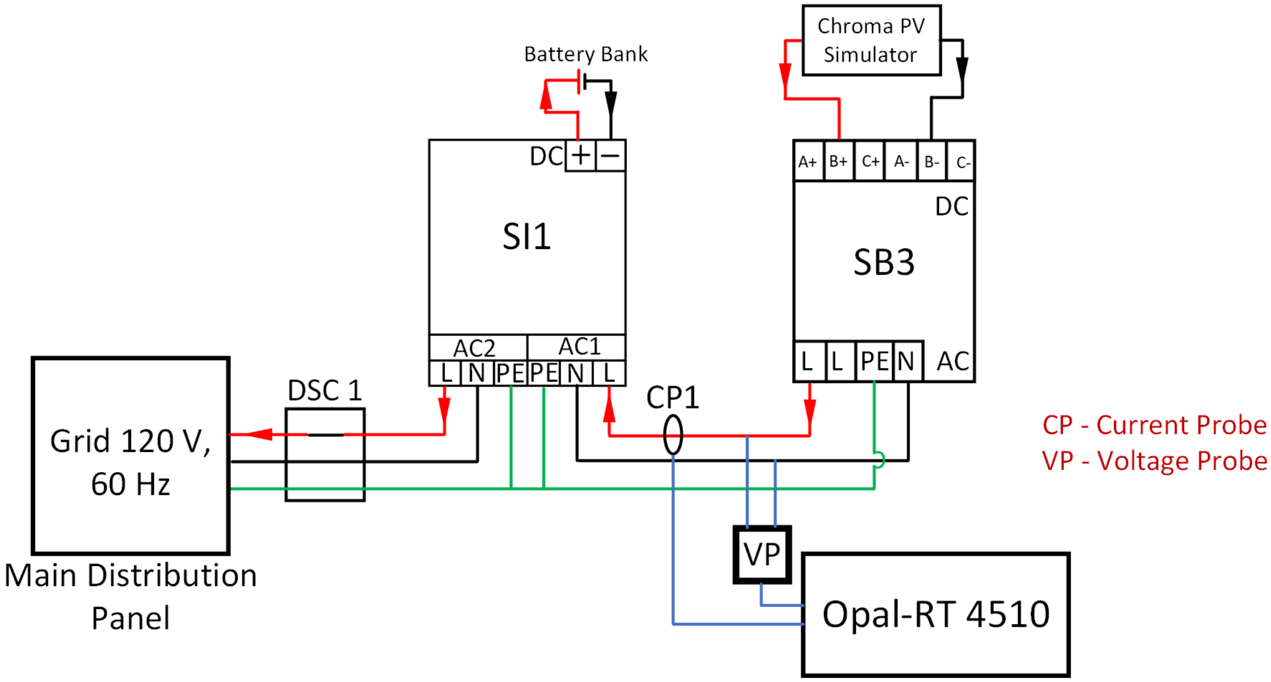

Figure 4.8 Schematic of Sunny Boy inverter experimental setup.

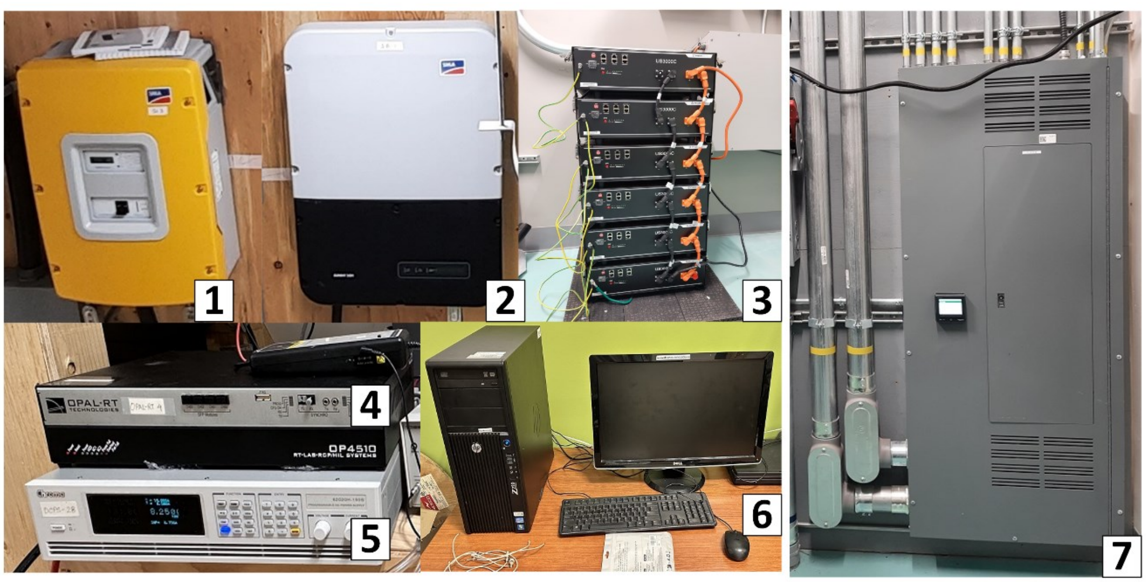

Figure 4.9 Sunny Island experimental setup: 1) Sunny Island converter, 2) Sunny Boy inverter, 3) Battery Bank, 4) Opal-RT 4510 for logging data, 5) Chroma DC source, 6) PC, 7) Main distribution panel (the grid).

4.3.2 Observation

Figures 4.10 and 4.11 show the observations taken during the experiment.

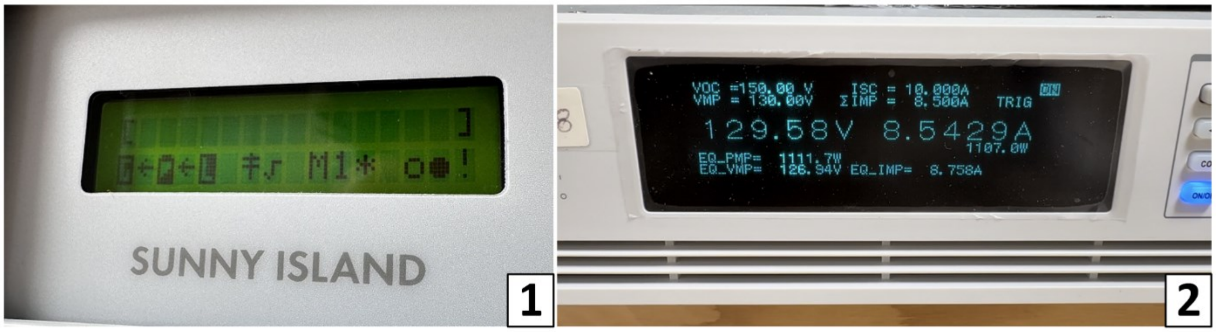

Figure 4.10 Sunny Boy inverter experimental observation: 1) Sunny Island converter display: power is sent from AC1 (load-side) to AC2 (grid-side), and at the same time, it charges the battery, 2) Chroma PV simulator display: the values 129.58 V and 8.54 A indicate

Figure 4.11 Sunny Boy inverter display: 1) DC input parameters (Chroma PV simulator is connected to B), 2) AC output parameters, 3) Power output and total energy.

4.3.3 Results

Figure 4.12 shows the Sunny Boy output voltage waveform; the measured value of voltage is 119.4 V RMS.

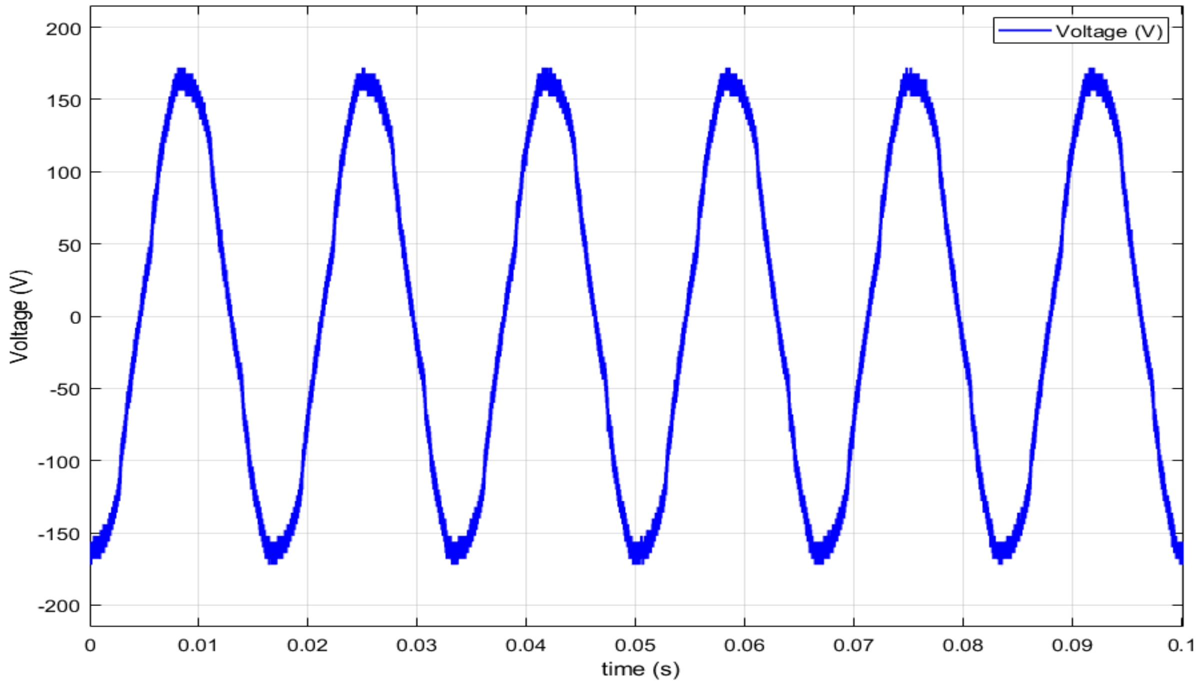

Figure 4.12 Experimental results of the Sunny Boy inverter: output voltage (time segment: 0 - 0.1 s).

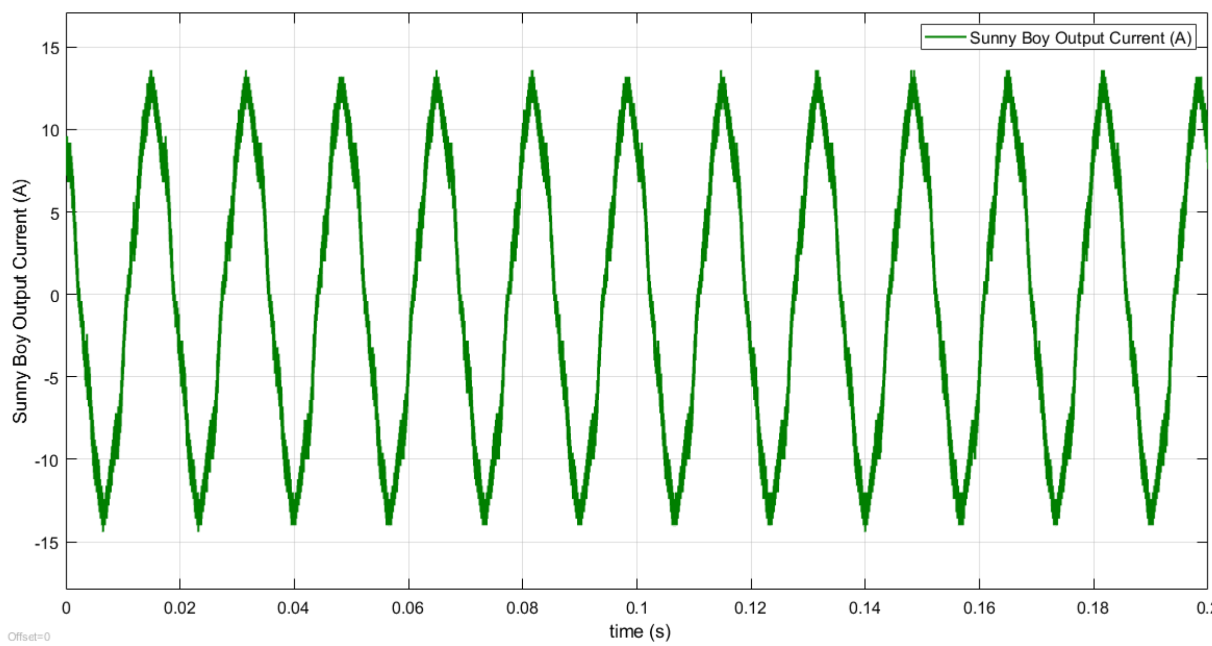

Figure 4.13 Experimental results of the Sunny Boy inverter: output current (time segment: 0 - 0.2 s).

Figure 4.13 shows the Sunny Boy output current waveform. Distortion can be noted in the sinusoidal waveform. The measured RMS value of the current is 8.5 A.

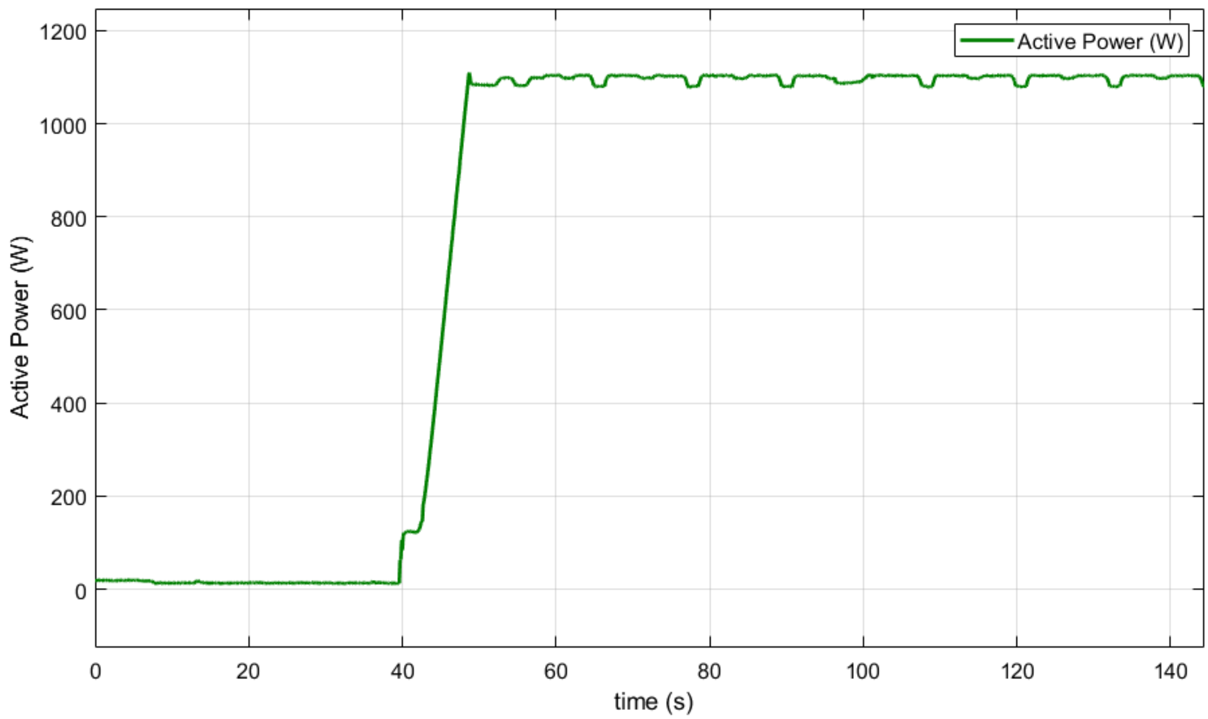

Figure 4.14 Experimental results of the Sunny Boy inverter: output power (time segment: 0 - 140 s).

Figure 4.14 shows the Sunny Boy's output power. When the Sunny Boy inverter is turned on at 40 s, it starts tracking the MPP and achieves maximum power after a few seconds. The AC output power of the Sunny Boy inverter is 1036 W, as displayed on the inverter in Figure 4.11.

Figures 4.15 and 4.16 show the FFT analysis of the voltage and current waveforms.

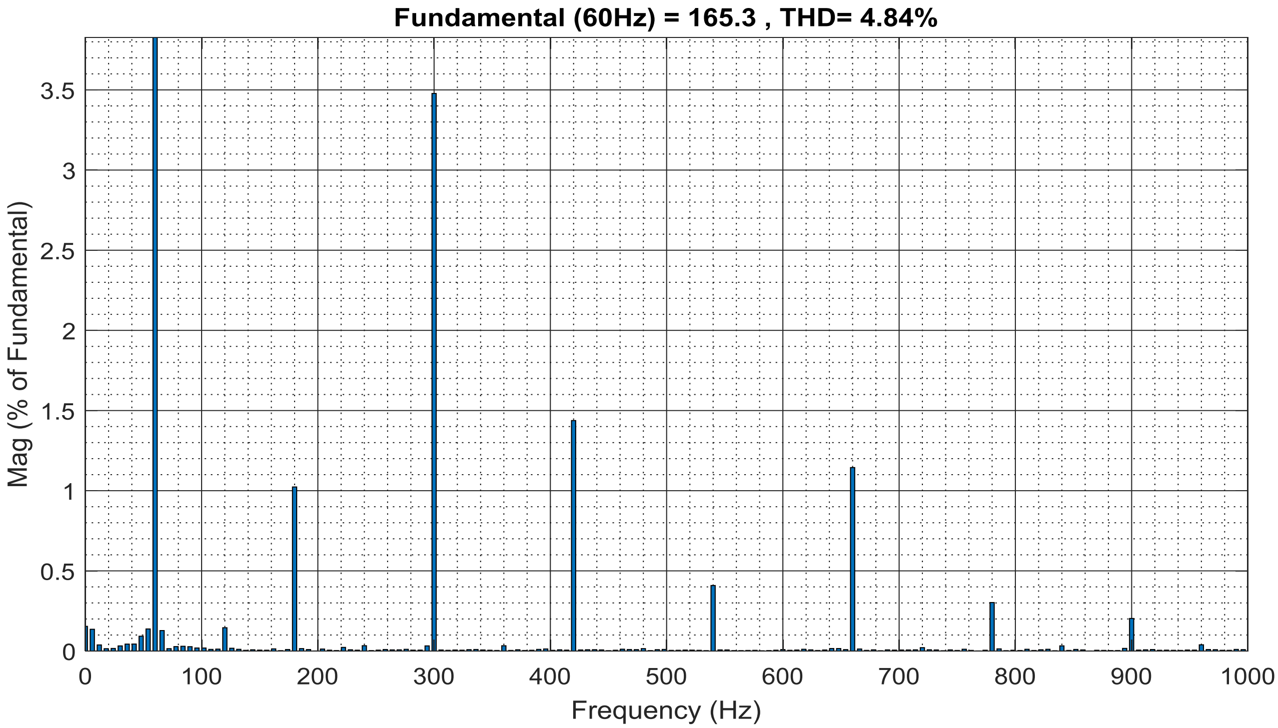

Figure 4.15 FFT analysis for the output voltage of the Sunny Boy inverter.

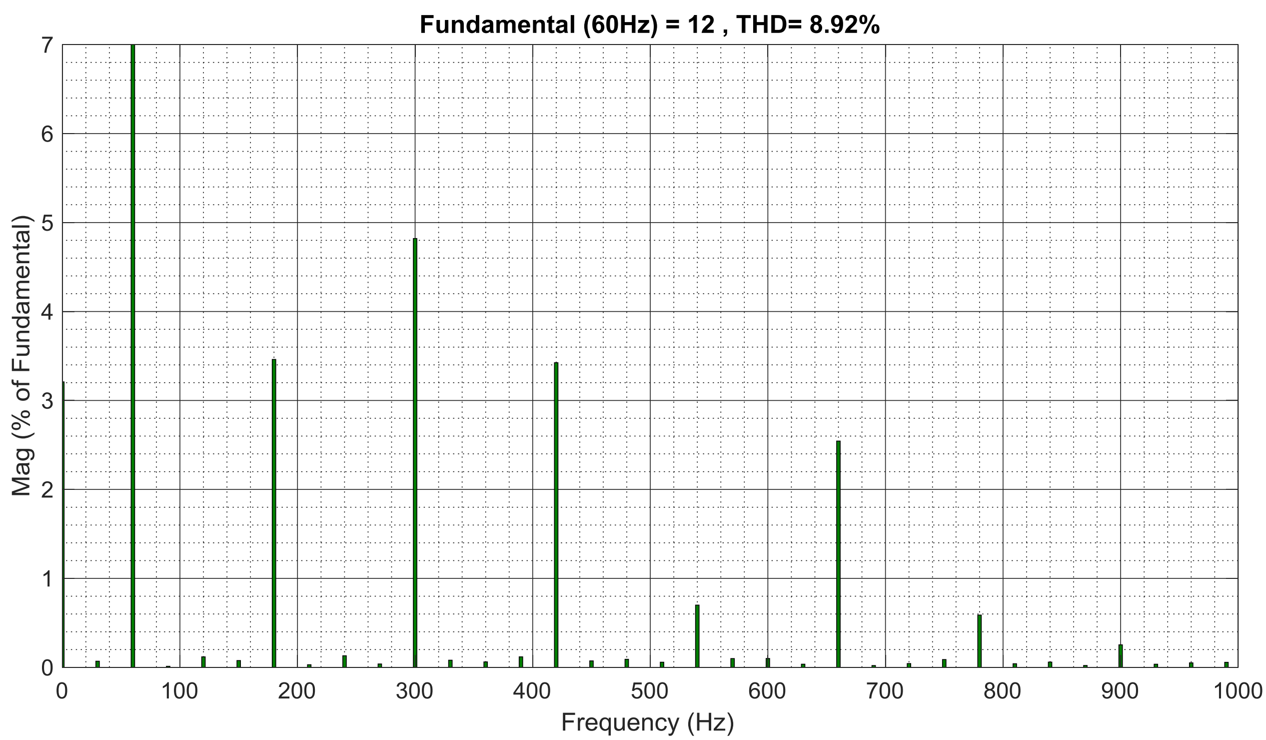

Figure 4.16 FFT analysis for the output current of the Sunny Boy inverter.

The dominant harmonics are the odd harmonics, such as 3rd, 5th, 7th, 9th, 11th, and 13th, as shown in the FFT analysis. The voltage THD is 4.84%, which is within the IEEE 519 standard. The injected current into the grid has a high THD value of 8.92%. One of the reasons behind this behavior is the non-linear loads, such as lighting, computer, security and communication devices, connected to the main panel in the FBL. In addition, the Sunny Boy's output power is also rectified by the Sunny Island to charge the battery, which causes distortion in the waveform.

4.4 Integrated System

To analyze the converters' frequency shift power control, the Sunny Island and Sunny Boy converters are operated in off-grid conditions with a variable load. In this test, the system's frequency, the Sunny Island and Sunny Boy output powers, and the load power consumption are measured when the loads vary.

4.3.4 Experimental Setup

The integrated system test data are logged using Opal-RT. Three current probes and a voltage probe are connected, as shown in Figure 4.17. A Chroma PV simulator is connected to the DC

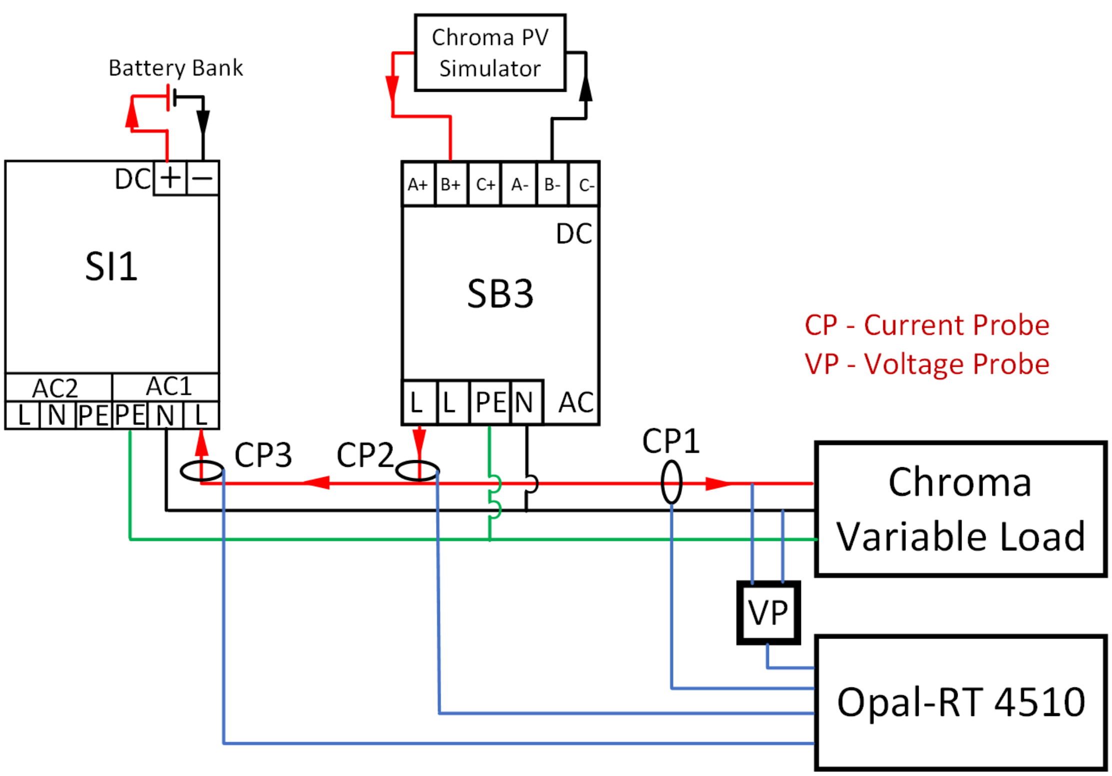

Figure 4.17 Schematic diagram of the integrated system.

side of the Sunny Boy inverter. The DC parameters are the same as mentioned in Table 4.1. The resistive load is varied in steps of 5 Ω, starting from 25 to 40 Ω using the Chroma variable load device. The actual devices are shown in Figure 4.18.

Figure 4.18 Experimental setup of the integrated system: 1) Sunny Island converter, 2) Sunny Boy inverter, 3) Battery Bank, 4) Opal-RT 4510, 5) Chroma PV simulator, 6) PC, 7) Chroma variable load.

4.3.5 Results

Figure 4.19 shows the result of the integrated system. Some part of the Sunny Boy power (green trace) is used by Sunny Island (blue trace) to charge the battery, and the load consumes part of the power. The charging power is around 200 W. It is observed that when the load decreases, the system's frequency increases, and the output power of the Sunny Boy inverter reduces. When the load decreases, momentarily, the difference in the power goes to the Sunny Island from the Sunny Boy, and the Sunny Boy starts decreasing its output power.

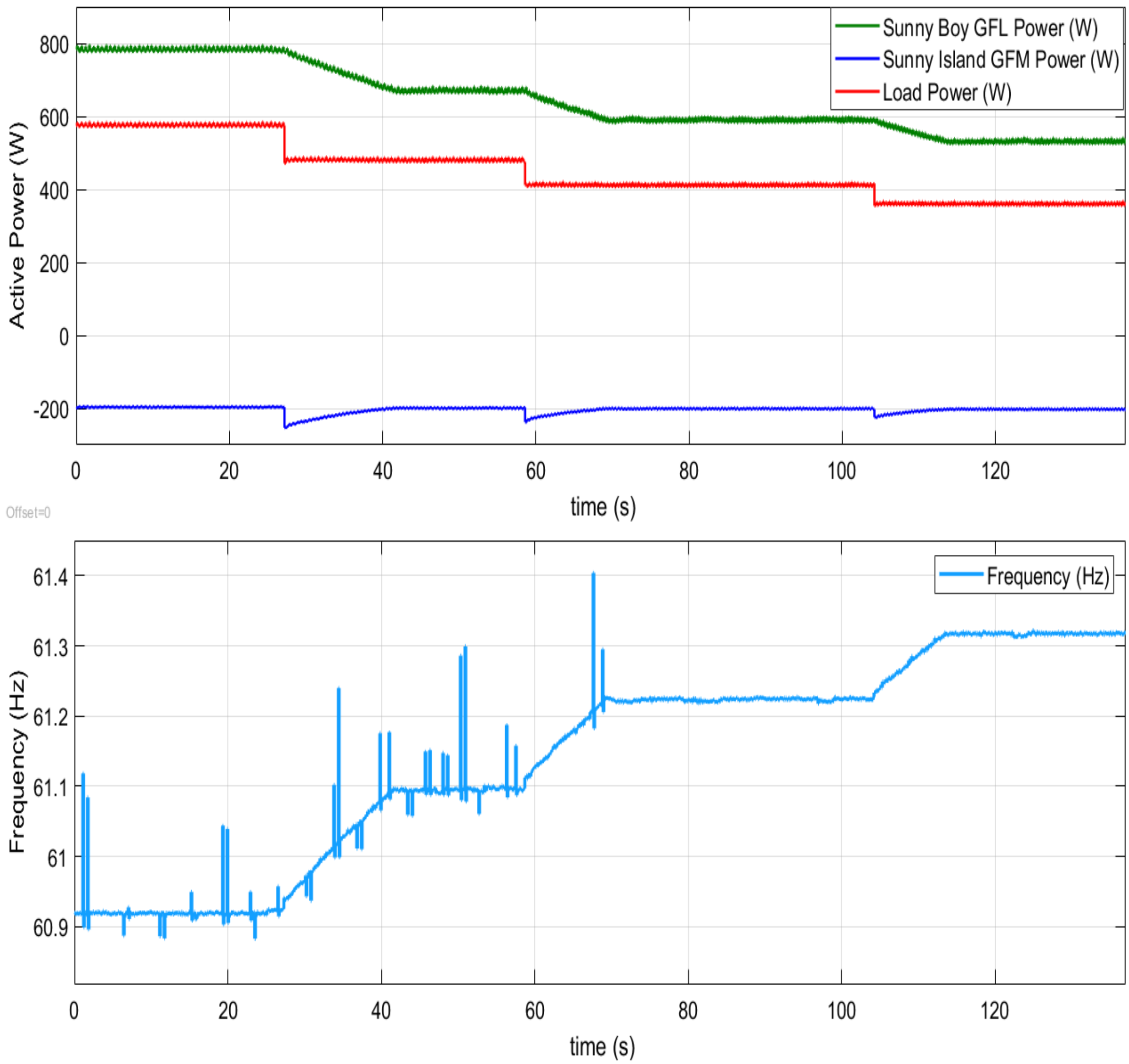

Figure 4.19 Power and frequency of the integrated system while reducing the load.

.

4.5 Comparison of the Experimental results of the Dynamics of Integrated system with Simulation results

Figure 4.20 compares the simulated and experimental results of the dynamics of the integrated system. The same load steps of 5 Ω, starting from 25 to 40 Ω are implemented. The ramp rate of change of power with frequency is slow in the experiment compared to the simulation. The additional setting in the Sunny Boy allows changing the rate and response time. Furthermore, in the experiment, the Sunny Island converter uses a part of the Sunny Boy inverter power to charge the battery bank. The negative 200 W shows the power consumed by the Sunny Island converter.

In both experimental and simulated results, initially, when the load decreases, momentarily, the excess power of the Sunny Boy (GFL) inverter goes into the Sunny Island (GFM) converter. Then, the Sunny Boy (GFL) inverter decreases its output power according to the frequency change.

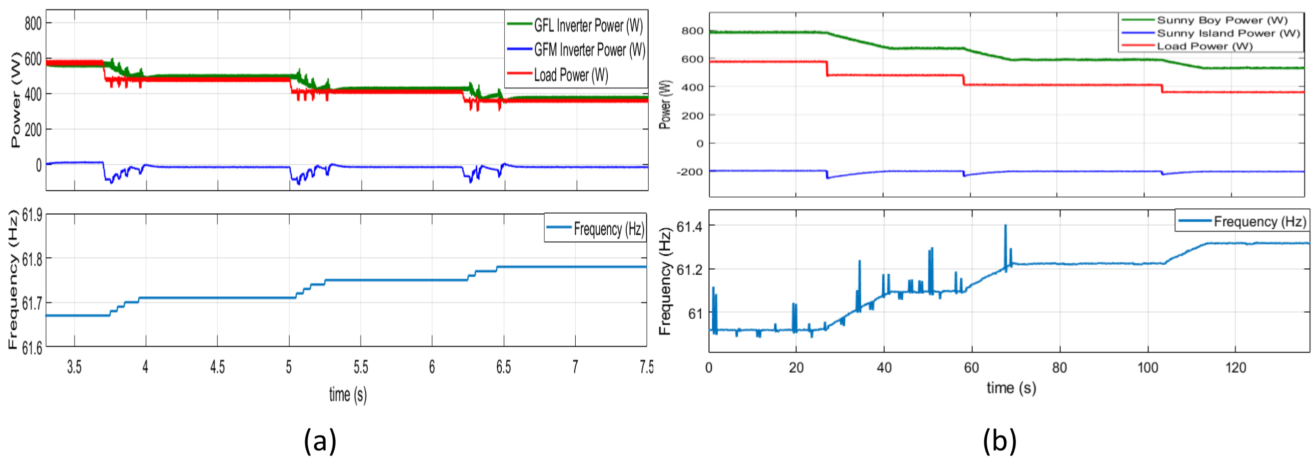

Figure 4.20 Power and frequency of the integrated system while reducing the load. a) Simulation results, b) Experimental results

5 Integration of V2L and V2H at the FBL

5.1 Introduction

As concerns over environmental issues and dependence on fuel increase, the need for clean energy continues to rise. Electric vehicles (EVs) have gained significant interest from governments, industries, and consumers [43-44]. With the significant development of EV technologies, the use of EVs in modern energy systems enables users to optimize energy sharing with homes and the grid [45-46]. In the following sections of this chapter, the two modes, vehicle to load (V2L) and vehicle to home (V2H), are demonstrated.

5.2 Vehicle to Load (V2L)

The V2L system is a very creative feature found in many EVs, such as Nissan Leaf, Ford F-150, Kia Niro, Hyundai Ioniq 6, and many more. This feature enables supplying power to the AC appliances of a house, and it also works as a portable power source. The EVs can store excess renewable energy and use it in times of emergency as a backup. The simulation and design of the V2L inverter is presented in [47]. This V2L mode of the Nissan Leaf EV is tested at the FBL using a Setec Power inverter. The specification of the Setec inverter is mentioned in Table 5.1. The inside power electronic hardware and microcontroller are shown in Figure 5.1. In the V2L

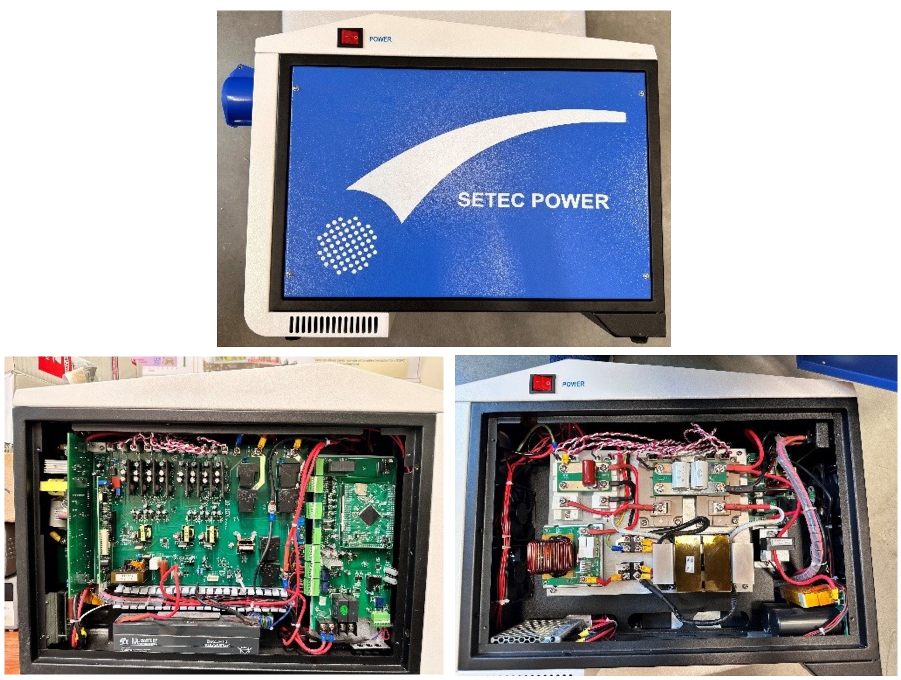

Figure 5.1 Setec Power Inverter

mode V2L mode, the Nissan Leaf is connected to the Setec inverter with a CHAdeMO plug. The AC side of the Setec inverter is connected to the load.

Table 5.1 Setec Power Inverter Specification

Rated input voltage	450 V
Rated capacity	6 kVA
Rated output power	4.2 kW
Rated output current	Max 38A/21A

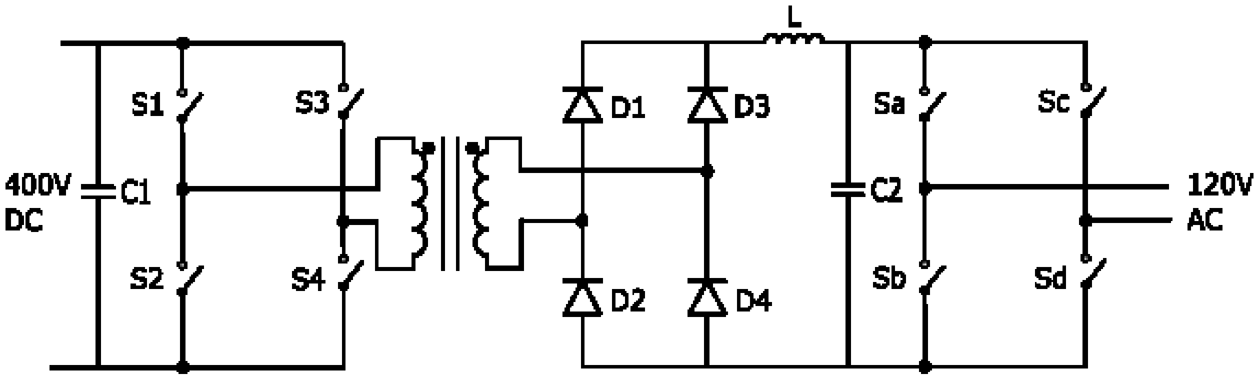

Figure 5.2 Investigated Topology of Setec Power Inverter

From the investigation of the power electronic components of the Setec inverter, a topology is formed and presented in Figure 5.2. The DC power from the EV goes to the first H-bridge (S1, S2, S3, S4); this H-bridge converts DC to AC of the high fundamental frequency. The switches used in both the H-bridges are IGBTs. The transformer is used to provide the electric isolation in the circuit. The diode rectifier converts the high-frequency AC to DC; then, the DC is inverted to AC with a 60 Hz fundamental frequency.

5.2.1 Experimental Setup

In the following experiment, the Nissan Leaf supplies power to a 1.5 kW load through the Setec inverter. The load is resistive, and the rated capacity of the Setec inverter is 6 kVA So, the percentage loading of the Setec inverter is 25%. Figure 5.3 shows the charging ports of the Nissan Leaf; the CHAdeMO port is used for DC fast charging, and the J1772 port is used for AC charging. The Setec inverter is connected to the CHAdeMO port through a cable. The AC side of the inverter is connected to the load. Figure 5.4 demonstrates the experimental setup and the connections. An oscilloscope is used to capture the output voltage and current of the V2L experiment.

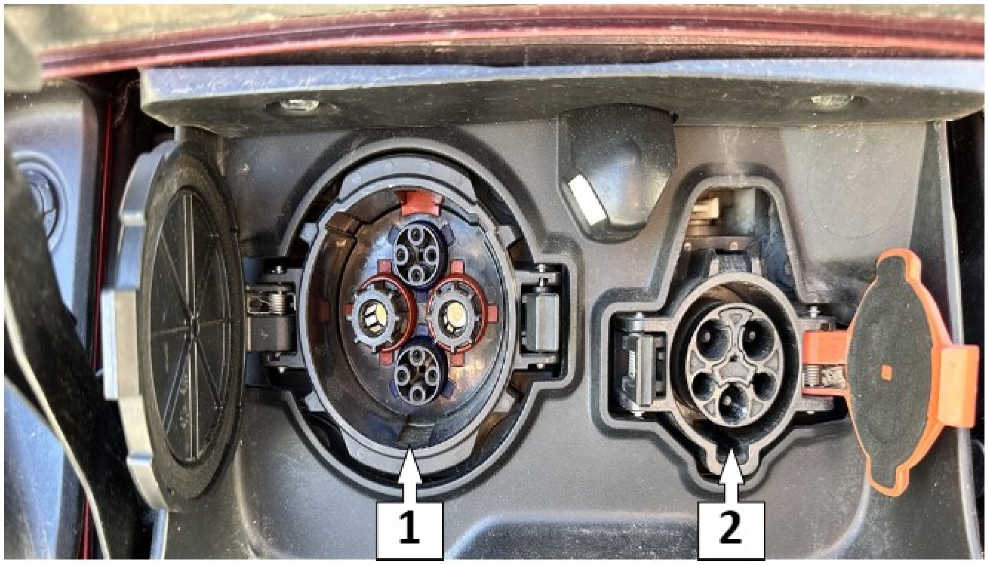

Figure 5.3 Charge ports of Nissan Leaf: 1) CHAdeMO (DC fast charging), 2) J1772 Type 1 and type 2 (AC charging)

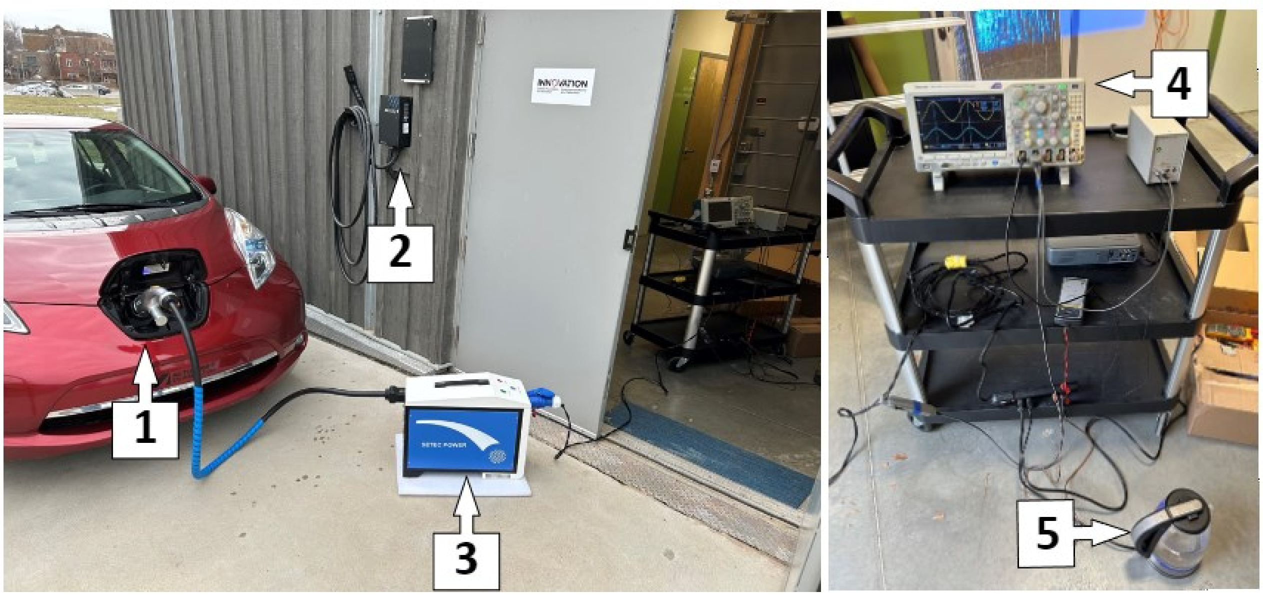

Figure 5.4 Experimental Setup: 1) CHAdeMO connector plugged into the Nissan Leaf 2) Grizzl-E Classic EV charger, 3) Setec inverter, 4) Oscilloscope, 5) Load

5.2.2 Results

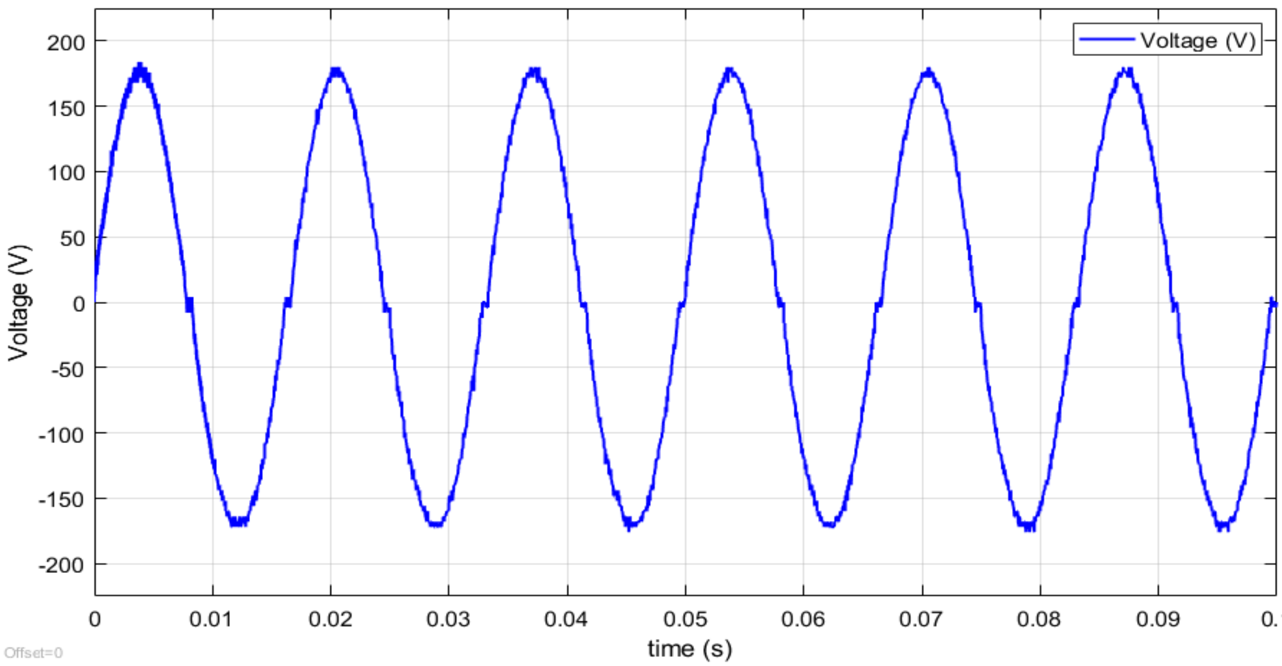

Figure 5.5 Experimental results of V2L test: Setec inverter output voltage.

Figure 5.5 shows the output voltage waveform of the Setec inverter. A distortion can be observed at the zero crossing of the sinusoidal waveform. The reason for the distortion is the presence of lower-order harmonics in the waveform due to dead time. The RMS value of the measured voltage is 121.8 V.

Figure 5.6 shows the output current waveform of the Setec inverter. The measured RMS value of the current drawn by the water kettle is 12.16 A. Since the load is resistive, the sinusoidal current waveform has the same distortion at zero crossing as the voltage waveform.

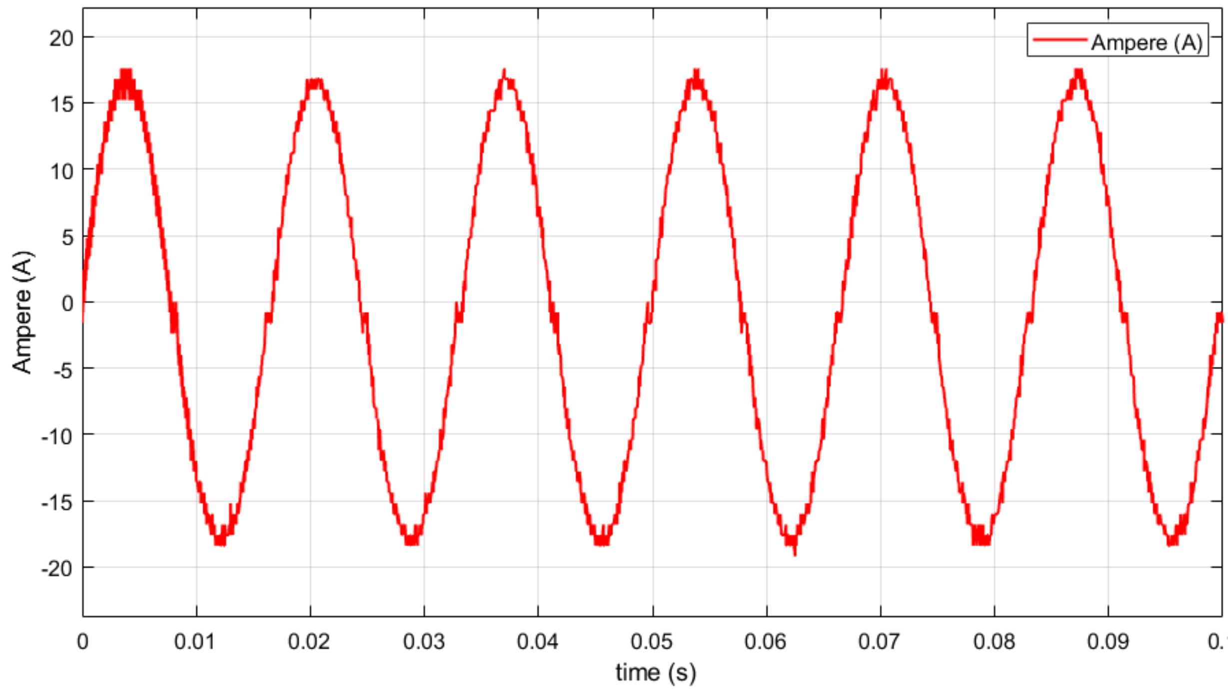

Figure 5.6 Experimental results of the V2L test: Setec inverter output current.

A FFT analysis of the output voltage of the Setec inverter is shown in Figure 5.7. The Total Harmonic Distortion (THD) of voltage is 3.87%. According to the IEEE 519 standard, the THD of a system having a voltage less than 1kV should be less than 8%, and the individual harmonics should be less than 5%. From the analysis, apart from the presence of the old harmonics, the presence of even harmonics such as 2^{nd} and 4^{th} are noted. The THD and the individual harmonics are within the IEEE 519 standard.

The THD of the Setec inverter's output current is 4.93%, as shown in Figure 5.8. The second harmonic is also observed in the FFT analysis of the current waveform. The AC instantaneous power of the inverter oscillates at twice the frequency (2f) due to the product of two sinusoids. Because of the second harmonic power oscillation, the DC side experiences a pulsating power demand at twice the AC frequency. If the DC link capacitor is not adequate, this pulsating power can cause a second harmonic distortion on the AC side.

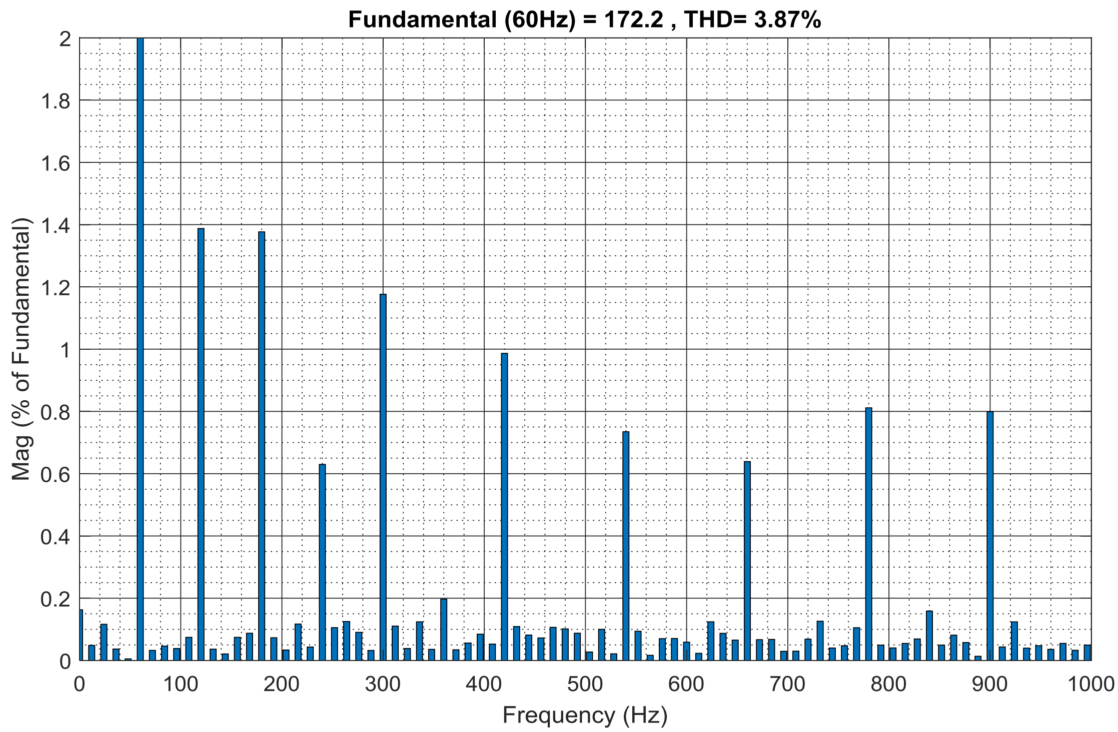

Figure 5.7 FFT analysis of the output voltage of the Setec inverter.

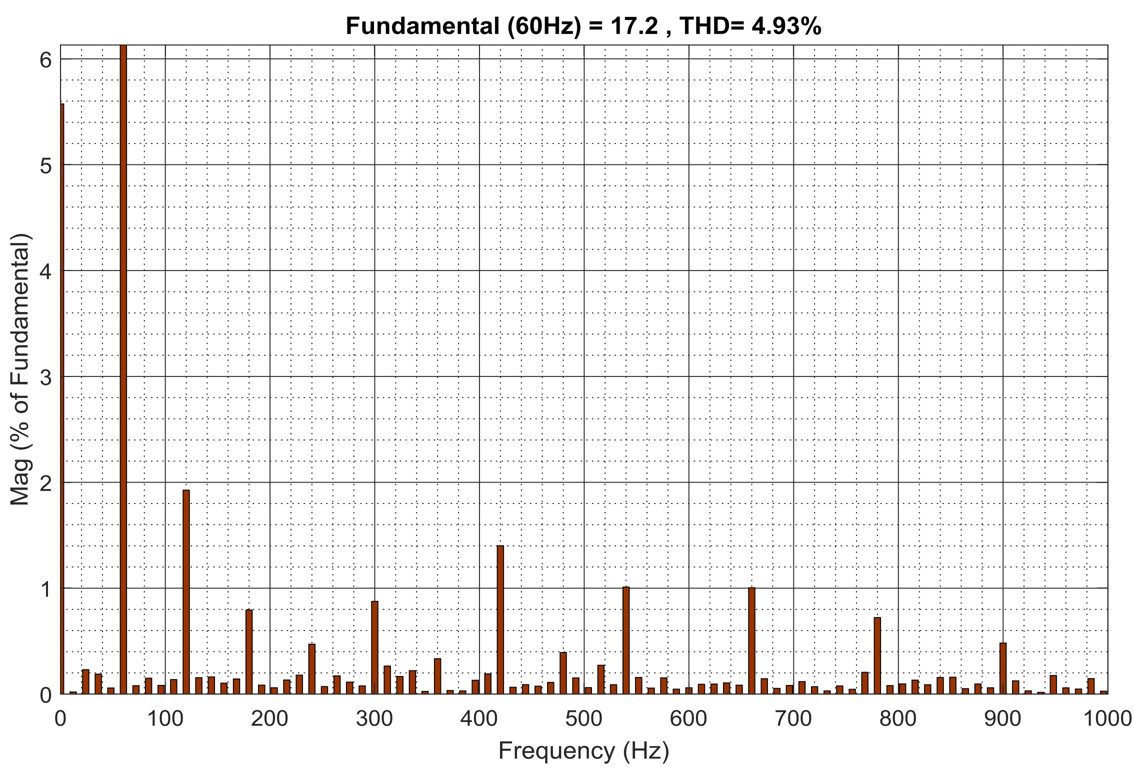

Figure 5.8 FFT analysis of the output current of the Setec inverter.

5.3 Vehicle to Home (V2H)

In the V2H system, the EV is connected to the house's electrical system. Depending on the battery capacity and the inverter power, this type of system can supply power to critical loads or the entire house. This system helps consumers reduce energy bills by charging the vehicle at cheaper tariff periods or off-peak hours and using that stored energy at peak hours. It helps optimize the renewable energy system by providing extra energy storage.

To integrate the V2H in the FBL, the critical loads of the house are separated and placed in a subpanel. The loads connected to the C-phase will be connected to the V2H system in case of a power outage. The capacity of the Setec Power inverter is 6 kVA, so the connected load should be less than that. The critical load of the C-phase is kept at a total of 4.49 kVA. Table 5.2 shows the loads connected to the V2H system.

Table 5.2 Critical loads of V2H system

No.	Load	VA
1	Ground floor lighting	891
2	Ground floor lighting	1424
3	Intrusion Alarm box	500
4	Greenheck fan	75
5	Air Exchanger	500
6	Communication Panel	500
7	Fire Alarm Control Panel	500
8	Door Controller Panel	100
Total		4490

5.3.1 Experimental Setup

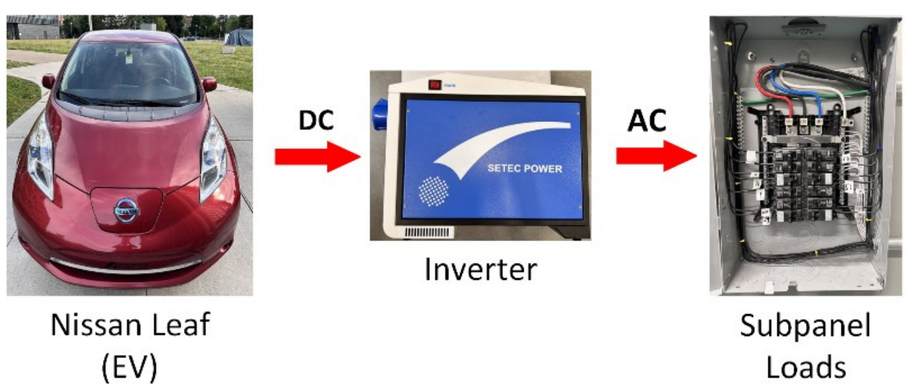

Figure 5.9 Layout of the V2H system

A general layout of the V2H system is shown in Figure 5.9. The detailed wiring diagram is shown in Figure 2.2. The transfer switches change the supply between the SMA, grid, or V2H systems. The switches' positions shown in Figure 5.10 are used to obtain supply from the traction battery of the Nissan Leaf through the V2H system. The AC socket outside of the house is used to take the power inside the house to the sub-panel through the transfer switches. The experimental setup is shown in Figure 5.11. During the V2H system test, most of the power was consumed by the lighting loads.

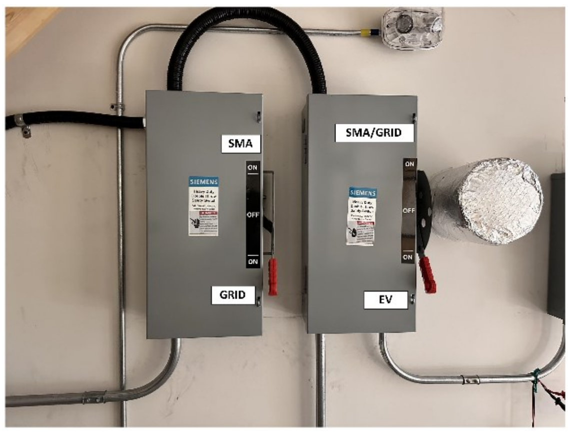

Figure 5.10 Transfer switches' position for the V2H test

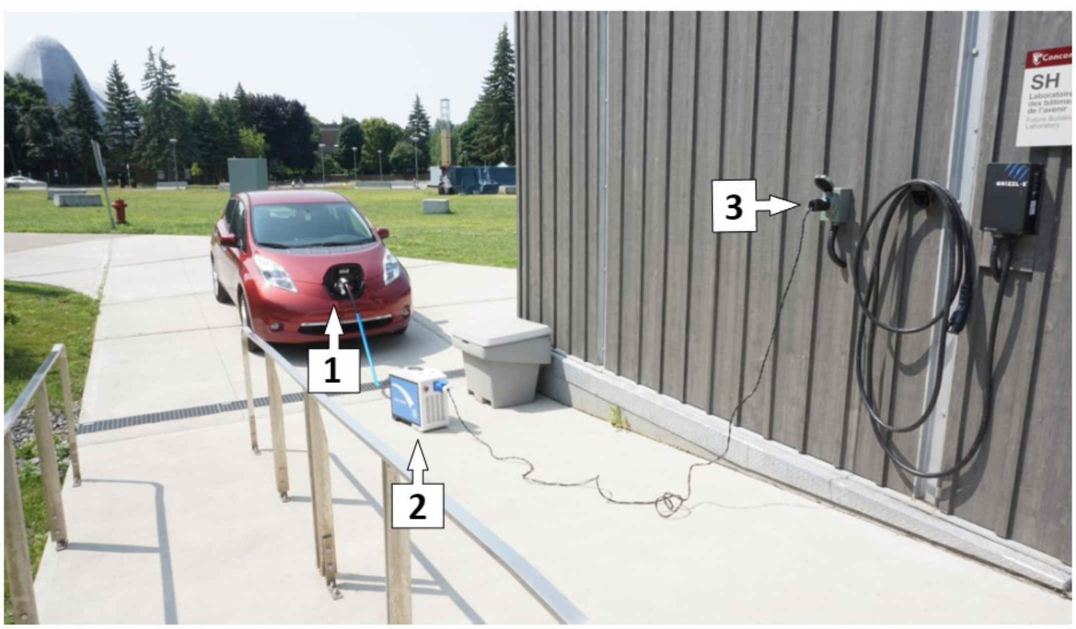

Figure 5.11 Experimental setup for the V2H system: 1) A CHAdeMO connector is plugged into the Nissan Leaf, 2) Setec inverter, 3) AC socket

5.3.2 Results

Figure 5.12 shows the experimental result of the output voltage of the V2H system. The voltage waveform is sinusoidal, with distortion caused by the lower-order harmonics. The RMS value of the voltage is 119.7 V.

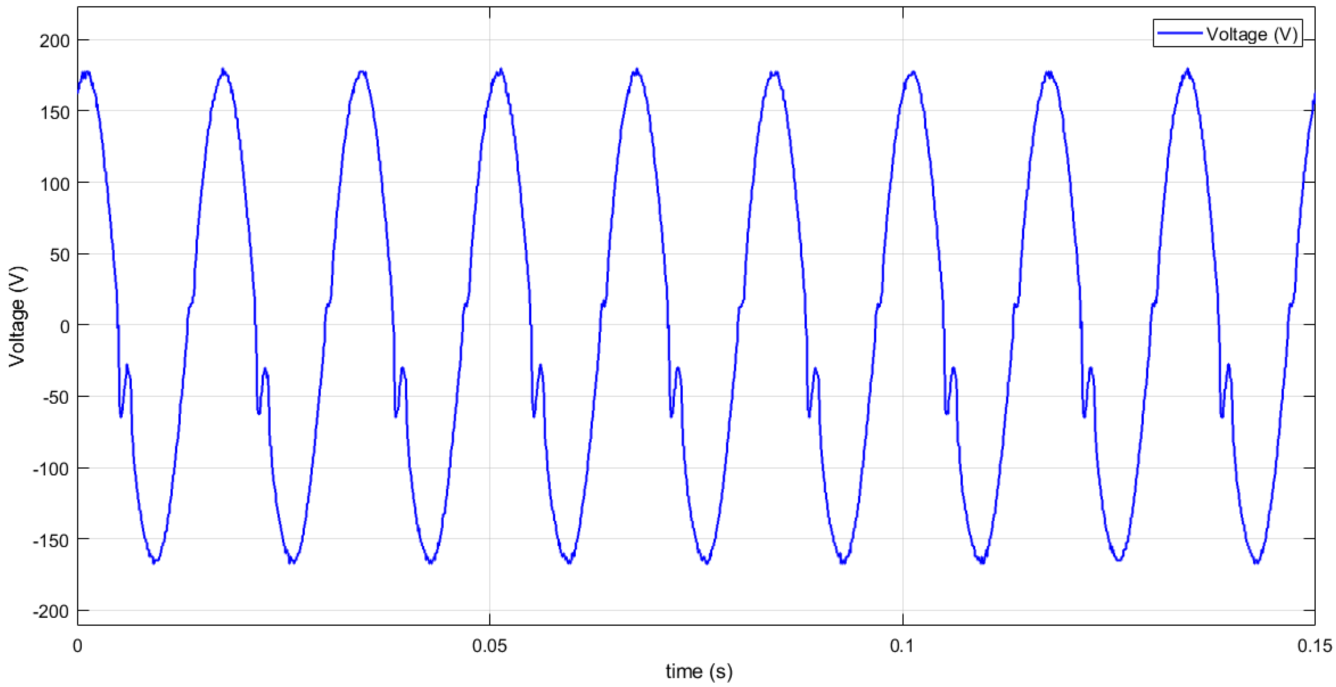

Figure 5.12 Experimental results of the V2H test: the output voltage of the Setec inverter.

Figure 5.13 shows the load current waveform. The RMS value of the current is 11.6 A. The distortion in the sinusoidal waveform is caused by the presence of non-linear loads, the non-linearity of switching devices, and inadequate capacitance.

Figure 5.14 shows the FFT analysis of the voltage waveform. The THD is 10.13%. This THD is higher than the IEEE 519 standard limit because of the presence of highly non-linear loads in the system. The individual harmonic distortion is less than 5%. All the lower-order even and odd harmonics are present in the spectrum.

During the V2H system experiment, the lighting load consumes most of the power. In the experiment, the lighting load consists of LEDs, which are non-linear loads. The distortion in the current and voltage waveforms is due to the non-linear loads [48]. These loads are responsible for the higher harmonic injection in the system.

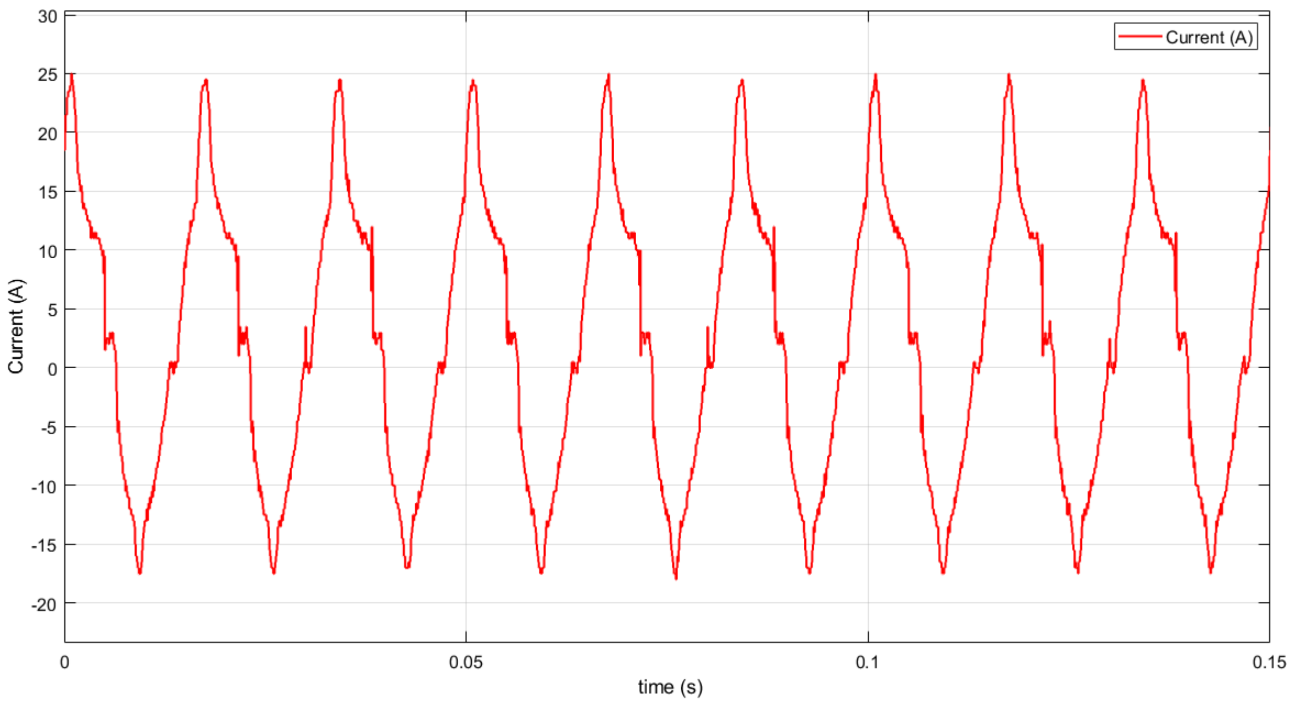

Figure 5.13 Experimental results of the V2H system test: the load current.

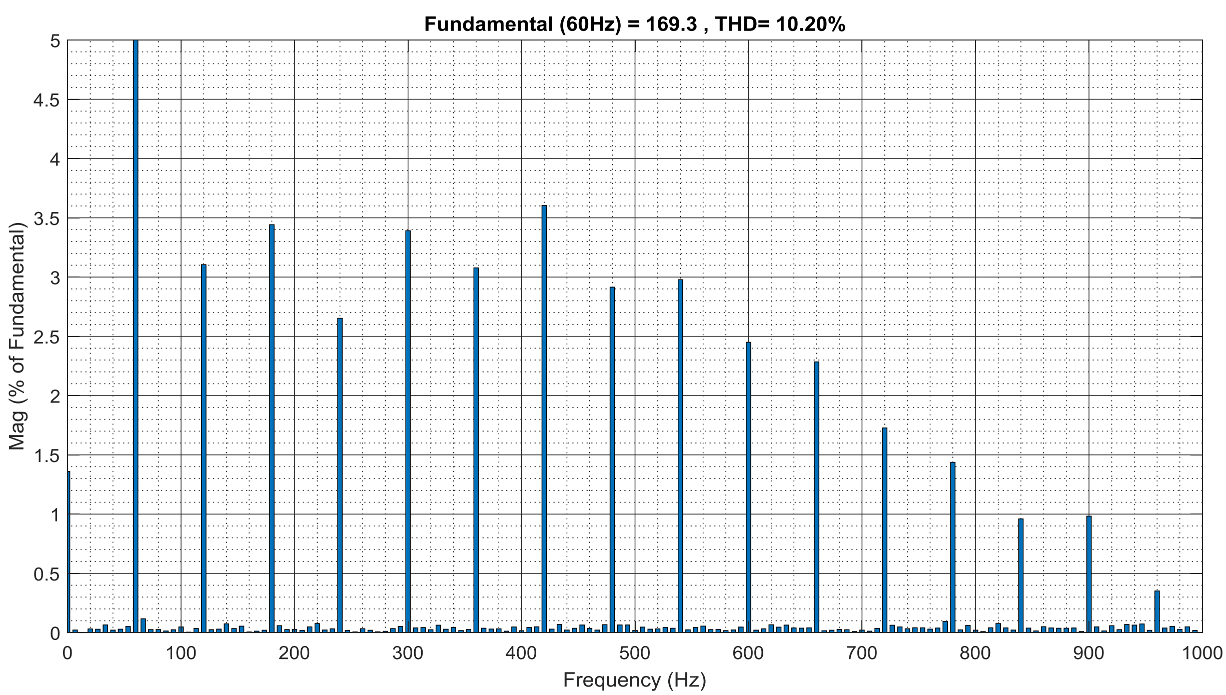

Figure 5.14 FFT analysis of the output voltage of the V2H system.

Figure 5.15 shows that the current THD is 20.34%, which is very unusual. The lower-order harmonics are high, and similar results are also mentioned in [48]. Apart from the odd harmonics, 4th, 6th, 8th, 10th, 12th, and 14th-order even harmonics are present in the analysis. The 3rd harmonic is around 14%, causing most of the distortion in the current waveform.

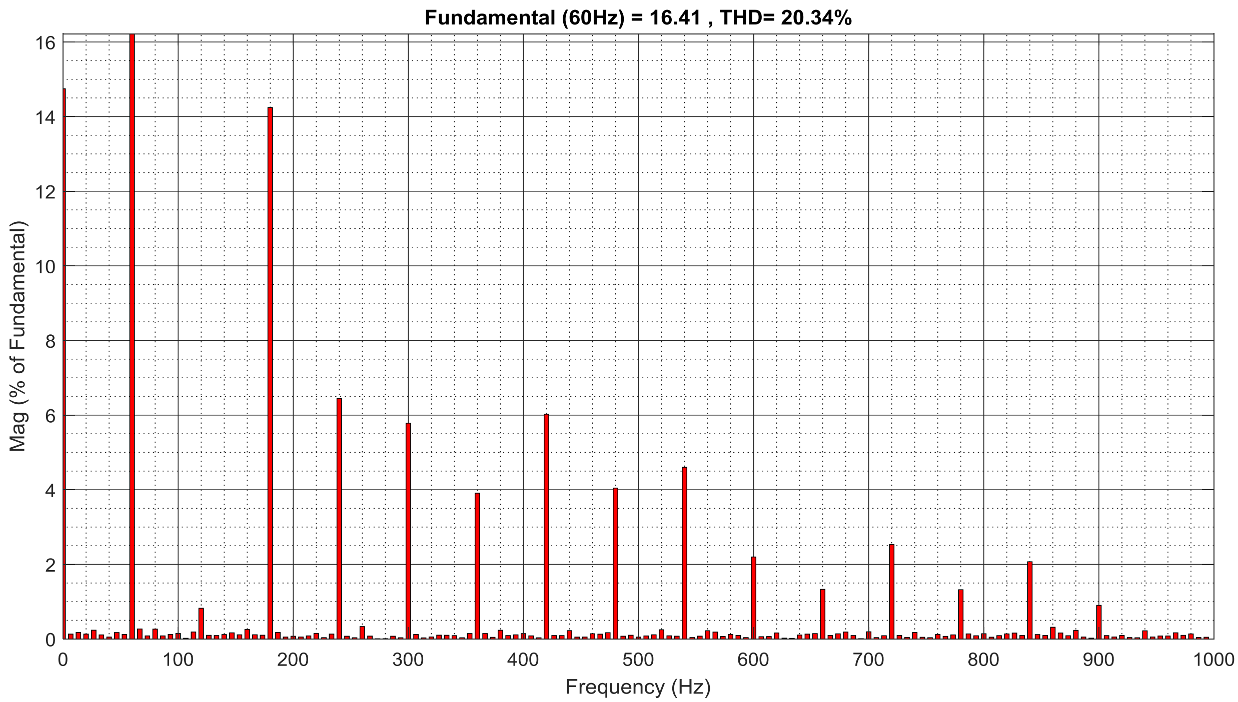

Figure 5.15 FFT analysis of the load current of the V2H system.

5.4 Vehicle to Home (V2H) 3 Phase

The V2H system mentioned earlier can supply power to single-phase house loads. A three-phase V2H system is required to supply power to three-phase house loads such as the elevator, boiler, and heating unit from the Electric Vehicle (EV).

5.4.1 Experimental Setup for 3 Phase Induction Motor

A 3-phase V2H system is developed using the existing converters at FBL. This system uses a 6 kVA Setec Power inverter, three 5.75 kW SMA Sunny Island converters, and a 48 V Pylontech battery bank. As a 3-phase load, a 3-phase induction motor (208 V, 3 hp) is used at no load. Before starting this system, the whole electrical system should be turned off. Then, the Setec inverter is turned on first. Then, the master Sunny Island is turned on, and after that, the other two Sunny Islands are turned on. The full load current of the motor is 8.4 A, and the starting current is 5 times the full load current. The starting current is less than the rated output current of the Sunny Island converter, so the induction motor is started directly.

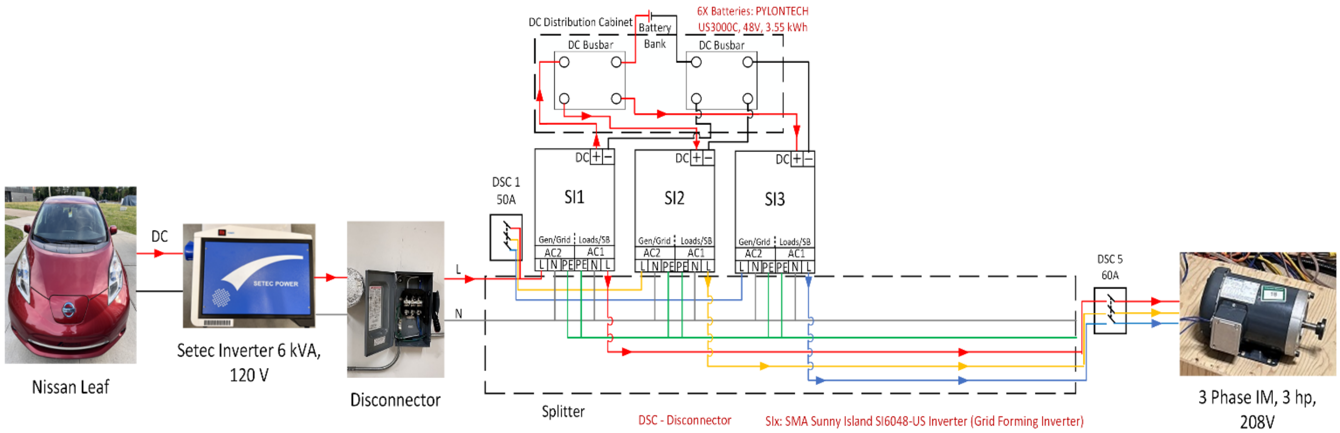

Figure 5.16 Schematic of 3-Phase V2H system to run 3-phase motor

As shown in Figure 5.16, the Setec inverter is connected to the master Sunny Island (SI1) converter through a disconnect switch at terminal AC2. The AC2 terminals of SI2 and SI3 are not connected to the grid. The AC1 terminals of the 3 Sunny Islands are connected to the induction motor through a disconnect switch.

5.4.2 Results of V2H system connected to 3-phase IM

The three line-line voltages and the no-load current of the A phase are measured using an oscilloscope. Table 5.3 gives the 3-phase V2H system line voltages. Figure 5.17 shows the 3-line voltage waveform of this V2H system. The waveforms are sinusoidal and 120 degrees apart.

Table 5.3 Three Phase V2H system line voltages

V_{ab}	203.1 V
V_{bc}	202 V
V_{ca}	203.4 V

The test confirms that this setup is capable of supplying the house's three-phase loads. Figure 5.18 shows the induction motor's no-load current. The waveform is distorted.

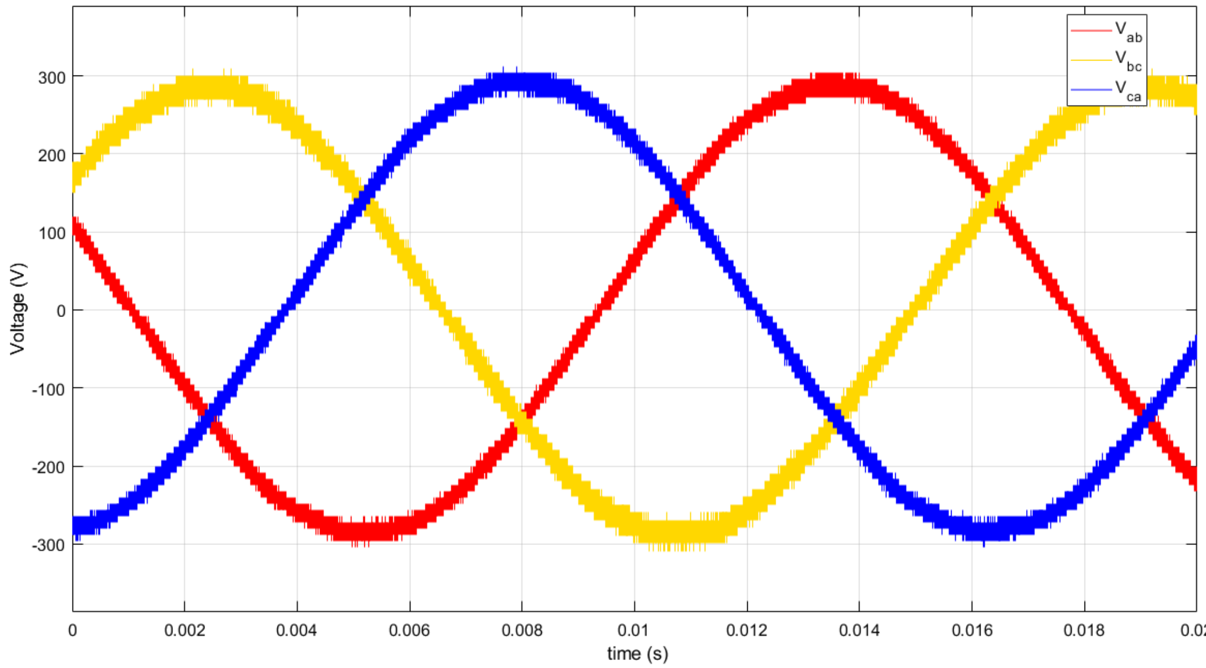

Figure 5.17 Experimental results of the three-phase V2H system test: line voltages.

.

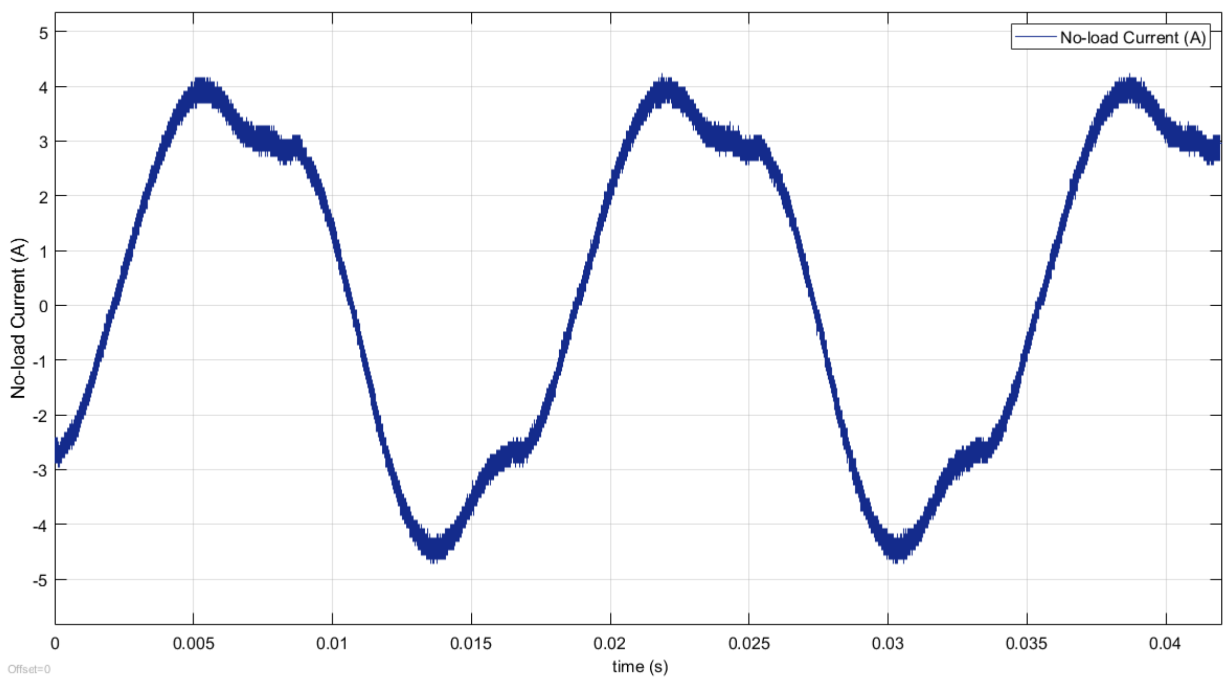

Figure 5.18 Experimental results of the three-phase V2H system test: no-load motor current.

The current that flows in the system is mentioned in Table 5.4. The Setec inverter gives 15.6 A to the SI1 at AC2; part of it feeds the a-phase of the motor, and the remaining is rectified to 30.3 A DC. From 30.3 A DC, 5.9 A and 7.6 A DC are used by SI2 and SI3, respectively, to supply AC current of 2.2 A and 3.1 A to the motor. The remaining DC current from SI1 is used to charge the battery bank. Therefore, it can be concluded that no power from the battery bank is used. In fact, the EV supplies power to the 3-phase motor and also charges the battery bank.

Table 5.4 Three-Phase V2H system test results to run a 3-phase motor

	SI-1		SI-2		SI-3	
	Current	Power	Current	Power	Current	Power
Going in AC2	15.6 A	1872 W	0 A	0 W	0 A	0 W
Coming out of AC1	2.8 A	336 W	2.2 A	264 W	3.1 A	372 W
DC side (DC)	30.3 A	1490 W	-5.9 A	-290.1 W	-7.6 A	-373.7 W

5.4.3 Experimental Setup for 3-Phase Sub-panel Loads of Home

In this section, the 3-phase V2H system is tested with the actual house loads. Figure 5.19 shows the 3-phase motor replaced by the subpanel in the schematic for the V2H system. The loads in the subpanel are already mentioned in Chapter 2.

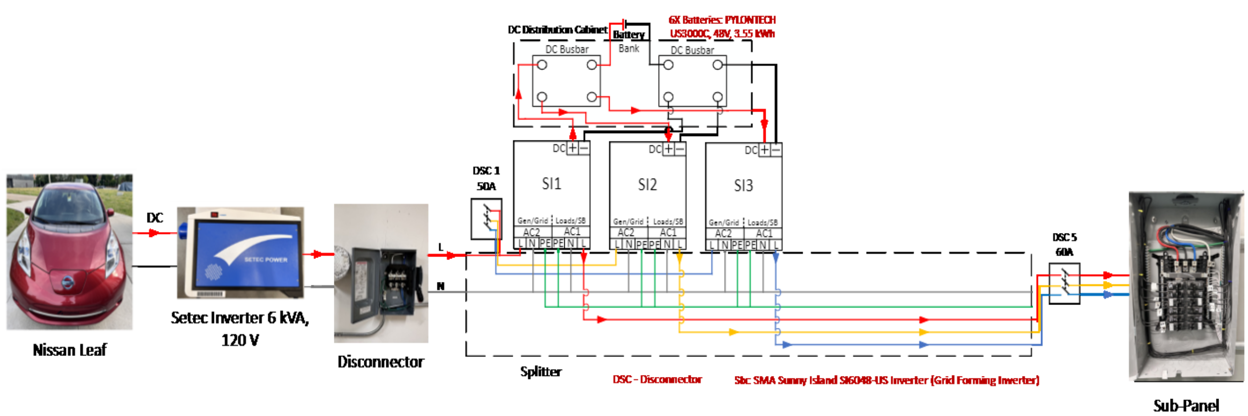

Figure 5.19 Schematic of 3 Phase V2H system connected to Sub-panel

5.4.4 Results of V2H system connected to Sub-panel

The loads of the sub-panel do not consume power all the time. As shown in Table 5.5, the B-phase does not consume any power. 6.6 A and 8.2 A are the A-phase and C-phase currents, respectively. The rectified 21.1 A DC is used by SI2 and SI3. A 0.2 A DC is consumed by SI2 to keep the converter ON. 20.3 A DC is inverted by SI3 to feed the loads connected to the C-phase.

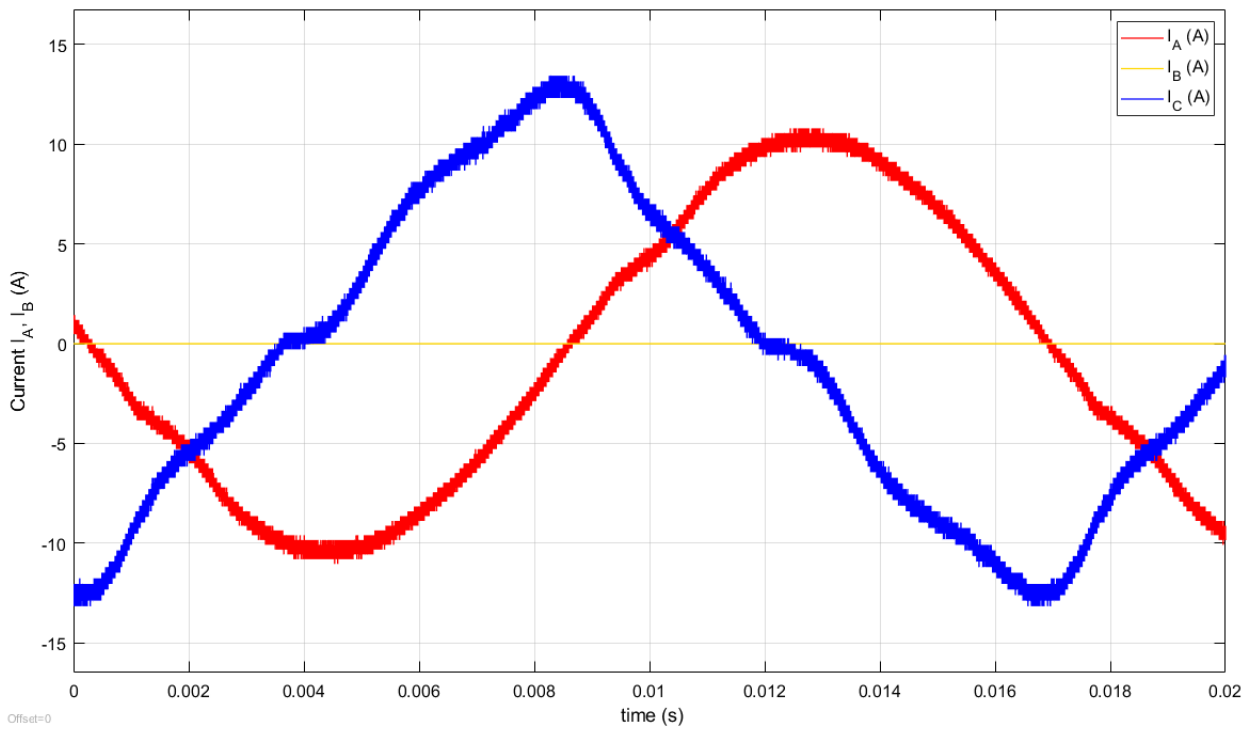

Figure 5.20 Experimental results of the three-phase V2H system test: Sub-panel load

Figure 5.20 shows the load current consumed by the sub-panel loads. The distortion in the current is because of the presence of the non-linear loads (LEDs).

Table 5.5 Three-phase V2H system test result to run a 3-phase sub-panel load

	SI-1		SI-2		SI-3	
	Current	Power	Current	Power	Current	Power
Going in AC2	15.6 A	1872 W	0 A	0 W	0 A	0 W
Coming out of AC1	6.6 A	792 W	0 A	0 W	8.2 A	984 W
DC side (DC)	21.1 A	1034 W	-0.2 A	-10 W	-20.3 A	-995 W

SI1 receives 1872 W power from the Setec inverter, and from that, the loads on the A-phase consume 792 W. 1034 W is obtained at the DC side (1872 – 792 = 1080 W), which means 46 W is the AC to DC conversion power loss. This 1034 W DC power is converted to 984 W AC power by SI3, and SI2 is consuming some power to keep the converter ON. Some power loss is also noted during DC to AC conversion.

6 Conclusion and Future Works

6.1 Conclusion

This research integrates a solar renewable energy system to the Future Building Laboratory (FBL) of Concordia University, Montreal, Quebec, and tests its performance and modes of operation in both off-grid and grid-connected scenarios. The simulated results of the system show that the used topologies and controllers resemble the actual system's behavior. The experimental results of the vehicle-to-load (V2L) and vehicle-to-home (V2H) systems show the potential of EVs as an emergency backup source.

A brief of the chapters is mentioned below.

Discussion of the challenges of rural electrification. The renewable energy system is a sustainable solution for electrifying rural areas. Examples of off-grid rural electrification projects include generating clean energy and helping reduce greenhouse gas emissions.

Presented the FBL's modified electrical power system. The major components of the FBL and the critical loads in the subpanel are mentioned, and the different modes of operation of the power system are discussed.

Investigated the components and the topology of the Sunny Island converter. This helped accurately simulate the standalone grid-forming converter. A grid-following inverter that consists of a maximum power point tracking (MPPT) stage was simulated and controlled. In addition, a frequency shift power control strategy is proposed for parallel operation of grid forming and grid following converters in off-grid mode.

Illustrated the experimental setup installed at the FBL to obtain the experimental results. The performed tests were 1) a Sunny Island converter feeding the house loads in a standalone condition, 2) a Sunny Boy inverter injecting power into the grid, and 3) a Sunny Island and Sunny Boy converters working in parallel to feed the house loads in an off-grid mode. The experimental results obtained of these modes of operation showed that the behavior of the real converters was the same as in the simulation.

Implemented the vehicle-to-home (V2H) system in the Future Building Laboratory (FBL) as a backup option using a Nissan Leaf. A power system was designed to integrate the V2H system alongside the renewable energy system at the FBL. This was realized through manual transfer switches and a subpanel. The system was tested, and the experimental data was analyzed.

6.2 Future Works

For future work, the modes of operation mentioned in Chapter 2 can be tested with the actual solar panels at FBL and compared with the simulated model. A separate three-phase V2H system can be designed without a Setec inverter and SMA converters to supply to the FBL's three-phase loads. Furthermore, with a modification in the design of the V2H inverter, the vehicle-to-grid (V2G) mode can also be realized and tested.

References

[1] "Access to Electricity", SDG7: Data and Projections, [online]. Available: https://www.iea.org. [Accessed June 2024]

[2] Makoto Kanagawa, Toshihiko Nakata, "Assessment of access to electricity and the socio-economic impacts in rural areas of developing countries", Energy Policy, Volume 36, Issue 6, 2008, Pages 2016-2029, ISSN 0301-4215, [online]. Available: https://doi.org/10.1016/j.enpol.2008.01.041. [Accessed June 2024]

[3] "Share of Population with access to Electricity, 2021", Access to Energy, [online]. Available: https://ourworldindata.org [Accessed June 2024]

[4] "Clean Energy Projects in Remote Indigenous and Northern Communities" Market Snapshot, [online]. Available: https://www.cer-rec.gc.ca [Accessed June 2024]

[5] "Renewable Energy for Remote Communities", International Renewable Energy Agency (IRENA), [online]. Available: https://www.irena.org. [Accessed Feb 2025]

[6] N. Sadullaev and S. Nematov, "Micro-grid Based Power Supply of Remote Consumers Located Away from the Centralized Power Grid," 2020 IEEE International Conference on Advent Trends in Multidisciplinary Research and Innovation (ICATMRI), Buldhana, India, 2020, pp. 1-6, doi: 10.1109/ICATMRI51801.2020.9398476.

[7] M. Juanpera, B. Domenech, L. Ferrer-Martí, A. Garzón, R. Pastor, Renewable-based electrification for remote locations. Does short-term success endure over time? A case study in Peru, Renewable and Sustainable Energy Reviews, Volume 146, 2021, 111177, ISSN 1364-0321, https://doi.org/10.1016/j.rser.2021.111177.

[8] E. Karimi and M. Kazerani, "Impact of renewable energy deployment in Canada's remote communities on diesel generation carbon footprint reduction," 2017 IEEE 30th Canadian Conference on Electrical and Computer Engineering (CCECE), Windsor, ON, Canada, 2017, pp. 1-5, doi: 10.1109/CCECE.2017.7946740.

[9] “Photovoltaic Electricity Potential”, 2020 The World Bank, Source: Global Solar Atlas 2.0, Solar resource data: Solargis, [online]. Available: https://solargis.com [Accessed June 2024]

[10] “Goal 7: Increase Canadians’ access to clean energy”, [online]. Available: https://www.canada.ca [Accessed June 2024]

[11] “ATCO Completes Canada’s Largest Off-Grid Solar Project in Partnership with three Alberta Indigenous Nations”, [online]. Available: https://electric.atco.com [Accessed June 2024]

[12] “3NE Solar Farm”, [online]. Available: https://www.3ne.ca [Accessed June 2024]

[13] “Old Crow Solar Project”, [online]. Available: https://electric.atco.com [Accessed June 2024]

[14] “Powered by Nature: The Old Crow Solar Project”, GBP CREATIVE, [online]. Available: https://arctic-council.org [Accessed June 2024]

[15] “Community micro grid project now online”, [Online]. Available: https://www.opg.com [Accessed June 2024]

[16] “Gull Bay First Nation”, [online]. Available: https://www.hydrooneremotes.ca [Accessed June 2024]

[17] Z. Asadi, A. M. Aljehaimi and P. Pillay, "Solar Power Electronics System Design for the Future Building Laboratory at Concordia University," *2023 IEEE 14th International Conference on Power Electronics and Drive Systems (PEDS)*, Montreal, QC, Canada, 2023, pp. 1-6, doi: 10.1109/PEDS57185.2023.10246500.

[18] Secondary control with grid-forming inverters for an island grid restoration approach without communication Author: Iwo Bekker,Lutz Hofmann,Axel Mertens Available: https://www.sciencedirect.com

[19] D. Pattabiraman, R. H. Lasseter. and T. M. Jahns, "Comparison of Grid Following and Grid Forming Control for a High Inverter Penetration Power System," *2018 IEEE Power & Energy Society General Meeting (PESGM)*, Portland, OR, USA, 2018, pp. 1-5, doi: 10.1109/PESGM.2018.8586162.

[20] T. Ackermann, T. Prevost, V. Vittal, A. J. Roscoe, J. Matevosyan and N. Miller, "Paving the Way: A Future Without Inertia Is Closer Than You Think", *IEEE Power and Energy Magazine*, vol. 15, no. 6, pp. 61-69, Nov.-Dec. 2017.

[21] REX POWER MAGNETICS – Name Plate Rating

[22] SMA Solar Technology America LLC [online] Available: https://files.sma.de/downloads/SI4548-6048-US-BE-en-21W.pdf

[23] SMA Solar Technology America LLC [online] Available: https://files.sma.de/downloads/SBxx-US-1XP-41-BA-en-11.pdf?_ga=2.83633430.1443162467.1694444603-84926377.1694444603

[24] PYLONTECH-US3000C Li-ion Battery [online] Available: https://en.pylontech.com.cn/products/c23/121.html

[25] P. Soth et al., "Robust Dual-Current Control of a Three-Phase Grid-Tied Inverter under Unbalanced Grid Voltage Using LMI Approach," 2023 International Electrical Engineering Congress (iEECON), Krabi, Thailand, 2023, pp. 6-11, doi: 10.1109/iEECON56657.2023.10126574.

[26] J. Lin et al., "Frequency Coupling Suppression Control Strategy for Single-Phase Grid-Tied Inverters in Weak Grid," in IEEE Transactions on Industrial Electronics, vol. 69, no. 9, pp. 8926-8938, Sept. 2022, doi: 10.1109/TIE.2021.3112989.

[27] Z. Zhang, R. Schürhuber, L. Fickert, G. Chen and Y. Zhang, "Low Voltage Ride Through Characteristics of Grid Forming inverters," 2020 21st International Scientific Conference on Electric Power Engineering (EPE), Prague, Czech Republic, 2020, pp. 1-6, doi: 10.1109/EPE51172.2020.9269240.

[28] A. B. Nassif et al., "Improving Frequency Stability and Minimizing Load Shedding Events by Adopting Grid-Scale Energy Storage with Grid Forming Inverters," 2023 IEEE PES Innovative Smart Grid Technologies Latin America (ISGT-LA), San Juan, PR, USA, 2023, pp. 5-9, doi: 10.1109/ISGT-LA56058.2023.10328328.

[29] D. Huang, Z. Fang, S. Zhang, X. Li, Z. Wei and L. Jin, "A short-circuit fault ride-through method based on adaptive dual-mode control of grid-forming inverters," 2023 IEEE PELS Students and Young Professionals Symposium (SYPS), Shanghai, China, 2023, pp. 1-6, doi: 10.1109/SYPS59767.2023.10268207.

[30] A. Quedan, W. Wang, D. Ramasubramanian, E. Farantatos and S. Asgarpoor, "Dynamic behavior of combined 100% IBR transmission and distribution networks with grid-forming and grid-following inverters," *2023 IEEE Power & Energy Society Innovative Smart Grid Technologies Conference (ISGT)*, Washington, DC, USA, 2023, pp. 1-5, doi: 10.1109/ISGT51731.2023.10066356.

[31] J. Gluščević, Ž. Janda, J. Dragosavac and L. Ristić, "Enhancing Stability of Grid-Following Inverter for Renewables," *2023 22nd International Symposium on Power Electronics (Ee)*, Novi Sad, Serbia, 2023, pp. 1-6, doi: 10.1109/Ee59906.2023.10346158.

[32] R. Teodorescu, M. Liserre, and P. Rodriguez, Grid Converters for Photovoltaic and Wind Power System. John Wiley & Sons, Ltd, Jul. 2011.

[33] Q. Ma, S. An, M. Liu, J. Jiao, M. Li and W. Xie, "Emergency Switching Control Strategy of Grid-Forming and Grid-Following for Centralized Photovoltaic," *2023 IEEE International Conference on Power Science and Technology (ICPST)*, Kunming, China, 2023, pp. 61-66, doi: 10.1109/ICPST56889.2023.10164937.

[34] Prasad, J. & Bhavsar, Tushar & Ghosh, Rajesh & Narayanan, G.. (2009). Vector control of three-phase AC/DC front-end converter. Sadhana. 33. 591-613. 10.1007/s12046-008-0045-y.

[35] N. S. D'Souza, L. A. C. Lopes and X. Liu, "Peak Current Control Based Maximum Power Point Trackers for Faster Transient Responses," 2006 Canadian Conference on Electrical and Computer Engineering, Ottawa, ON, Canada, 2006, pp. 659-663, doi: 10.1109/CCECE.2006.277590.

[36] H. A. Sher, A. F. Murtaza, A. Noman, K. E. Addoweesh, K. Al-Haddad and M. Chiaberge, "A New Sensorless Hybrid MPPT Algorithm Based on Fractional Short-Circuit Current Measurement and P&O MPPT," in IEEE Transactions on Sustainable Energy, vol. 6, no. 4, pp. 1426-1434, Oct. 2015, doi: 10.1109/TSTE.2015.2438781.

[37] Reddy, D. & Satyanarayana, S. & Ganesh, Vaishnavi. (2018). Design of Hybrid Solar Wind Energy System in a Microgrid with MPPT Techiques. International Journal of Electrical and Computer Engineering. 81. 730-740. 10.11591/ijece.v8i2.pp730-740.

[38] Y. Chen et al., "A Novel Mixed Control Strategy with Grid-Following and Grid-Forming for Renewable Energy Grid-Connected Inverter," in 2023 6th International Conference on Electronics Technology (ICET), Chengdu, China, 2023, pp. 781-786, doi: 10.1109/ICET58434.2023.10211867.

[39] F. Sadeque, D. Sharma and B. Mirafzal, "Power-Sharing between Grid-Forming and Grid-Following Inverters," in 2021 IEEE 22nd Workshop on Control and Modelling of Power Electronics (COMPEL), Cartagena, Colombia, 2021, pp. 1-5, doi: 10.1109/COMPEL52922.2021.9646073.

[40] R. Mishan, M. Benidris and J. Zeng, "Autonomous Power Sharing Among Decentralized Inverters Using Modified Droop Control," in 2022 IEEE International Conference on Power Electronics, Drives and Energy Systems (PEDES), Jaipur, India, 2022, pp. 1-6, doi: 10.1109/PEDES56012.2022.10080845.

[41] R. Rosso, X. Wang, M. Liserre, X. Lu and S. Engelken, "Grid-Forming Converters: Control Approaches, Grid-Synchronization, and Future Trends—A Review," in IEEE Open Journal of Industry Applications, vol. 2, pp. 93-109, 2021, doi: 10.1109/OJIA.2021.3074028.

[42] Z. Zhou, W. Wang, T. Lan and G. M. Huang, "Dynamic Performance Evaluation of Grid-Following and Grid-Forming Inverters for Frequency Support in Low Inertia Transmission Grids," 2021 IEEE PES Innovative Smart Grid Technologies Europe (ISGT Europe), Espoo, Finland, 2021, pp. 01-05, doi: 10.1109/ISGTEurope52324.2021.9640034.

[43] C. Liu, K. T. Chau, D. Wu and S. Gao, "Opportunities and Challenges of Vehicle-to-Home, Vehicle-to-Vehicle, and Vehicle-to-Grid Technologies," in Proceedings of the IEEE, vol. 101, no. 11, pp. 2409-2427, Nov. 2013, doi: 10.1109/JPROC.2013.2271951

[44] L. Dickerman and J. Harrison, "A New Car, a New Grid," in IEEE Power and Energy Magazine, vol. 8, no. 2, pp. 55-61, March-April 2010, doi: 10.1109/MPE.2009.935553.

[45] Arya, Tanmay & Saxena, Devansh & Misra, Priya. (2023). Optimizing Electricity Bill, Grid Performance, and User Satisfaction in a Comprehensive Home Energy Management System with Electric Vehicles and Home-to-Grid Capabilities. 1-6. 10.1109/ELEXCOM58812.2023.10370103.

[46] Yousafzai, Adnan & Khan, Asif & Javaid, Nadeem & Hussain, Hafiz Majid & Abdul, Wadood & Almogren, Ahmad & Alamri, Atif & Niaz, Iftikhar. (2017). An Optimized Home Energy Management System with Integrated Renewable Energy and Storage Resources. Energies. 10. 549. 10.3390/en10040549.

[47] T. Osmancik, A. M. Aljehaimi and P. Pillay, "An Electric Vehicle Circuit for Powering Independent Loads," *2023 IEEE 14th International Conference on Power Electronics and Drive Systems (PEDS)*, Montreal, QC, Canada, 2023, pp. 1-5, doi: 10.1109/PEDS57185.2023.10268828.

[48] A. Syafiqa Shamsuddin, R. Ishak, A. Syahiman Mohd Shah and A. Sharizli Abdullah, "Harmonic Injection by LEDs and CFLs in Electrical Distribution System," 2020 11th IEEE Control and System Graduate Research Colloquium (ICSGRC), Shah Alam, Malaysia, 2020, pp. 10-15, doi: 10.1109/ICSGRC49013.2020.9232631.

Appendix

A. Commissioning

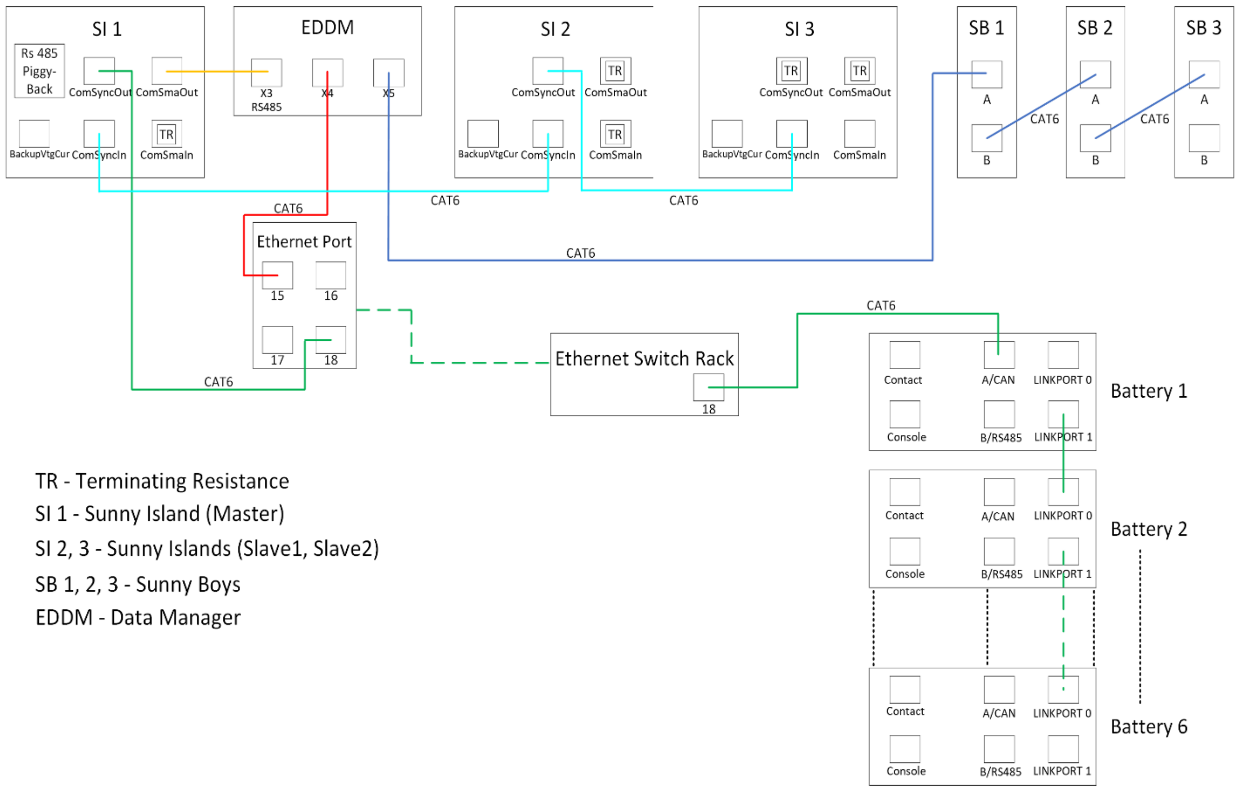

Figure A-1 Communication Network of inverters, battery bank, and data manager

I. Sunny Island Converter

SI 1 serves as the master Sunny Island (SI). To enable RS 485 communication, a Piggy-Back module is installed inside the master SI. The ComSmaOut port (RJ-45 connector) of the master SI is connected to the X3 (RS485) port of the EDDM. The X3 port has 6 terminals, and the connections for the RS 485 protocol are as follows: terminal 1 - green strip in white, terminal 3 - orange, terminal 4 - green, and terminals 5-6 are jumper. A terminating resistor is connected at the ComSmaIn. SI 2 and SI 3 are configured as Slave 1 and Slave 2, respectively (with the only adjustment being their designation as slaves). The Sunny Islands are interconnected using a CAT6 cable, as depicted in Figure A-1.

Initial commissioning Steps:

1. It is recommended to configure the Sunny Islands (SIs) in off-grid mode. Therefore, ensure that the grid disconnect switch on the back of the wooden wall is turned off.

2. Verify that the power connection between the batteries and the SIs is established, and ensure that the batteries are charged to at least 20%. If the batteries are fully discharged, the SIs will not function.
3. Ensure the communication wiring between the batteries and the SI Master is properly connected, as shown in Figure A-1. Also, confirm that the communication wiring between all three SIs is properly set up, as shown in Figure A-1.
4. Begin the configuration with Slave 2. Always start with Slave 2, then move to Slave 1, and configure the SI Master last. For any SI unit, turn the switch on, then immediately press and hold the "Enter" button until you hear three beeps (same process to reset the SIs). This will take you to the settings display. For the slave SIs, the only configuration required is to select "New System" and set the inverter mode to "Slave."
5. For the SI Master, select "New System" and then proceed to the battery settings. Configure the battery type as "Lithium-ion with External BMS" and input the total Ah capacity of the battery bank. Then, set the external source to "Grid" and adjust the grid current according to the fuse rating. (For example: If the fuse is rated 15 A, set the grid current to 10 A. The 10 A setting allows the battery to be charged at 3.6 kW (calculated as 10 A * 120 V * 3 phases). This results in a total DC charging current of 3.6 kW / 48 V = 75 A, with 25 A supplied by each inverter. If we assume equal charging across all six batteries, each battery would receive 12.5 A. The manufacturer's recommended charge/discharge current for each battery is 37 A). Set the battery voltage (48 V), battery bank capacity (74 Ah * 6 = 444Ah), time, and baud rate (1200).
6. Once the parameters in the master SI are set, the system will ask to press and hold enter to start the converter.

II. Sunny Boy Inverter

Sunny Boy inverters do not have a control panel to change the parameters of the Sunny Boy inverter; a connection to the web server is used.

Initial commissioning Steps:

1. Ensure that the AC power connection of the sunny boy (SBs) is established, and verify that the sunny islands (SIs) are powered on. Once confirmed, switch on the three Sunny Boys AC disconnect switches located on the back of the wooden wall.

2. At this point, the AC terminal voltage of the SBs should be 208 V if connected in L-L fashion or 120 V if connected in L-N fashion.
3. The complete configuration of the SBs requires both AC and DC power. However, one can still perform the configuration with only the AC power on, except for the "Grid Standard" setting, which will remain inaccessible until the DC power is available.
4. Connect a laptop to one SB (A or B port) using a CAT 6 Ethernet cable.
5. On the laptop, ensure that the network's TCP/IPv4 settings are set to "Automatic", as shown in the below figure A-2.

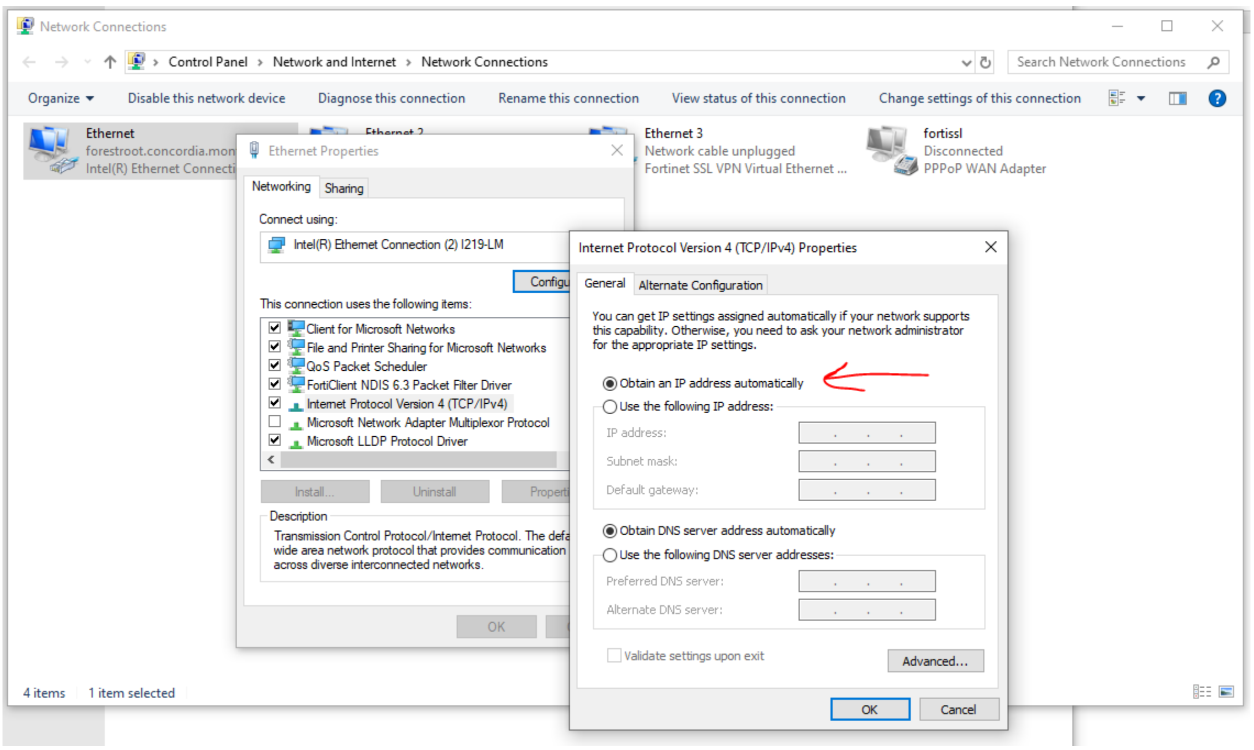

Figure A-2 Laptop's TCP/IPv4 network settings (Automatic)

6. On the laptop, ensure that the "Packet Priority & VLAN" option in the Ethernet network configuration is disabled, as shown in Figure A-3. If this option is enabled, the laptop will not detect the Sunny Boy (SB), as it will prioritize the Wi-Fi connection, which needs to remain on during configuration. Disabling "Packet Priority & VLAN" instructs the laptop to search for the Ethernet connection in addition to the Wi-Fi.

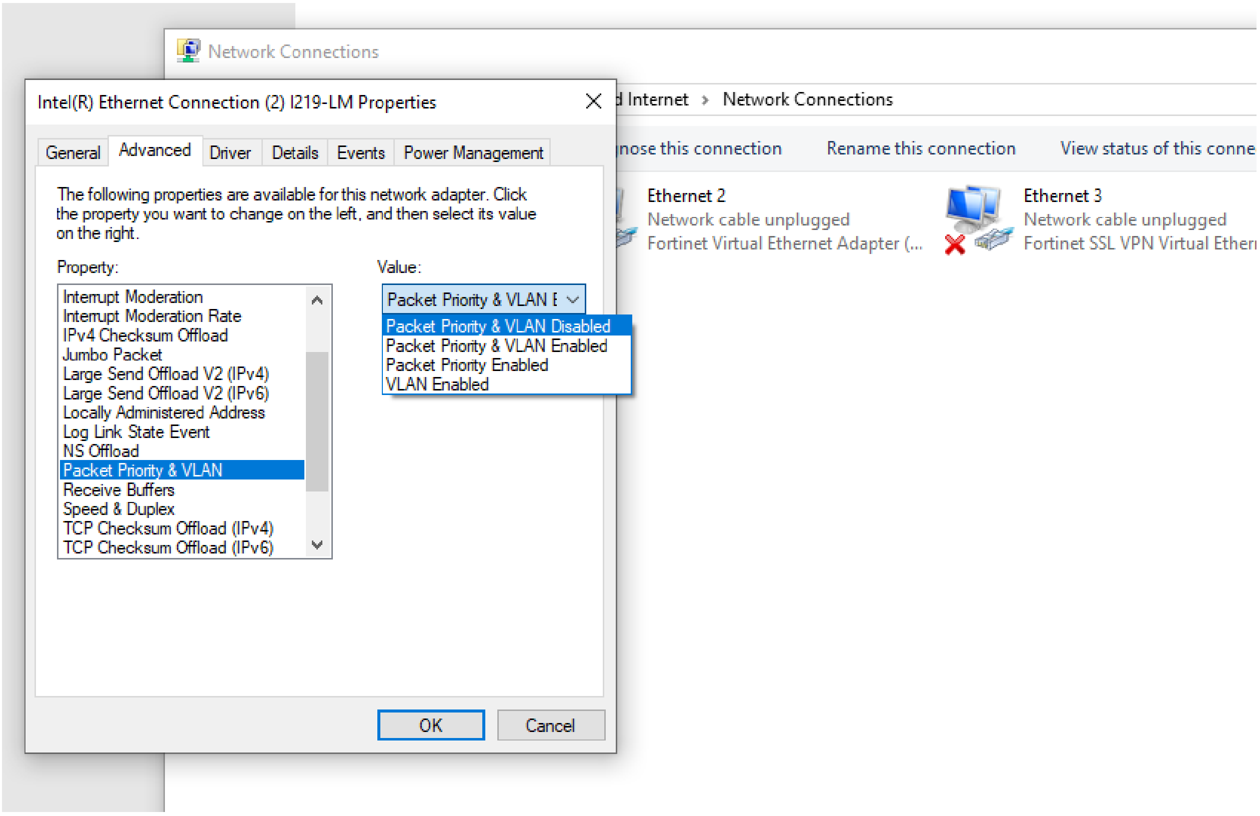

Figure A-3 Laptop network configuration (Packet Priority & VLAN)

7. Next, open a web browser and enter the SBs' default IP address, which is https://169.254.12.3. The first time you log in, you must set a username and password. If credentials have already been set, enter them to log in.
8. At this point, you can also update the SB's firmware. To do this, download the latest firmware version from the SMA website on the laptop. Select "Update the firmware," as shown in Figure A-4, and follow the instructions. The update process takes about five minutes, during which the SB will restart.

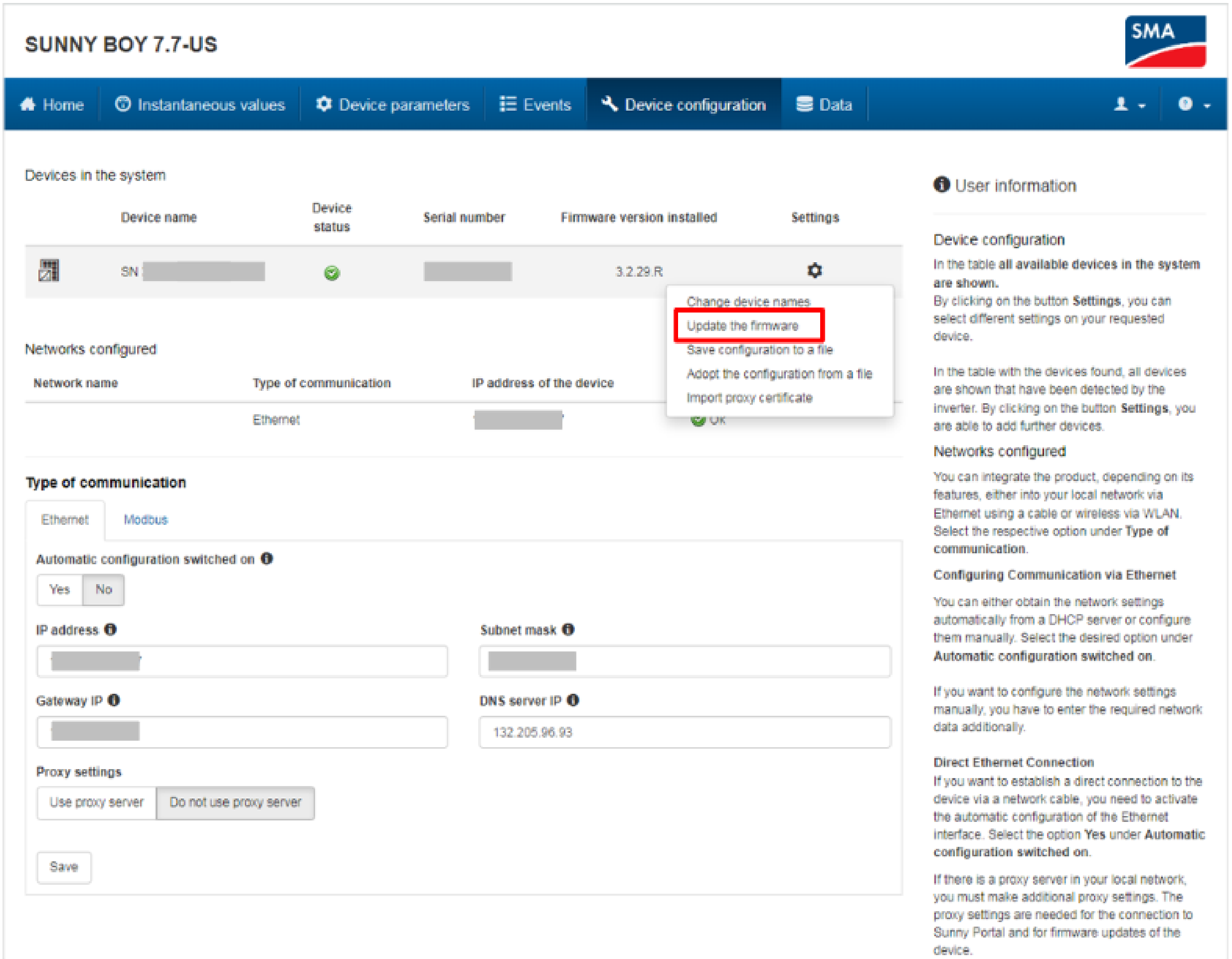

Figure A-4 SB firmware update

9. After the firmware update, again login and follow the Setup Assist Guide as shown in Figure A-5. Click on "Start the installation assistant," which contains eight steps. In step 1 of the Setup Assist Guide, set the date and time as presented in Figure A-6. Then, change the IP address of the SB to the IP assigned (let's take an example: 192.166.122.117) by the network department (available IPs in the present network).
10. After updating the IP settings of the SB, you will lose the connection. To reconnect, go to Step 5 and change the TCP/IPv4 network settings to static by selecting "Use the following IP address" (IP address: 192.166.122.200, which is in the range of 192.166.122.117).
11. Then, open the browser again and enter (updated IP address) https://192.166.122.117. Log in with your credentials (Step 7), and you will notice the SB's IP address has been updated to the newly assigned one. Continue with the Setup Assist Guide until you have completed all the

steps. After configuring and updating the firmware of all three SBs, establish the communication wiring between the SBs and the data manager, as shown in Figure A-1.

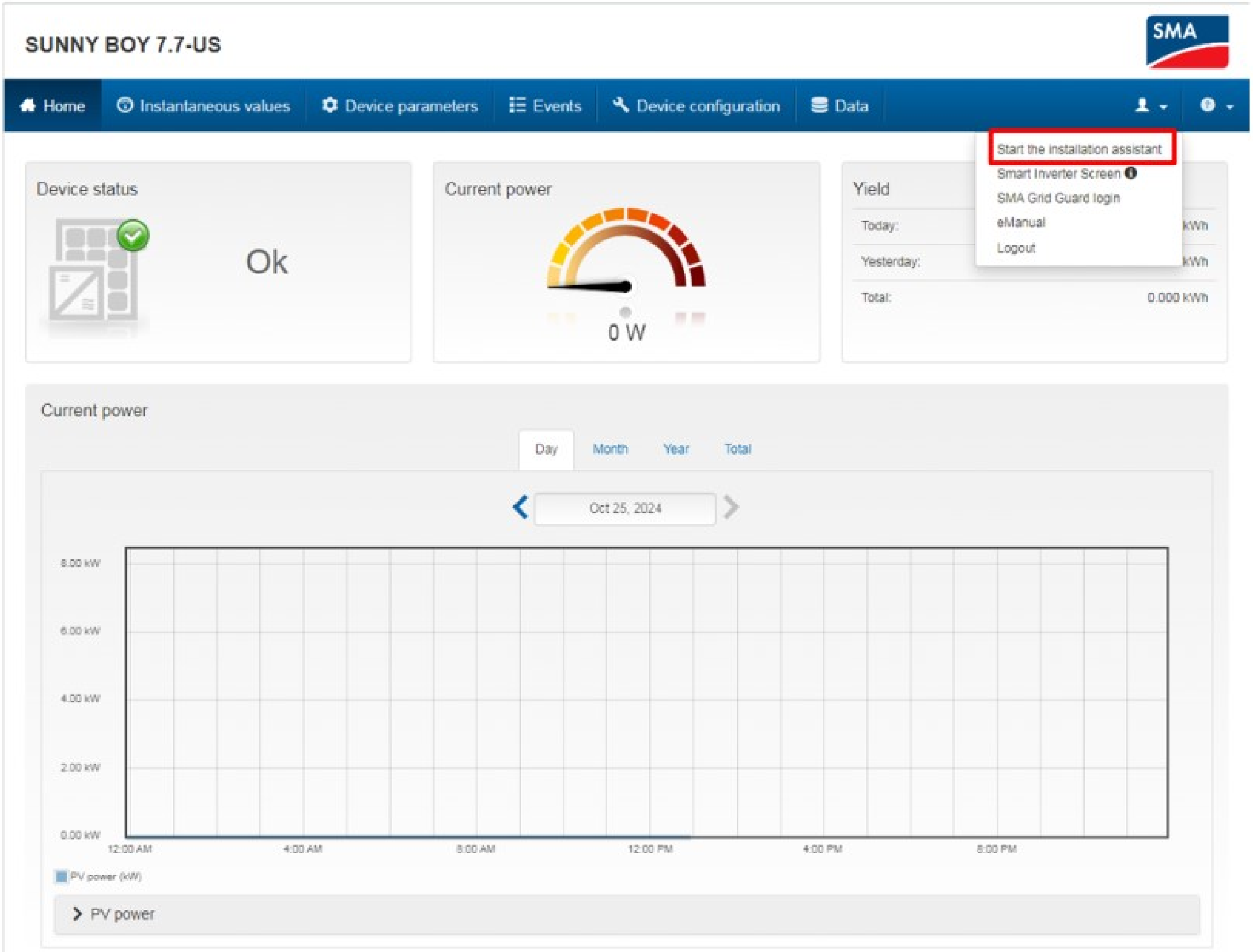

Figure A-5 Starting the installation assistant

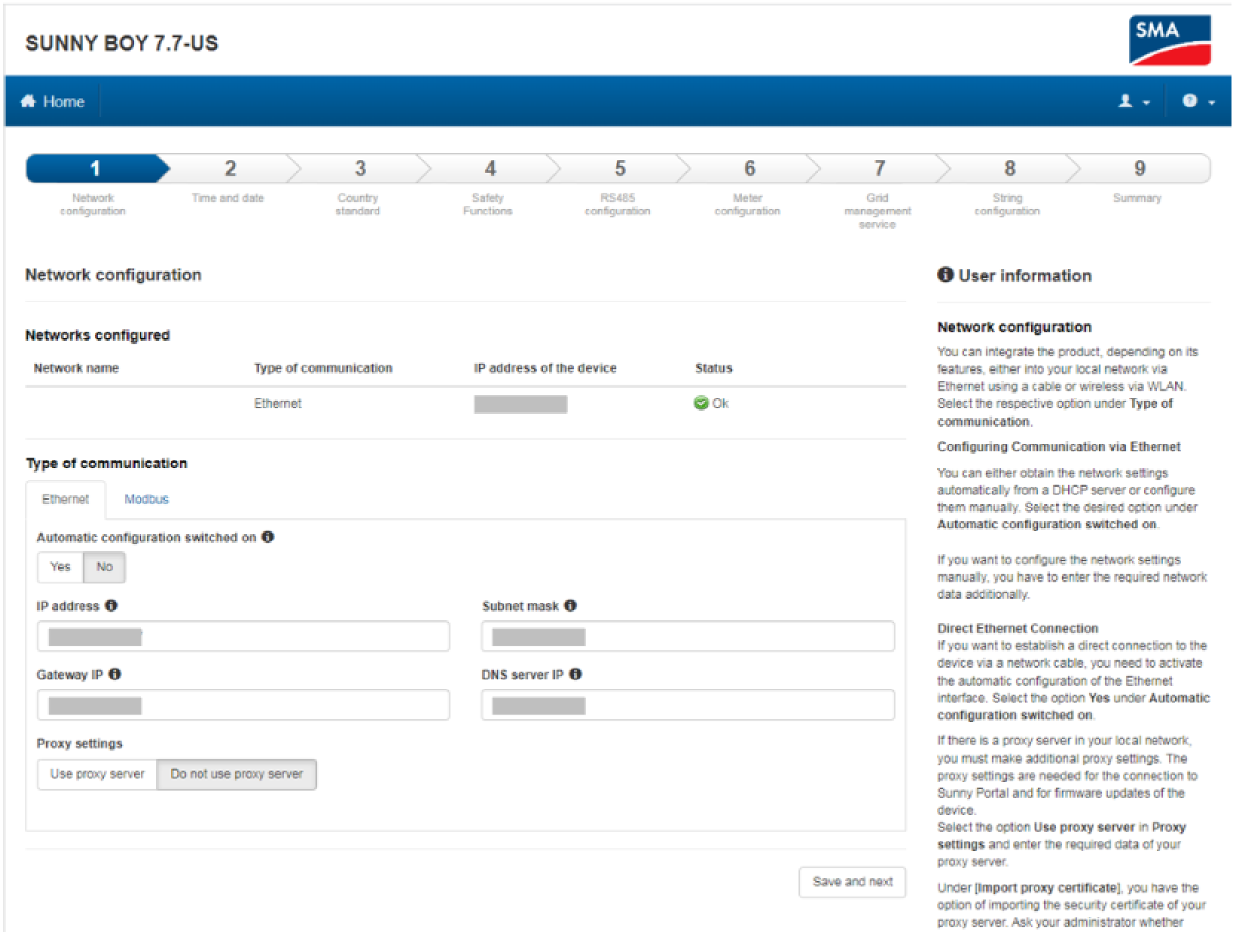

Figure A-6 Installation steps

III. Data Manager (EDMM)

The EDMM needs a 24 V DC power supply, an AC/DC converter is used to get the 24 V DC supply.

The following steps are followed for configuring EDMM:

1. Ensure that the AC power connection of the sunny boys (SBs) is established, and verify that the sunny islands (SIs) are powered on. Once confirmed, switch on the three sunny boys. Check all the communication wiring between the SBs, SIs, and the EDMM.
2. If everything is connected correctly, the top LED on the EDMM should be solid green, and the bottom LED should be blinking green. Establish the Ethernet connection between the laptop and the EDMM via CAT6 cable. The CAT6 cable should be plugged into the EDMM's X4 port.

3. Set the laptop's TCP/IPv4 network setting to "Automatic," as done in configuring SB. Open the browser and type the EDMM's default IP: http://169.254.12.3.
4. This will open the ennexOS platform of the EDMM. For the first time, set the username and password. Also, fill in the information regarding the installer's name and email, date and time, system's name, and location.
5. To change the IP of the EDMM, select EDMM on the dashboard, then go to "Configuration" and select "Network Configuration". Once the IP is changed, the connection will be lost. To re-establish the connection, change the laptop TCP/IPv4 network to Static and enter the IP address and subnet mask in the range of the configured EDMM's IP.

6. Now, to add the master SI and SBs to the EDMM, go to "Configuration" and select "Device Administration." The page will have the plus sign to add the devices, as shown in Figure A-7.

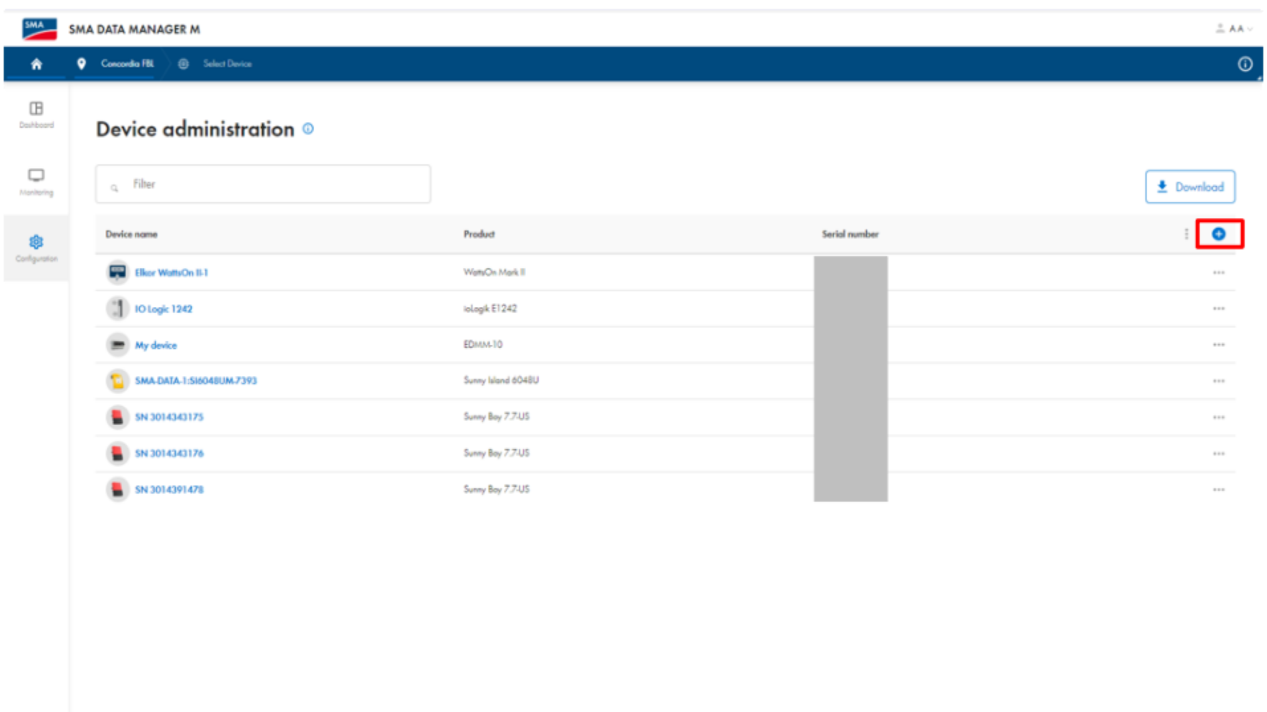

Figure A-7 Adding devices with EDMM

7. After clicking the add button, the "Device registration" page will open, as shown in Figure A-8. To add an SI master, select the "SMA Data1 devices" protocol and follow the steps to search and add the device. To add SBs, select the "SMA Speedwire devices" protocol and follow the steps to search and add the device. To add other Modbus devices, select "Modbus devices" protocol.

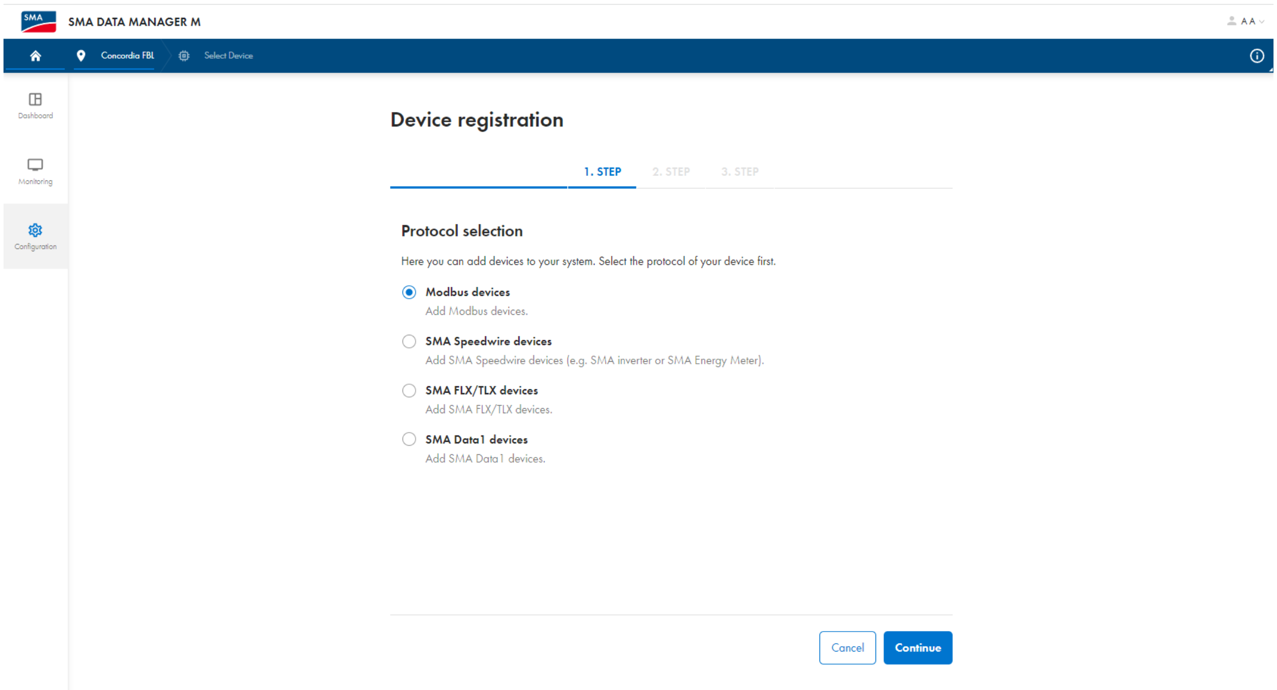

Figure A-8 Protocol selection to add the device in EDMM

The remote monitoring of the battery charge/discharge and the PV power is shown in Figures A-9 and A-10.

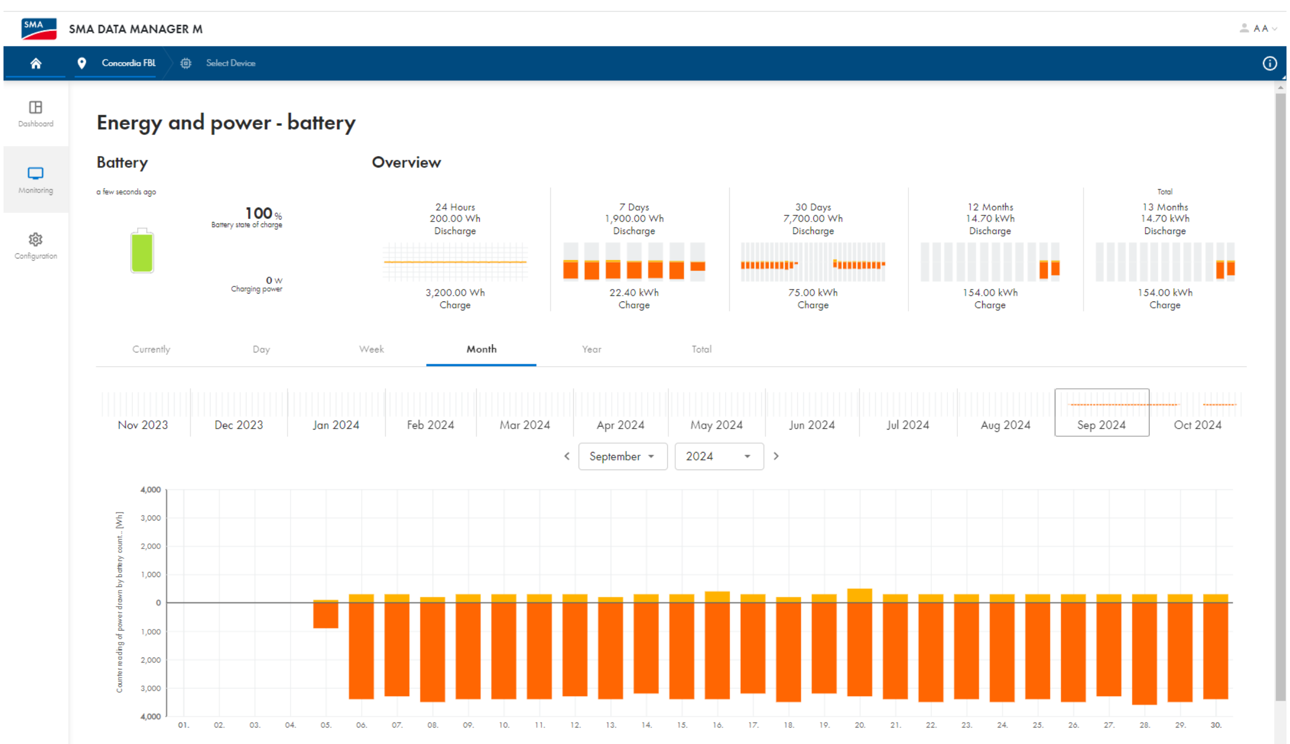

Figure A-9 EDMM battery status remote monitoring

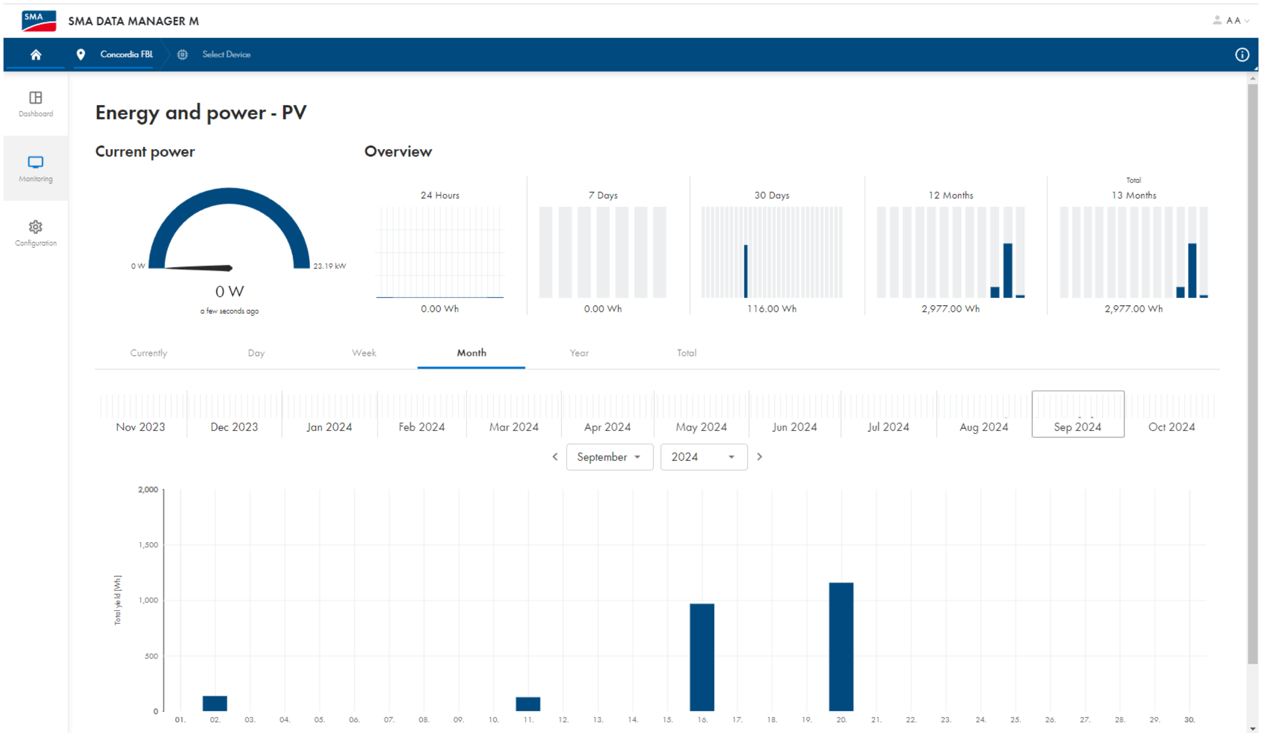

Figure A-10 EDMM PV energy status remote monitoring